Dissertation

submitted to the

Combined Faculties for the Natural Sciences and for Mathematics

of the Ruperto-Carola University of Heidelberg, Germany

for the degree of

Doctor of Natural Sciences

presented by

Dipl.-Biol. Sonja Welsch

born in: Heilbronn

Oral-examination: . .

Ultrastructural Analysis of HIV-1 Infection in Human Cells

Referees:

Prof. Dr. Hans-Georg Kräusslich

Dr. Jacomine Krijnse-Locker

Summary

Human immunodeficiency virus (HIV), the causative agent of Acquired Immune Deficiency Syndrome (AIDS), is a major infectious disease problem that affects over 40 million people worldwide, with an estimated 3 million deaths per year. Although major advances were made in the treatment of HIV-infected individuals, a protective vaccine or an effective way to eliminate HIV from infected individuals is still lacking. In this study, I combined cell biology and virology to obtain new insights into HIV-infection by quantitative electron microscopy. In the first part, I analyzed the localization of a cellular protein complex, termed ESCRT, recently found to be essential for HIV release from infected cells. ESCRT was also shown to be involved in protein sorting into, and formation of, intralumenal vesicles of a specialized endosomal compartment, the multivesicular body (MVB). ESCRT subunits localized throughout the endocytic pathway, including the plasma membrane and were found to be particularly concentrated on tubular-vesicular endosomal membranes but not on MVBs. Unexpectedly, ESCRT was not redistributed to the presumed site of HIV budding upon infection, the plasma membrane and endosomes in primary human T cells and macrophages, respectively. ESCRT localized more to the cell surface in T cells than in macrophages, collectively suggesting that endogenous ESCRT suffices for HIV budding. These findings also suggested a previously unknown role for tubular-vesicular endosomal membranes in the function of ESCRT.

In the second part of this study, the site of HIV budding and release from infected macrophages was studied in detail by EM. Recent studies suggested that HIV buds into MVBs of macrophages, thereby accumulating in an intracellular endosomal storage compartment. Such cellular reservoirs of HIV were proposed to hamper clearance of HIV from infected individuals. In agreement with previous data, EM analysis of macrophages showed that virions accumulated in large vacuolar structures. However, an assay that unequivocally discriminated endosomal membranes from the plasma membrane revealed a very complex morphology of the plasma membrane, displaying many protrusions and deep invaginations. HIV budding occurred on such deep invaginations of the cell surface, leading to the accumulation of virions in vacuolar structures that were limited by cell surface-derived membranes rather than endosomal membranes. This finding opens a new perspective on HIV infection of macrophages, in particular their proposed role in virus persistence. Finally, the combined studies have important implications for the presumed pivotal role of MVBs/endosomes in HIV budding as well as the role played by ESCRT in their biogenesis.

Zusammenfassung

Das Humane Immundefizienz-Virus (HIV) ist der Auslöser des erworbenen Immundefizienz-Syndroms (acquired immune deficiency syndrome, AIDS). HIV-Infektion, weltweit eine der problematischsten Infektionskrankheiten, betrifft etwa 40 Millionen Menschen und tötet schätzungsweise 3 Millionen Menschen jährlich. Obwohl die Behandlung von HIV-Patienten heute möglich ist, gibt es weiterhin keinen Impfschutz und keine Heilung. Mit der vorliegenden Arbeit habe ich Zellbiologie und Virologie vereint, um mittels quantitativer Elektronenmikroskopie (EM) neue Einblicke in die HIV-Infektion zu gewinnen. Im ersten Teil habe ich die Verteilung eines zellulären, ESCRT benannten, Proteinkomplexes analysiert. ESCRT ist essentiell für die Freisetzung von HIV aus infizierten Zellen und spielt sowohl beim Sortieren von Proteinen in die internen Vesikel eines multivesikulären endosomalen Kompartiments (multivesicular body, MVB) als auch bei der Bildung dieser Vesikel eine Rolle. ESCRT fand sich im gesamten endosomalen System einschliesslich der Plasmamembran, und war besonders an tubulär-vesikulären endosomalen Membranen, aber nicht an MVBs, angereichert. Entgegen der Erwartungen führte HIV-Infektion nicht zu einer Umverteilung von ESCRT zu den Orten der Virusfreisetzung aus Zellen, der Plasmamembran in primären humanen T-Zellen bzw. Endosomen in Makrophagen. In T-Zellen fand sich mehr ESCRT an der Plasmamembran als in Makrophagen, was darauf hindeutet, dass endogene ESCRT-Mengen für die HIV-Freisetzung hinreichend sind. Die Ergebnisse weisen auch auf eine bisher unbekannte Rolle von tubulär-vesikulären endosomalen Membranen bei der Funktion von ESCRT hin.

Im zweiten Teil habe ich den Ort der HIV-Freisetzung aus infizierten Makrophagen mittels EM untersucht. Neuere Studien wiesen darauf hin, dass neu gebildete HIV-Partikel in die Endosomen infizierter Makrophagen entlassen werden und somit in intrazellulären Speichern akkumulieren, die die Heilung infizierter Patienten erschweren könnten. Übereinstimmend mit bekannten Daten zeigte unsere EM-Analyse von Makrophagen, dass Viren in grossen, intrazellulären Vakuolen akkumulierten. Eine Methode zur eindeutigen Unterscheidung von endosomalen Membranen und der Plasmamembran offenbarte aber die komplexe Morphologie der Plasmamembran mit vielen Aus- und Einstülpungen. In diesen tiefen Einstülpungen, die nicht von endosomalen Membranen, sondern von der Plasmamembran begrenzt werden, wurden Viruspartikel freigesetzt und angehäuft. Dieses Ergebnis eröffnet einen neuen Blickwinkel auf die HIV-Infektion von Makrophagen, besonders deren mögliche Rolle bei der Persistenz von Viren. Zusammenfassend haben diese Daten eine wichtige Bedeutung hinsichtlich der scheinbar zentralen Rolle von MVBs/Endosomen bei der HIV-Freisetzung als auch der Rolle von ESCRT bei deren Bildung.

Table of Contents

List of Figures

List of Tables

Acknowledgements

I wish to thank Jacomine Krijnse-Locker, my irreplaceable supervisor and mentor, for bringing cell biology into my life and for unerringly guiding me through all this. I also wish to thank Hans-Georg Kräusslich, without whom this work could not have been initiated or completed, for offering me the opportunity of carrying out this study and for his invaluable help and guidance.

I want to thank Anja Habermann for sharing her masterly skills in electron microscopy and Stefanie Jäger for great collaboration and continuous critical discussion. Gareth Griffiths, the inexhaustible source of EM knowledge, for sharing his ideas, and Barbara Müller, Oliver Keppler and Oliver Fackler for their active and academic support and for critical discussions.

I wish to thank Bärbel Glass, and Ina Allespach for expertly taking care of all infection experiments. Marko Lampe, Eva Gottwein, Vanda Bartonova, Susanne Rauch and all everyone else at Virology department for being great colleagues. At EMBL, I would like to thank Claude Antony and Uta Haselmann, who run the EM facility, and Daniela Holzer, Mark Kühnel, Birgit Schramm, Antonino Schepis, Wiebke Möbius, Sybille Schleich, Stefan Bohn, Andrea Meiser, Sebastian Schröder and everyone else in the Griffiths group for constant support and for providing a good working atmosphere. Many people shared reagents and antibodies, among them I especially wish to thank Wesley Sundquist, Mark Marsh and Sylvie Urbé.

Mein innigster Dank gilt meinen Eltern, meiner Schwester Annett, und Klaus Greger, für Alles.

Chapter 1

1. Introduction

1.1 Human Immunodeficiency Virus (HIV)

Since the isolation of Human Immunodeficiency Virus (HIV) in 1983, modern antiretroviral drug development has transformed HIV infection into a treatable chronic disease in the developed world. Infection with HIV, the causative agent of Acquired Immune Deficiency Syndrome (AIDS), nevertheless remains a major infectious disease problem that affects over 40 million people worldwide, with an estimated 3 million deaths per year [1]. The course of HIV infection typically starts with acute viral illness, accompanied by loss of T cells, and is followed by development of a specific immune response during which T cell numbers are largely restored. During this second phase, viral load in the blood is controlled by the immune system and patients are generally asymptomatic, but viral replication is not eradicated. As viral replication continues, T cells are progressively destroyed, finally resulting in immune deficiency and the development of AIDS. Introduction of highly active antiretroviral therapy (HAART) has immensely prolonged the asymptomatic phase, but a protective vaccine or an effective way to eliminate HIV from infected individuals is still lacking.

Without doubt future directions of HIV therapy will have to take several recent findings into account. First, it is now becoming clear that the virus interacts with its host in a sophisticated way, both by modulating the hosts' immune response and by misusing host cell factors to complete the viral life cycle. Targeting of cellular proteins that play crucial roles in the HIV replication cycle may allow development of new potent drugs that block HIV replication, but a detailed understanding of the normal cellular functions of such proteins is essential. Second, cellular reservoirs of HIV were found to hamper clearance of HIV from infected individuals. Efficient treatment of HIV infection will depend on detailed knowledge about cellular HIV reservoirs and the mechanisms of virus storage and release.

1.1.1 Taxonomy of HIV

Human Immunodeficiency Virus (HIV) is a member of the Lentiviruses, one of seven genera that belong to the family of *Retroviridae* [2]. Retrovirus genomes are of (+)-sense RNA type and are reverse transcribed into double stranded DNA (dsDNA) by the viral enzyme reverse transcriptase (RT) after virus entry into host cells. This reverse transcription step is a hallmark of retroviral replication [3].

Lentiviruses are subdivided into five groups, each affecting different species. The primate lentivirus group is further subdivided into three subgroups of Immunodeficiency Viruses, HIV-1, HIV-2 and Simian Immunodeficiency Viruses (SIV). HIV-1 is the most extensively studied immunodeficiency virus as over 90% of cases of HIV infection in the developed world are due to HIV-1. Three distinct groups of HIV-1, group M, N and O, which are have emerged from three separate chimpanzee-to-human transmission events, are known [4]. All three groups display diversification into subtypes, but HIV-1 group M is believed to be the main group in the HIV-1 global pandemic. Based on phylogenetic association, it can be subdivided into multiple groups or subtypes. Furthermore, recombination of various group M strains constantly gives rise to circulating recombinant forms, with different geographic distributions. Thus, most HIV-1 laboratory strains are derived from group M isolates.

1.1.2 HIV structure and genome

Infectious HIV-1 virions are spherically shaped, enveloped particles with a mean diameter of 125 nm (Figure 1 and [5]). Virus particles are enveloped by a cellular membrane that is acquired during the process of virus budding from infected cells and contain a characteristic cone-shaped core that encases the viral RNA genome and proteins that are required for viral replication. Two copies of the HIV-1 genome are packaged into each infectious viral particle. This RNA genome encodes for nine proteins: the structural proteins Gag, Gag-Pol and Env, two regulatory proteins Tat and Rev, and the accessory proteins Vpu, Vpr, Vif and Nef (Figure 2 and [2]).

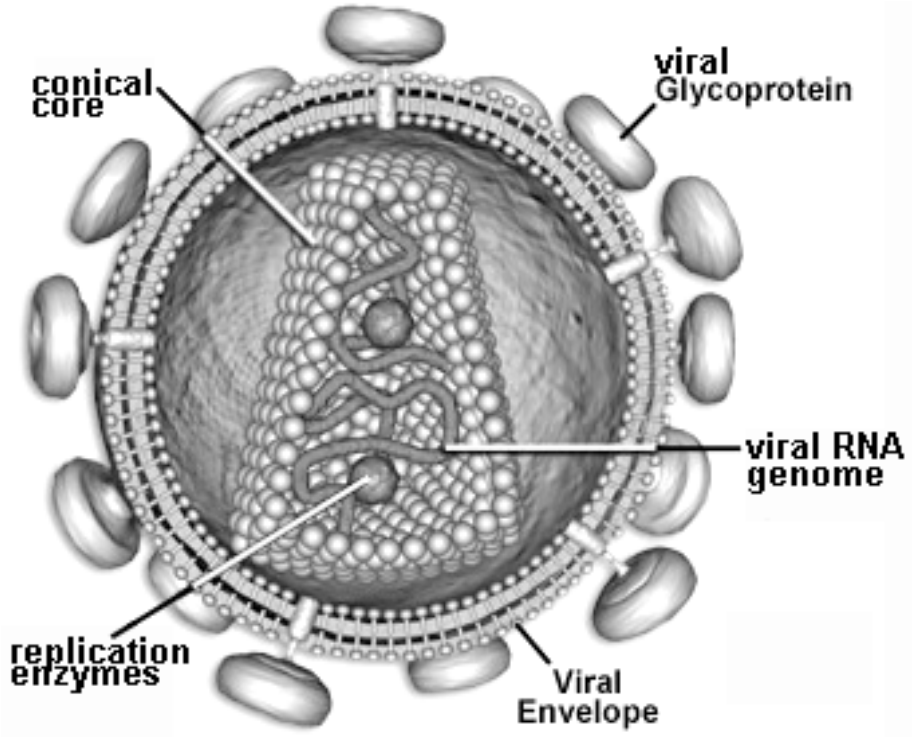

Figure 1: Structure of an HIV-1 particle.
Enveloped mature HIV-1 particles have a mean diameter of 125nm. The viral envelope consists of a cellular membrane with the incorporated viral Env glycoprotein. The envelope encases a conical proteinacious core, which harbors two copies of the viral genome and viral enzymes. Adapted from Molecular Expressions™ Images from the Microscope, National High Magnetic Field Laboratory, Florida State University, Tallahassee, Florida, USA.

The 9.3 kilobase (kb) RNA genome of HIV-1 is of (+)-strand polarity and is flanked by short repeats at both ends (U3 and U5, see Figure 2). Upon infection of a host cell, the RNA genome is reverse transcribed into dsDNA by the action of the viral reverse transcriptase (RT) enzyme. During reverse transcription, U3 and U5 are duplicated, giving rise to the long terminal repeats (LTRs, figure 2). Subsequent integration of the viral DNA into the host cell genome generates the 'provirus', the integrated form of HIV-1. Transcription of the proviral genome is controlled by a single promoter in the viral 5'-LTR and generates an approximately 9 kb primary transcript that has the potential to encode all nine HIV genes.

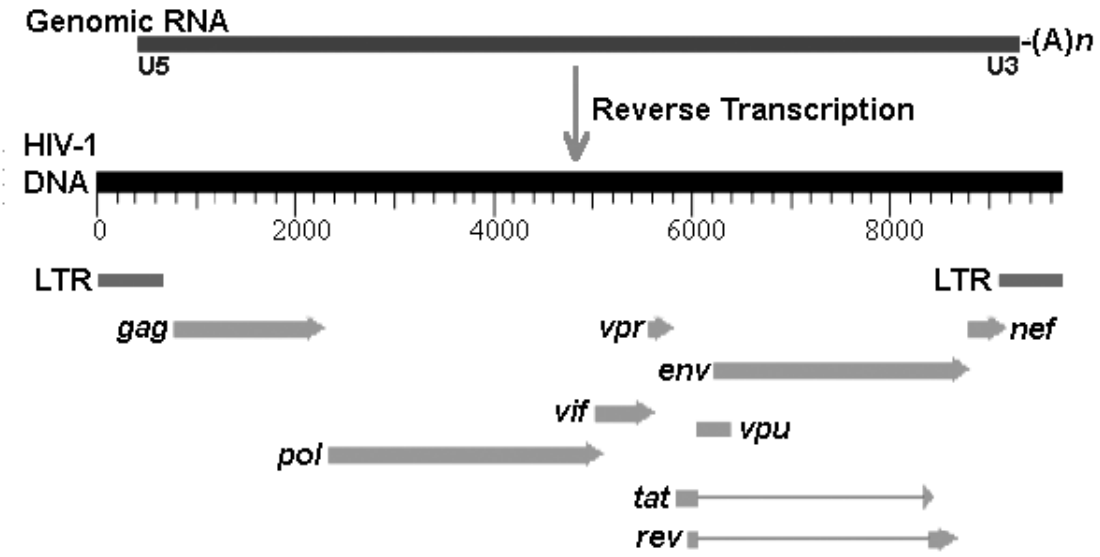

Figure 2: Genome organization of HIV-1.
The HIV-1 genomic RNA is reverse transcribed into dsDNA, which is inserted in the cellular genome, giving rise to the integrated provirus. Transcription from proviral DNA gives rise to viral transcripts encoding for nine viral proteins (see text for details). Adapted from web-books.com/MoBio.

The primary HIV-1 transcript is either packaged without further modification into virus particles, where it serves as the viral RNA genome or serves as an mRNA template for the synthesis of viral proteins (see section 1.1.4).

1.1.3 HIV proteins and their functions

HIV-1 Gag is the major structural protein of HIV-1 and is thus the determining factor for virus particle structure and shape. It is expressed as a 55kDa precursor polyprotein that is cleaved during viral maturation by the viral protease (PR, see below) into the proteins matrix (MA), capsid (CA), nucleocapsid (NC), p6 and two spacer peptides, sp1 and sp2 ([6] and figure 3).

Figure 3: Schematic model of the domains in HIV-1 Gag.
HIV-1 Gag is expressed as a polyprotein which is cleaved upon virus release into the Gag domains MA matrix, CA Capsid, NC Nucleocapsid, and two spacer peptides sp1, sp2.

HIV-1 Gag assembly at cellular membranes is the driving force for virus production, and Gag alone is sufficient for the formation of virus-like particles (VLPs) on cellular membranes [7]. Gag membrane association is mediated by MA, which is derived from the myristoylated N-terminus of Gag [8]. It binds to membranes via myristate and a basic cluster motif near its N-terminus. MA is thus associated with the envelope of budding virus particles, and its insertion into the virions' lipid bilayer stabilizes the immature particle [9]. The CA and NC domains mediate Gag-Gag interactions and oligomerization. Furthermore, NC has nucleic acid binding properties and is thus responsible for incorporation of the viral genome into particles [10]. The p6 domain of HIV Gag is crucial for HIV release. It carries two highly conserved motifs, the so-called late domain (L domain) motifs, which are required for the final membrane fission event during HIV release. Deletion of either of the two L domains in p6 inhibits binding to cellular proteins that are involved in endosomal protein sorting and recycling (see below) and blocks HIV release [11].

A ribosomal –1 frameshift at the C terminus of the *gag* reading frame occurs in about one in twenty of all Gag translation events and leads to the expression of a Gag-Pol fusion polyprotein. HIV-1 Pol encodes for the viral Protease (PR), reverse transcriptase (RT), RNAseH and integrase (IN). Dimerization of Gag-Pol molecules upon viral assembly leads to activation of PR, resulting in autocatalytic PR cleavage away from Gag-Pol. PR the catalyses cleavage of Gag and Gag-Pol into the above-mentioned proteins.

The glycoprotein Env is the only viral protein that is stably inserted into the envelope of mature virus particles. It consists of two glycoprotein (gp) domains, gp41 and gp120, which are generated from a gp160 precursor protein after cleavage by the cellular furin protease. The gp41 moiety contains the transmembrane domain of Env, while gp120 is located on the surface of the virion through non-covalent interactions with gp41; Env mediates CD4 virus receptor binding on the cellular surface and fusion of the viral membrane with the plasma membrane of the target cell. Thus, expression of Env on the surface of infected cells can lead to plasma membrane fusion with an adjacent cell bearing CD4, a process that leads to syncytium formation.

The regulatory proteins Tat and Rev are RNA-binding proteins that bind to viral transcripts in a sequence-specific manner. Tat is a transcriptional transactivator that facilitates elongation of viral transcripts by binding to a transactivation response

element (TAR), whereas Rev facilitates nuclear export of intron-containing viral DNA by binding to a secondary RNA structure, the Rev response element (RRE).

The accessory proteins of HIV-1, Nef, Vif, Vpr and Vpu are not absolutely required for HIV-1 replication in most cell types, but they play multiple roles as virulence factors in the viral life cycle (see table 1).

HIV-1 gene product		function(s)
Tat	Transcriptional activator	Binds TAR on viral RNA transcripts, enhances transcription from viral promoter/ RNA-Polymerase II elongation
Rev	Regulator of viral gene expression	Binds RRE on viral RNA, inhibits viral RNA splicing, promotes nuclear export of incompletely spliced viral RNA transcripts
Nef	'Negative effector'	down-regulates cell surface CD4 and MHC class I molecules, enhances virion infectivity, alters state of cellular activation
Vif	Viral infectivity factor	overcomes inhibitory effect of unknown host factor, stabilizes RT complexes
Vpr	Viral protein R	promotes cell cycles arrest, facilitates infection of nondividing cells/ nuclear import of viral genome
Vpu	Viral protein U	promotes CD4 degradation, influences virion release

Table 1. The functions for HIV-1 regulatory and accessory proteins in the viral replication cycle.

1.1.4 The HIV-1 replication cycle

HIV infection begins with binding of the gp120 domain of Env to the CD4 receptor on the plasma membrane of a host cell, followed by binding to a chemokine co-receptor. HIV-1 most commonly uses either of the co-receptors CXCR4 or CCR5, and thus virus strains are classified as either CXCR4-using (X4), CCR5-using (R5), or R5X4 strains (which can use both co-receptors), capable of infecting T cells or macrophages, respectively ([12] and below). Co-receptor binding leads to a conformational change in the gp41 transmembrane domain of Env, which allows fusion of the viral envelope with the plasma membrane or endosomal membranes of the host cell [13]. Consequently, the virus core is released into the cytoplasm, leaving the viral membrane and envelope proteins behind on the outer surface of the cell.

Once inside the cell, the core is uncoated in a mechanism that is poorly understood, and the viral nucleoprotein complex (composed of RNA and the viral enzymes RT, IN and RNAseH) is released. Catalyzed by RT, the RNA genome is reverse transcribed into DNA and enters the host cell nucleus as a component of the pre-integration complex, composed of IN, RT, MA, Vpr and at least one host cell protein. In contrast to other lentiviruses, HIV-1 is able to translocate its genome across intact nuclear envelopes (see for instance[14]). By the catalytic action of IN, the viral DNA is then integrated into the host cell genome; the integrated form of the HIV genome, the so-called 'provirus', can persist latently for long periods in resting cells. Activation of the host cell results in the transcription of viral DNA into a single mRNA transcript. In the early stages of gene expression, this transcript is multiply spliced, giving rise to mRNA templates for the early viral genes *tat*, *rev* and *nef*. The fully spliced transcripts of the early genes are exported into the cytoplasm, whereas the incompletely or unspliced viral transcripts of all other viral genes are retained in the nucleus. Their export depends on expression of the viral protein Rev, which binds to the Rev-responsive element (RRE) on incompletely spliced RNAs and channels these into the CRM1-dependent nuclear export pathway [15]. Once the transcripts of late genes *gag*, *pol*, *env*, *vif*, *vpu* and *vpr* are exported, the proteins are expressed in the cytoplasm. The Env glycoprotein precursor is synthesized on ER-associated ribosomes and undergoes modifications such as glycosylation and folding in the secretory pathway. Gag and Gag-Pol are translated on free ribosomes in the cytoplasm, from where they are targeted to the virus assembly site.

Gag assembles together with the other viral proteins and two copies of the RNA genome at a cellular membrane, where the virus then buds away from the cytoplasm. A final membrane scission event leads to release of immature virus particles [9]. Immediately after or during release, the viral PR catalyzes self-proteolysis from the Gag-Pol precursor and cleaves packaged polyproteins, which leads to major protein rearrangements in the virus and condensation of the conical core. This process is called maturation and gives rise to fully infectious, mature HIV-1 particles. A schematic overview of the HIV-1 life cycle is given in Figure 4.

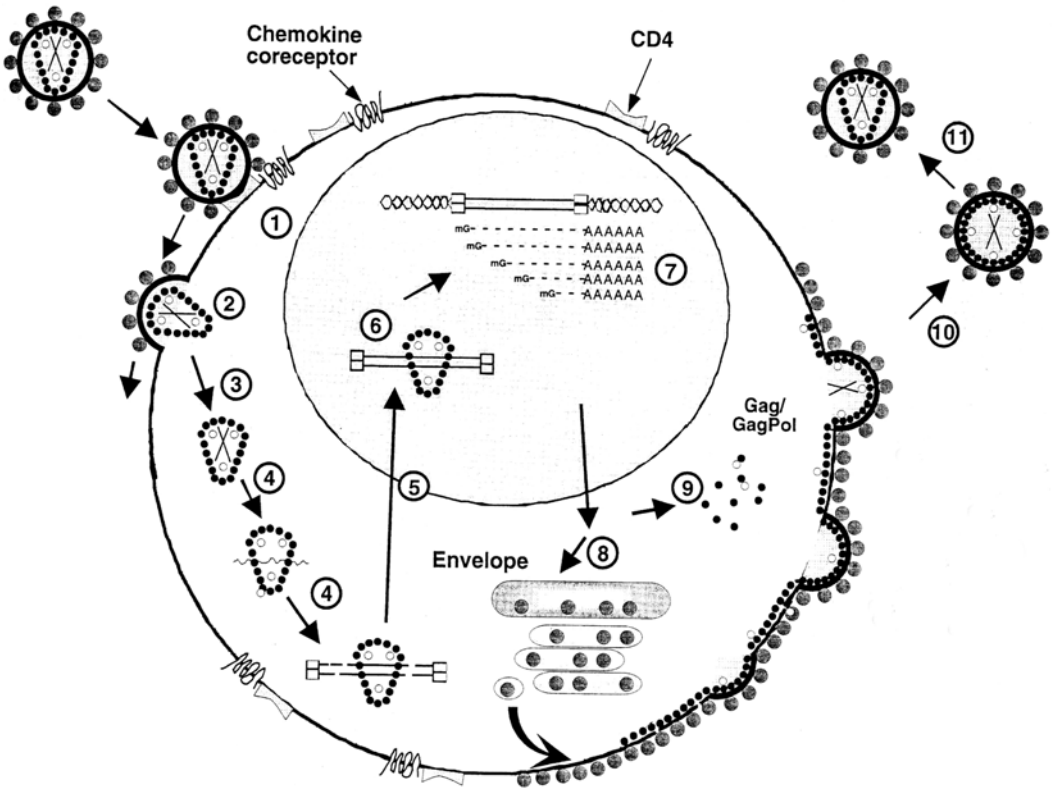

Figure 4: The HIV-1 replication cycle in T cells.
HIV-1 infection starts with the interaction of virus particles with the CD4 receptor and chemokine co-receptor (1), followed by fusion of viral and cellular membranes (2) and release of the viral core into the cytoplasm (3). Reverse transcription of the viral RNA genome occurs within subviral particles in the cytoplasm (4) and the double stranded DNA transcript is translocated into the nucleus (5) where it is integrated into the cellular genome (6). Integrated provirus serves as a template for synthesis of viral RNA transcripts (7), which are translated into proteins in the cytoplasm (8, 9). The viral Env protein (8) and Gag/Pol polyproteins (9) are transported via independent pathways to the plasma membrane. Virus particles assemble and bud from the plasma membrane and are released as immature particles (10). Subsequent proteolysis of viral proteins generates mature infectious particles (11). Modified from [16] Chapter 59: HIVs and their replication.

1.1.5 HIV-1 budding and release

Like most enveloped viruses, HIV-1 is released from infected cells via budding at a cellular membrane (Figure 4, steps 9-11), which in most cell lines was shown to be the plasma membrane. The essential steps preceding viral budding are targeting of Gag to and formation of assembly complexes at the plasma membrane. How the Gag protein, after its synthesis on free ribosomes in the cytoplasm, is targeted to the plasma membrane is not entirely clear, but it was recently

hypothesized that Gag assembles on endosomes and traffics through the endosomal sorting pathway prior to virus assembly at the cell surface (see for instance [17]). Cellular proteins that are involved in endosomal protein sorting and recycling were shown to bind HIV Gag and to be part of viral assembly complexes on the plasma membrane (see below). Formation of assembly complexes initiates the 'late' stages of HIV release: membrane curvature, formation of viral buds and the final active membrane fission event that leads to the release of virus particles [11].

The preferred site of HIV release from infected cells is discussed with some controversy: it is well established that HIV-1 buds from the surface of many cell lines including monocytic cells [18, 19], and it is generally believed that the virus buds exclusively from the plasma membrane of primary T lymphocytes. The site of HIV assembly and release in primary macrophages is, however, less well defined. Assembly and budding of HIV in monocytes and *in vitro* differentiated, monocyte-derived macrophages has been addressed in various electron microscopy (EM) studies [18, 20-30]. Early ultrastructural studies showed budding from plasma membrane derived pseudopods [30] or the accumulation in and budding into cytoplasmic vacuolar structures that seemed to be part of the Golgi complex [20, 24]. Recent data suggested that these cytoplasmic vacuolar structures are of late endocytic origin [28, 29]. This was based on the observation that viruses collected inside large membrane-bounded vacuoles and acquired late endosomal proteins such as CD63, lamp-1 as well as major histocompatibility class II (MHC II) molecules. EM images also suggested that the virus-filled vacuoles sometimes released their viral content into the extracellular environment in an exosome-like fashion [28] (for a definition of 'exosome', see section 1.4). Based on these observations it therefore seemed reasonable to propose that in macrophages the virus budded and accumulated in late endosomes. Upon certain stimuli, for instance contact with T cells, these viruses could then be released from endosomes into the extracellular environment [31]. This scenario also fitted the proposal that macrophages may constitute a reservoir of infectious HIV-1 (see below). However, *in vivo* this model has not been proven yet.

1.2 HIV-1 susceptible cells

HIV-1 infects cells of the immune system, namely CD4 positive T lymphocytes (CD4+ T cells), macrophages and dendritic cells (DCs). Like all cells of the vertebrate immune system, they originate in the bone marrow, where common lymphoid and common myeloid progenitor cells are produced upon division of hematopoietic stem cells [32].

T lymphocytes bear antigen-specific receptors, the so-called T cell receptors (TCRs) and either of the two co-receptors CD4 or CD8. Naïve T cells travel with the blood stream to the peripheral lymph nodes, where they recognize and bind antigen that is presented via MHC II molecules on the surface of DCs. If naïve CD4+ T cells encounter their specific antigen, they become activated, resulting in proliferation and differentiation into armed effector T cells, which re-enter the blood stream and activate macrophages or B lymphocytes displaying specific antigen. Activation of macrophages and B cells in turn leads to efficient degradation of ingested pathogens and production of pathogen-specific antibodies, respectively.

Monocytes traveling through the bloodstream either differentiate into phagocytic macrophages upon entering tissues or develop into precursor DCs. Precursor DCs differentiate into highly phagocytic immature DCs upon entering peripheral tissues and efficiently take up pathogens, such as viruses, by macropinocytosis. This results in activation and maturation of DCs into professional antigen-presenting cells (APCs), presenting antigen to CD4+ T cells via MHC II molecules. Thus, DCs are APCs that induce the first line of adaptive immune response. Phagocytic macrophages bind pathogens via surface receptors, resulting in macrophage activation, phagocytic uptake of the pathogen and its lysosomal degradation. Macrophages also act as APCs and present antigen together with co-stimulatory molecules on their surface, resulting in activation of CD4+ T cells and induction of an adaptive immune response.

1.2.1 Role of T cells, DCs and macrophages in HIV-1 infection

As CD4 is the primary receptor for HIV binding to the cell surface, CD4+ T cells are major targets of HIV. Early in the course of infection, most HIV replication is believed to take place in activated, proliferating CD4+ T cells and thus T cells account for the major population of newly made virus in infected individuals. Resting

T cells (that do not support HIV replication) may, however, play an important role in the persistence of the virus [33]. As the average half-life of productively infected T cells is only about two days, the number of T cells profoundly decreases during the course of HIV infection, finally leading to a failure of immune response.

The role of DCs in HIV infection is poorly understood. As they express moderate amounts of CD4 on their surface, HIV can enter DCs, but it is not entirely clear if DCs can be productively infected with HIV-1. It has been shown that the HIV glycoprotein can bind to DCs via the cell surface molecule DC-SIGN and that this interaction leads to viral uptake of virus into a mildly endocytic compartment that may serve as a viral storage compartment. It was shown that virions are released from DCs and transmitted to T cells upon contact via 'virological synapses' (reviewed in [34]). This argues for a model in which DCs play a dual role: first, transmission of endocytosed infectious HIV-1 to T lymphocytes and second, activation of the same T cells by presenting viral antigen [35, 36].

Macrophages are, besides CD4+ T cells, the major target for HIV-1 infection [37]. It was shown that HIV is able to replicate in macrophages, although fully differentiated macrophages do not undergo mitosis. During initial infection, macrophages are believed to be among the first cells targeted by HIV and they may contribute to HIV infection in several ways: First, macrophages are less susceptible to the cytopathic effects of HIV and more resistant to HIV-induced apoptosis compared to T cells. This allows infected macrophages to survive over long periods of infection [38, 39] and thus they contribute significantly to persistence of infection. Second, ultrastructural analysis of HIV-1-infected monocytes and macrophages showed the presence of virions in intracellular vacuoles [22, 26, 28, 29]. Whether these viruses accumulate upon *de novo* replication or, at least partially, represent endocytosed virus is not entirely clear. In both cases, this intracellular virus-containing compartment may provide a cellular reservoir of infectious HIV, which is protected from the hosts' immune system. Third, as HIV-infected macrophages potentially encounter and activate T lymphocytes in lymphoid tissues, reverse signaling from the T cell to the infected macrophage may induce directed release of virus particles onto T cells and thereby support viral spread.

1.3 The ESCRT protein complex

Endosomal Sorting Complex Required for Transport (ESCRT) is a multiprotein complex that was originally identified in yeast. Genetic studies in *Saccharomyces cerevisiae* identified over 40 vacuolar protein sorting (Vps) factors [40-43], 18 of which were classified as class E Vps factors. Yeast mutant strains defective for one of these class E Vps proteins display enlarged, aberrant endosomal structures, the so-called 'class E compartment', and defects in protein sorting to the vacuole [44]. In yeast, ESCRT functions in the sorting of mono-ubiquitinylated proteins to the vacuole and is involved in formation of the intra-lumenal vacuolar vesicles to which ubiquitinylated proteins are targeted for degradation. Some class E Vps factors, such as Vps27, Vps31 and Vps4 were not found to be part of ESCRT, but are additionally required for ESCRT function [45-47].

ESCRT is highly conserved from yeast to human, and mammalian homologs of all known yeast class E Vps proteins have been identified [48-50]. Compared to yeast, some Vps proteins have up to four isoforms in human cells, and the complex is therefore composed of at least 19 subunits [50, 51]. The class E Vps factors allocated to ESCRT were further subdivided into the three subcomplexes ESCRT-I, -II and –III [52-55]. It is believed that these subcomplexes are recruited to membranes in a sequential manner.

Many of the initial findings in yeast have recently been confirmed in mammalian cells. A now well-established function of ESCRT in mammalian cells is the down-regulation of cell surface receptors. As in yeast, human ESCRT was shown to mediate targeting of cell surface receptors to the intra-lumenal vesicles of multi-vesicular endosomes (MVEs) or multivesicular bodies (MVBs), from where the receptors are transported into lysosomes for degradation. Ubiquitination of cell surface receptors is an important sorting signal into this pathway, and at least three ESCRT proteins were shown to have ubiquitin-binding activity (Figure 5 and [56-58], reviewed in [59]). Furthermore, ESCRT is believed to be responsible for the formation of intralumenal MVB vesicles, and mutation of mammalian class E Vps proteins results in the formation of an aberrant endosomal compartment, similar to the class E compartment of yeast [60]. Thus, interaction with (endosomal) membranes is a crucial factor in the well-established functions of mammalian ESCRT. However, sequence analysis of ESCRT proteins showed that ESCRT subunits have no

membrane-spanning domains and, with the exception of Hrs, none of the ESCRT proteins is currently known to be capable of membrane association [61]. Previous studies suggested that ESCRT proteins were mostly cytosolic, but such localization studies were mostly based on fluorescence microscopy of overexpressed proteins and ultrastructural data on ESCRT localization were missing until the onset of this study. Furthermore, despite extensive data on protein-protein interactions of class E Vps factors, the function of the entire ESCRT protein network in eukaryotic cells is not completely understood. It is not clear why human cells have additional Vps protein isoforms and, because of its higher complexity, it is likely that ESCRT has additional functions, which may be related to the endocytic pathway, in higher eukaryotes.

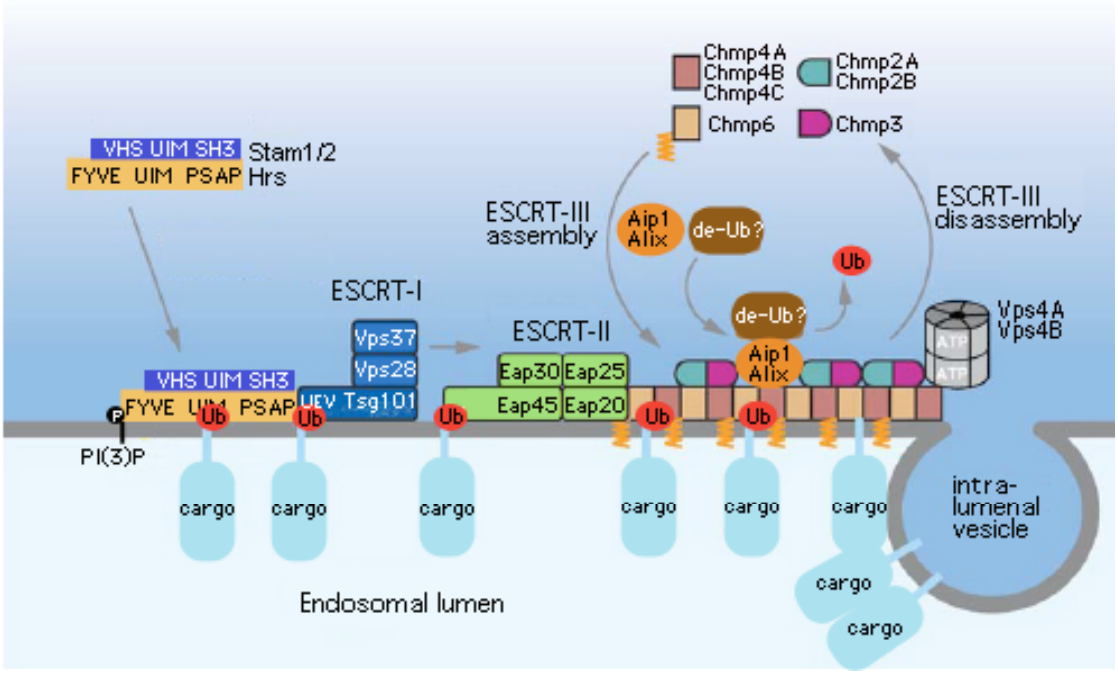

Figure 5: The human ESCRT complexes in endosomal sorting.
The Hrs protein is targeted to endosomal membranes via its FYVE domain that binds PI(3)P, and its UIM domains, which bind ubiquitinated cargo. Hrs subsequently binds and activates the ESCRT-I complex via the PSAP motif in its C-terminal domain that also interacts with Tsg101 in ESCRT-I. Ubiquitinated cargo is recognized by ESCRT-I via the UEV domain of TSG101 and by ESCRT-II (presumably via EAP45). ESCRT-III coordinates the association of accessory factors such as Aip1/Alix and hypothetical deubiquinating enzymes that remove ubiquitin from cargo. The AAA-type ATPases Vps4A and Vps4B catalyze the dissociation of ESCRT complexes. Together, these complexes appear to direct formation of intralumenal endosomal vesicles and vesicle fission. This speculative model is based on potential similarities between endosomal vesicle formation in yeast and human. Abbreviations: de-Ub, deubiquitinating enzyme; Ub, ubiquitin. Adapted from [46].

1.3.1 The ESCRT proteins Hrs, Tsg101, Aip1/Alix and Vps4

Within this work, four subunits of the ESCRT machinery were studied in detail. First, hepatocyte growth factor-regulated tyrosine kinase substrate (Hrs, Vps27 in yeast). Second, tumor susceptibility gene 101 protein (Tsg101, Vps23 in yeast). Third, ALG-2 interacting protein 1/ ALG-2 interacting protein X (Aip1/Alix, Vps31 in yeast) and fourth, the AAA-type ATPase Vps 4B (Vps4 in yeast). Although only Tsg101 is currently classified as a *bona fide* ESCRT component, all four proteins were shown to be required for ESCRT function in mammalian cells.

Hrs binds to membranes via a FYVE domain capable of binding to phospholipids and two coiled-coil domains that mediate membrane association. Furthermore, Hrs binds ubiquitinated cargo protein through a ubiquitin-interaction motif (UIM) and forms a complex with the ubiquitin-binding proteins STAM1, STAM2 and the endocytic regulator Eps15 [62]. This complex is often referred to as ESCRT-0. It functions in recruiting mono-ubiquitynated cargo onto (endosomal) membranes and delivering it to the ESCRT-I component Tsg101. Tsg101 binds ubiquitinated cargo via its E2 ubiquitin-conjugating domain and recruits other ESCRT-I components onto endosomal membranes. This is followed by recruitment of the ESCRT-II and-III complexes and their associated proteins. The ESCRT-associated class E Vps factor Aip1/Alix was shown to bind both Tsg101 and ESCRT-III subunits and thus serves as a bridging molecule between ESCRT-I and -III [50]. Finally, the ATPase activities of Vps4A and 4B were shown to be required for ESCRT function, presumably by disassembling ESCRT complexes and recycling them for further rounds of protein sorting [60, 63].

1.3.2 ESCRT function in HIV-1 budding and release

Budding of HIV-1 away from the cytoplasm mechanistically resembles the formation of intra-lumenal endosomal vesicles, consistent with a role for ESCRT in both processes. Recent literature shows that egress of several enveloped viruses, including HIV-1, depends on interaction with functional ESCRT complexes [11, 64-66]. In the case of HIV-1, two highly conserved motifs within the p6 region of Gag were shown to bind class E Vps proteins [67, 68]. These short amino acid sequences, a PTAP motif binding to Tsg101 and a LXXLF motif (with X being any amino acid) binding to Aip1/Alix, are referred to as late domain (L domain) sequences, since

mutations in these sequences have been shown to play a critical role in the late steps of the HIV-1 replication cycle [65, 66, 69]. Specifically, binding of L domains to Tsg101 as well as to the ESCRT-associated protein Aip1/Alix was shown to be essential for efficient virus release [19, 50, 68, 70], and abrogation of L domain binding leads to retention of virus buds on the plasma membrane. In analogy with ESCRT-mediated sorting of ubiquitinated cell surface receptors, ubiquitination was shown to play a role in the release of HIV-1 and other enveloped viruses that utilize a PTAP L domain for ESCRT binding. HIV-1 Gag is ubiquitinated at multiple sites and it was shown that ubiquitin is required for the release of HIV-1 [71, 72]. Recent data showed that the MA, CA, sp2, NC and p6 domains of HIV-1 Gag are ubiquitinated, and mutation of multiple ubiquitination sites in these Gag domains dramatically interfered with HIV-1 release [73], confirming the functional relevance of Gag ubiquitination.

Since HIV-1 release at the plasma membrane depends on ESCRT, it has been proposed that HIV-1 Gag actively recruits ESCRT to its site of budding. The latter idea was supported by immunofluorescence analyses, showing that overexpression of Gag results in the recruitment of ESCRT to the site of Gag accumulation [69, 74]. However, the latter studies did not analyze the localization of endogenous ESCRT proteins under HIV-1 infection conditions in detail, and a direct quantitative comparison of ESCRT localization in HIV-infected and uninfected cells has not been done before the onset of this work.

1.4 The endocytic pathway

The cellular endocytic pathway functions in uptake of extracellular material such as proteins and lipids, its intracellular sorting and transport as well as in recycling and degradation of endocytosed material. This function is carried out by a morphologically complex network of membrane-bounded endocytic structures, distributed through the peripheral and perinuclear regions of the cytoplasm [75]. A simplified classification of endocytic structures found in any vertebrate cell distinguishes four types of structures: primary endocytic vesicles, early endosomes (EEs), late endosomes (LEs) and lysosomes (Figure 6). However, the endocytic pathway comprises a sophisticated network of vacuoles, tubules and vesicles that can

differ significantly between cell types [76, 77]. The classification of early and late endocytic structures is generally based on detailed pulse-chase EM analyses with fluid phase markers (see below) and on immuno-EM labelings with antibodies against endosomal proteins.

Endocytic uptake of material at the plasma membrane is often initiated by stimulation of cell surface receptors, followed by receptor-mediated endocytosis. This process involves invagination of specialized areas of the cell surface and subsequent formation of small intracellular vesicles carrying internalized transmembrane or lumenal cargo. Many of these small endocytic vesicles are encased by a proteinacious coat that assembles from cytosolic proteins that are recruited to the plasma membrane. A key component of this protein coat is clathrin, which, in association with adaptor protein 2 (AP2), drives endocytic vesicle formation at the cell surface [78]. Other coat complexes that mediate clathrin-independent endocytosis have been identified and their number is still growing [79-81]. One important example of clathrin-independent uptake is fluid-phase endocytosis, an uptake mechanism that can occur constitutively without receptor stimulation. Constitutive fluid phase endocytosis and receptor-mediated endocytosis originate from different plasma membrane regions, and thus fluid phase uptake gives rise to a different set of (non-coated) early endocytic vesicles.

It is generally believed that both clathrin-coated and non-clathrin vesicles enter the same endocytic pathway at the level of EEs, although examples of convergence of the two systems at later steps of the endocytic pathway have been reported [82, 83]. Transport of endocytosed material is regulated by a complex molecular machinery, which delivers endocytic cargo into early endosomes (EEs) and transports it into a tubulo-vesicular compartment that is defined as the sorting endosome. From the sorting endosome, cargo is either recycled back to the plasma membrane (generally referred to as the ‘default pathway’) or transported to late endosomes (LEs) and then to lysosomes for degradation. Whether transport from EEs to LEs involves maturation of EEs or occurs via vesicular intermediates (similar to transport mechanisms within the secretory pathway) is not entirely clear, but computational three-dimensional analysis of serial cell sections revealed the existence of discrete endocytic vesicles without membrane continuity to other endocytic structures [84]. In favor of the latter mechanism is the finding that, upon blocking

dynein function and therefore directed movement of endocytic vesicles, endocytosed material accumulates in a distinct spherical endocytic compartment containing multiple internal vesicles and never reaches LEs [85, 86]. It was therefore postulated that this compartment, which morphologically resembles MVBs (which they termed endosomal carrier vesicles or ECVs), was the carrier vesicle mediating transport along microtubules from peripheral EEs to more perinuclear located LEs (Figure 6). The idea that ECVs or MVBs are intermediates between EEs and LEs is substantiated by uptake experiments of fluid phase markers, showing that MVBs are filled with such markers before LEs (see, for instance, section 3.1.2).

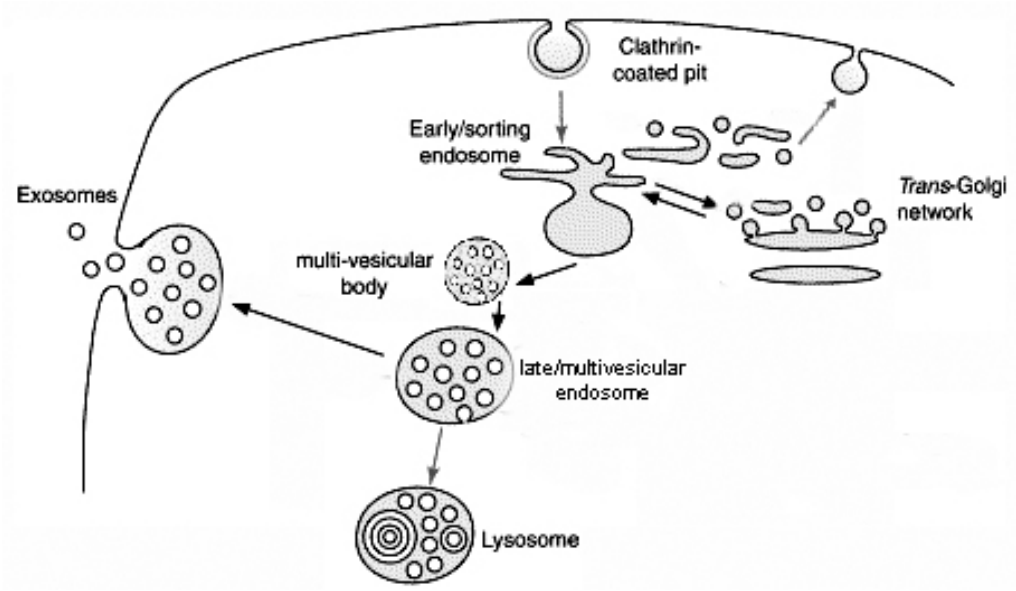

Figure 6: Overview of the endocytic pathway.
For details, see text. Adapted from [87].

With the discovery of ESCRT, the biogenesis of MVBs or multivesicular endosomes (MVEs) has gained much attention; it is now generally believed that endosomal cargo destined for degradation first localizes to the limiting membrane of MVBs/ MVEs, but is then sorted into its internal vesicles. This process seems to be ESCRT-dependent, and ubiquitination may provide a general sorting signal for cargo entry into MVBs/ MVEs (see above). ESCRT has furthermore been linked to the formation of the internal vesicles of MVBs and MVEs [88, 89]. As is clear from the above, the term ‘MVB’ and ‘MVE’ are generally used indiscriminately in the ESCRT literature, suggesting that these represent the same structures. However, throughout

this study we defined MVBs as an intermediate compartment between EEs and LEs that contains multiple internal vesicles and that has a distinct spherical shape and size. This is based predominantly on the fact that MVBs take up fluid phase markers before LEs/MVEs. Furthermore, MVBs generally display low labeling for typical late endosomal proteins that are abundantly found on MVEs/LEs.

In some cell types such as professional APCs, MVBs can serve as an intermediate storage compartment, from which intralumenal vesicles can be released into the extracellular space upon fusion of the limiting MVB membrane with the plasma membrane. The released vesicles are termed exosomes, and the limiting membrane of these 40-100nm exosomes was shown to be specifically enriched in MHC II molecules, which are typical for the late endocytic compartment of APCs [90].

1.4.1 EM analysis of the endocytic pathway

The endocytic pathways of different cell types vary greatly, both morphologically and functionally. This reflects the different functions of cells, as professional APCs, for instance, are specialized in processing and presenting antigen and are therefore equipped with a complex and extended endocytic system. This cell-type dependent complexity and diversity of endocytic compartments requires reliable assays to discriminate, at least roughly, different endocytic compartments. Immuno-electron microscopy (EM) using antibodies against established endosomal marker proteins may in some cases not be sufficient since such marker proteins can show cell type dependent differences in their localization ([91], see also section 3.1.2). Endocytic uptake of electron dense material into cells prior to their processing for EM is thus a more reliable method for studying endocytic compartments (see, for instance, [92, 93]).

To study the endocytic pathway by EM, various endocytic tracer molecules can be used. Useful molecules have in common that they are electron dense (or specifically form electron dense reaction products) and are not membrane permeable. Gold particles are widely used for localizing cell components with a variety of immunocytochemical techniques, because they can easily be visualized in biological specimens by various microscopic methods. The particulate nature and electron density of gold particles allows their simple visualization on thin sections by electron

microscopy, and gold particles can be prepared with defined diameters and narrow variation in particle size. Colloidal gold particles associate with a wide range of organic compounds such as bovine serum albumin (BSA), immunoglobulins (Ig) or protein A [94]. Conjugates such as BSA coupled to gold particles (BSA gold) are especially suitable for uptake by fluid phase endocytosis, as BSA gold is readily taken up into endosomal compartments of endocytically active cells. In ultrathin sections of such cells, the BSA-gold content of endocytic compartments allows simple and rapid identification of endosomes without any additional contrasting techniques. The progression of gold particles through the endocytic pathway can be studied in pulse-chase experiments and by sequential endocytosis of gold particles with different diameters. This allows specifying the endocytic pathway by morphology and tracer uptake kinetics. Combined pulse-chase and immuno-EM experiments with antibodies to established endosomal markers allow the detailed localization of an antigen throughout the endocytic pathway.

1.5 Aim of this work

This work aimed at addressing two topics related to HIV-1 budding and release.

First, we wanted to study the subcellular localization of the ESCRT protein complex, which was recently found to be essential for HIV release from infected cells. The aim was to gain insight into the normal localization and function of ESCRT in HIV-susceptible cells and to test if the ESCRT protein complex was relocalized to the site of HIV budding upon infection. A direct approach to address these questions is studying the localization of endogenous ESCRT subunits in HIV-1 susceptible cells by electron microscopy (EM). Within the first part of this work, subunits the cellular ESCRT protein complex were localized in great detail by immuno-EM in HIV-infected and uninfected human T cells and macrophages.

Second, we wanted to determine the site of HIV-1 budding and release in macrophages. The aim was to examine in detail if HIV-1 particles were released into an intracellular, endosomal compartment (as recently suggested) or from the cell surface (as in T cells). The most direct approach to address this question is the analysis of HIV-infected primary human macrophages by EM. Thus, we used EM to

study the morphology of primary macrophages and to determine the site of HIV budding and release in these cells.

Chapter 2

2. Materials and Methods

2.1 Buffers and solutions

2.1.1 Electron and light microscopy

0.4M PHEM, pH 6.9	240mM PIPES, 100mM HEPES, 8mM $MgCl_2$, 40mM EGTA; pH 6.9 adjusted with KOH
0.4M Sodium Cacodylate buffer, pH 7.2	8.56g Sodium Cacodylate ad 100ml; pH 7.2 adjusted with HCl
immuno-EM fixative I	4% PFA, 0.1 GA in 0.1M PHEM (pH 6.9)
immuno-EM fixative II	4% PFA in 0.1M PHEM (pH6.9)
immuno-EM pickup solution	2.3M sucrose, 2% methyl cellulose; mixed 1+1
grid coating solution	1% Formvar in chloroform
EPON embedding mixture, medium hardness	10 ml solution A, 10 ml solution B, 300µl DMP-30
EPON fixative I	2.5% glutaraldehyde (GA) in 0.1M sodium cacodylate buffer, pH 7.2
EPON fixative II	2% osmium tetroxide in 0.1M sodium cacodylate buffer, pH 7.2
EPON embedding solution A	50ml DDSA, 31ml glycid ether
EPON embedding solution B	44.5ml MNA, 50ml glycid ether
Fixative for immunofluorescence (IF)	4% PFA in PBS
IF blocking solution	5% FCS, 50mM glycine, in PBS
IF permeabilization solution	0.5% Triton-X100 in PBS

IF/ EM wash solution	50mM glycine in PBS
immuno-EM blocking solution (PBG)	1% fish skin gelatin, 0.8% BSA, 50mM glycine in PBS
Reynold's lead citrate stain	0.44g lead nitrate, 0.55g sodium nitrate in 10 ml freshly boiled double-dH_2O, pH12 (adjusted with 1N KOH)

2.1.2 Cell culture and biochemical assays

12x SDS-PAGE stacking gel buffer	1.5M Tris (pH 6.8), 0.4% SDS
3x SDS-PAGE sample buffer	187.5mM Tris (pH 6.8), 6% SDS, 30% glycerol, 0.003% bromophenol blue, 15% β-mercaptoethanol
8x SDS-PAGE running gel buffer	3M Tris (pH 8.8), 0.4% SDS
hypotonic buffer	10mM Tris (pH 8.0), 1mM $MgCl_2$
PBMC wash buffer	PBS, 2mM EDTA, 0.5% FCS
PBS	140mM NaCl, 5.4mM KCl, 9.7mM Na_2HPO_4, 2mM KH_2PO_4; pH 7.4
PBST	0.1% Tween-20 in PBS
1000x protease inhibitor cocktail	aprotinin 1mg/ml H_2O, leupeptin1mg/ml H_2O, pepstatin 1mg/ml ethanol
SDS-PAGE running buffer	50mM Tris, 0.38M glycine, 0.1% SDS
TNE buffer	50mM Tris (pH 8.0), 150mM NaCl
Western Blot blocking buffer	5% (w/v) non-fat dry milk in PBST
Western Blot transfer buffer	48mM Tris, 39mM glycine, 0.037% SDS, 20% methanol

2.2 Antibodies

A detailed list of antibodies and working dilutions is provided in appendix II. Rabbit polyclonal anti-Hrs was a kind gift of Sylvie Urbé (Liverpool University, UK). Mouse monoclonal anti-Tsg101 was purchased from Biozol (Eching, Germany). Rabbit polyclonal anti-Aip1/Alix and anti-Vps4B were kind gifts from Wesley

Sundquist (University of Utah, Salt Lake City, USA), and were affinity purified using purified antigen as described (von Schwedler 2003). Anti-CD63 was from Sanquin (Amsterdam, NL), anti-transferrin receptor from Zymed (Berlin, Germany), anti lamp-1 (H4A3) from DSHB, Iowa, USA and anti-actin (C-11) and anti-14-3-3γ and θ (C-16 and C-17, respectively) from Santa Cruz (Heidelberg, Germany). Culture supernatant of the monoclonal antibody 'P5D4' was a kind gift of Thomas Kreis. Polyclonal rabbit antiserum against HIV-1 CA was raised against bacterially expressed and purified protein. Anti-CD63 (1B5, used for immuno EM analyses) was a kind gift from Mark Marsh (University College London, London, UK), anti-CD63 was from Sanquin (Amsterdam, NL) and anti-CD44 (F10-44-2) from Chemicon (Hampshire, UK). Rabbit-anti mouse IgG was from ICN biomedicals. Anti-rabbit and anti-mouse IgG coupled to Cy3 or to horseradish peroxidase (HRP) were from Dianova, Hamburg, Germany.

2.3 Chemicals and reagents

All chemicals and reagents not listed here were purchased from Sigma, Heidelberg, Germany or from Merck, Darmstadt, Germany.

2.3.1 Tissue culture reagents

1000x L-glutamine (2M)	Gibco BRL, Division of Invitrogen, Karlsruhe, Germany
1000x penicillin (100.000U/ml), 1000x streptomycin (100mg/ml)	Gibco BRL
Dulbecco's modified Eagle's Medium (DMEM, high glucose)	Gibco BRL
EDTA-trypsin	Gibco BRL
fetal calf serum (FCS), heat inactivated	Gibco BRL
Ficoll Paque™ Plus	Amersham Biosciences
human AB serum (HAB), heat inactivated	Sigma, Heidelberg, Germany
interleukin-2 (IL-2)	Roche Diagnostics, Mannheim, Germany
phytohemagglutinin (PHA)	Sigma, Heidelberg, Germany

RPMI 1640	Gibco BRL

2.3.2 Chemicals and reagents for biochemistry

acrylamide 30% :bisacrylamide 0.8% solution acrylamide 40% : bisacrylamide 0.2% solution	BioRad, Munich, Germany
annealed siRNAs against Tsg101 and Aip1/Alix	Ambion, Huntingdon, UK
enhanced chemoluminescence (ECL) detection system	Amersham Pharmacia, Freiburg, Germany
Ficoll Paque™ Plus	Amersham Pharmacia,
fluorescent mounting medium	Dako Cytomation
FuGene6 transfection reagent	Roche, Mannheim, Germany
HEPES	Biomol, Hamburg, Germany
Hoechst 3342 dye (Hoechst)	Sigma, Heidelberg, Germany
Immobilon-P PVDF membrane	Millipore, Bedford, MA, USA
Optiprep™	Axis-Shield, Oslo, Norway
Protran® nitrocellulose membrane	Schleicher & Schuell, Dassel, Germany

2.3.3 Electron microscopy chemicals

16% paraformaldehyde (PFA, aqueous solution)	EMS (Hatfield, USA), Cat. #15710
25% glutaraldehyde (GA, aqueous solution)	EMS (Hatfield, USA), Cat. #16220
4% osmium tetroxide (OsO_4, aqueous solution)	EMS (Hatfield, USA), Cat. #19150
BSA Fraction V	(biomol, Hamburg, Germany), Cat. #01400
DDSA (EPON hardener)	Serva (Heidelberg, Germany), Cat. #20755
DMP-30	Serva (Heidelberg, Germany), Cat. #36975

Formvar	Plano, Wetzlar, Germany
gelatin for embedding of immuno-EM samples	La Bovida, Nanterres, France
glycid ether	Serva (Heidelberg, Germany), Cat. #21045
gold-III chloride	Sigma Cat. #G-4022
MNA (EPON hardener)	Serva (Heidelberg, Germany), Cat. #29452
propylene oxide	Serva (Heidelberg, Germany), Cat. #33715
protein A gold (PAG)	Utrecht University, Netherlands
Ruthenium Red	Serva (Heidelberg, Germany), Cat. #34580
tannic acid	Serva Cat. #35753
uranyl acetate	Fluka (Buchs SG, Switzerland)

2.4 Cell biological and virological methods

2.4.1 Cells and cell culture

All cells and cell lines were cultured at 37 ºC and 5% CO_2. All cell culture media were supplemented with 100U/ml penicillin, 100µg/ml streptomycin, 2mM glutamine and 5 or 10% heat inactivated FCS (referred to as /5% or /10%), unless otherwise indicated. MT4 cells [95] and primary CD4+ T cells were maintained in RPMI1640/10%. Primary human macrophages were cultured in DMEM/10% and 10% heat inactivated human AB serum (HAB). 293T cells [96] were maintained in DMEM/10%. The human 293T cell line is a highly transfectable derivative of the epithelial 293 cell line into which the Simian Virus 40 (SV40) tumor antigen was inserted. The human epithelial cell line HeLa (ATCC CCL-2) and its derivatives HeLaP4 [97] and HeLa SA48 [98] were grown in DMEM/10%. HeLaP4 are stably transfected with the HIV-1 CD4 receptor and express the CXCR4 and CCR5 coreceptors and are thus infectable with HIV-1. HeLa SA48 stably express sialyl-transferase (ST) tagged with a vesicular stomatitis virus G protein epitope. Tagged ST

was shown to localize to the TGN [98] and can readily be detected with the monoclonal antibody 'P5D4'.

2.4.2 Isolation of primary cells

Peripheral blood mononuclear cells (PBMCs) were isolated from buffy coats of healthy, HIV-1 seronegative blood donors (DRK Blutspendezentrale Mannheim, Germany) by density gradient centrifugation (Ficoll Paque™ Plus). Buffy coats were mixed 1:1 with PBS and carefully placed on top of 15 ml Ficoll Paque™ Plus in a 50 ml tube. Gradients were centrifuged for 30 min at 2000rpm (Heraeus Megafuge 1.0) and 4°Cwith slow deceleration. The PBMC layer was harvested, washed twice with PBS, and red blood cells were lysed by brief suspension (5 seconds) of cells in dH_2O. Lysis was stopped by immediate addition of 45ml of PBS to the cell suspension. This step was repeated when necessary until no red blood cells were left in the PBMC pellet.

CD4+ cells were separated from PBMCs by negative magnetic cell sorting (Miltenyi Biotec CD4+ T Cell Isolation Kit II), as instructed by the manufacturer. $5x10^6$ cells/ml were cultured over night in RPMI/10% with 0.5 μg/ml IL-2 and medium was replaced on the following day with RPMI/10% + 0.5μg/ml IL-2 and 200U/ml PHA. Every third day one third of medium was replaced with fresh RPMI/10% with IL-2 and PHA.

To obtain primary macrophages, isolated PBMCs were washed in PBS/2mM EDTA/0.5% FCS, resuspended in DMEM/5% and 5-7.5 x 10^7 PBMCs/ml were plated onto 15cm cell culture dishes in DMEM/5%. Cells were allowed to attach for 2 hours, after which unattached cells were washed off with PBS. Adherent monocytes were incubated in DMEM/10% with 10% HAB. After 2 days, cells were washed with PBS, detached by treatment with PBS/0.005% trypsin and gentle scraping, replated onto 6-well or 12-well tissue culture plates (2 x 10^6/ml) and allowed to differentiate into macrophages for 3-5 days. Medium was replaced with fresh DMEM/10% containing 10% HAB every third day.

2.4.3 Virus preparation and infections

Infection of MT4 cells and primary T lymphocytes as well as HIV-1 p24 ELISA measurements were done by Baerbel Glass; Infection of primary macrophages was done By Ina Allespach (both at Virology Department, University of Heidelberg).

MT4 cells were infected with HIV-1 strain NL4-3 [99] by mixing 10% of previously infected cells with 90% of uninfected cells. Cells were harvested for EM 24 hrs after initiation of co-cultivation. This method routinely leads to productive infection of >90% of cells, as assessed by immuno-EM of ultrathin sections that were labeled with an antibody to the viral CA protein (see below).

Virus inoculum for infection of primary CD4+ cells was prepared from MT4 cells infected as above. Virus-containing culture supernatant was cleared by low-speed centrifugation, filtered through 0.45-μm-pore-size cellulose-acetate filters (Schleicher & Schuell, Dassel, Germany), and analyzed for antigen content by a CA-specific enzyme-linked immunosorbent assay (p24 ELISA, [100]). After addition of Il-2 and PHA, the cell-free supernatant was used directly for infection of prestimulated CD4+ cells. Three days after infection, the inoculum was replaced with RPMI/10% + IL-2 and PHA.

Primary human macrophages were infected with HIV-1 strain YU-2 [101] or Ba-L, a kind gift of Oliver T. Keppler, using 50-75ng CA antigen per $7x10^5$ cells in DMEM/10% +10% HAB for 2 days. Cells were then washed 3 times with DMEM/10% containing 10% HAB and maintained as described above. Infection of primary cells was monitored by p24 ELISA. Cells were fixed when the ELISA signal reached a plateau (7-10 days for T cells, 12-17 days for macrophages), which corresponded to infection rates of 40-50% as assessed by anti-CA labeling of cryosections (see below).

2.5 Biochemical assays

2.5.1 RNA interference (RNAi)

RNAi is an evolutionary conserved process of gene silencing by which double-stranded short interfering ribonucleic acids (siRNAs) cause sequence-specific degradation of homologous cellular mRNA. Interaction of siRNAs with the cellular RNA-inducing silencing complex (RISC) and homologous mRNAs leads to

endonuceolytic cleavage and degradation of the target mRNA. This results in a decrease or shutdown of target mRNA translation into protein. Knockdown of target protein synthesis can be triggered in mammalian cells by transfection of 21-23 bp siRNA molecules identical with target mRNA sequences.

siRNA transfections of 293T cells were carried out by Stefanie Jaeger, Virology Department, University of Heidelberg. 293T cells were grown in 6cm dishes and transfected with siRNAs against Tsg101 or Aip1/Alix applying a standard calcium phosphate transfection protocol. At 60% confluency, cells were transfected with 600pmol siRNA, followed by cell splitting after 12 h and a second transfection with 300 pmol of the same siRNA after another 12 h. At 48 h after initial transfection, cells were either lysed in SDS-PAGE sample buffer for Western blot analysis or fixed for immuno EM as described below.

2.5.2 Transfection of plasmid DNA

For transfection, HeLa or HeLaP4 cells were seeded on glass cover slips in 24-well plates or onto 6 cm dishes in DMEM/10% without antibiotics. After approximately twelve hours, when cells had reached ~70% confluency, they were transfected with the expression plasmid for dominant negative $Vps4_{E228Q}$-EGFP (a kind gift of W. Sundquist) using FuGene6 transfection reagent as instructed by the manufacturer. 3.5 µg of DNA were used per 6 cm dish. Medium was replaced with DMEM/10% + antibiotics after 8 to 12 hours. At 36 hours after transfection, cells were either fixed with 4% PFA in PBS for IF or as described below for EM. Alternatively, cells were directly used for membrane flotation experiments (see below).

2.5.3 Membrane flotation

HeLaP4 or HeLa cells, either transfected with $Vps4_{E228Q}$-EGFP (see above) or untransfected were grown until around 90% confluency, washed with ice-cold hypotonic swelling buffer (10 mM Tris pH 7.4, 1 mM $MgCl_2$ and protease inhibitor cocktail) and swollen on ice for 15 min in hypotonic buffer. Cells were detached by gentle scraping in a small volume of hypotonic buffer and lysed on ice by 25 strokes with a 25-gauge needle. Nuclei were spun down (1.000g, 3min, 4° C) and the postnuclear supernatant (PNS) was adjusted to 40% Optiprep™. 900μl of PNS were

placed at the bottom of a SW60 centrifuge tube, successively overlaid with 2.5 ml 28% Optiprep™ in TNE buffer (50 mM Tris, pH 7.4, 150 mM NaCl, 5 mM EDTA and protease inhibitor cocktail) and TNE buffer and centrifuged at 165.000g in a Beckman SW60 rotor for 3h at 4° C. 500 μl fractions were collected from top to bottom of the gradient and fractions were either directly mixed with SDS-PAGE sample buffer or proteins were precipitated from the fractions prior to SDS-PAGE (blots not shown). For this, 10% trichloroacetic acid (TCA) were added to each fraction, proteins were precipitated for 20 min on ice, collected by centrifugation (15 min, 13.000 rpm, 4° C), washed once with ice-cold acetone, air-dried and solubilized over night in SDS sample buffer. Samples were then analyzed by SDS-PAGE and western blotting.

2.5.4 SDS-Polyacrylamide gel electrophoresis (SDS-PAGE) and Western Blots

SDS-PAGE allows electric-field separation of proteins according to their mass. The detergent SDS dissociates and unfolds oligomeric proteins. SDS binding to polypeptides leads to formation of complexes with fairly constant charge to mass ratios. The electrophoretic migration of such complexes through a gel is therefore only determined by their mass. Transfer of separated proteins from an SDS-gel onto a nitrocellulose membrane in an electric field and specific protein detection by antibodies is referred to as Western Blotting.

SDS-PAGE and Western Blots of HIV-1 infected or uninfected MT4 cell lysates were done by Dr. Barbara Mueller, Western Blotting of siRNA transfected 293T cell lysates by Stefanie Jaeger (both Department of Virology, University of Heidelberg). 293T cells were scraped, MT4 and 293T cells were collected by centrifugation at 1000g for 15 min, washed with PBS and lysed in SDS-PAGE sample buffer. Cell lysates were separated by SDS-PAGE (15% acrylamide: bisacrylamide, 200 to 1) and analyzed by western blotting as described [50].

For Western Blot analysis of gradient fractions from HeLaP4 or HeLa membrane flotation experiments, samples were adjusted to 1x SDS-PAGE sample buffer, boiled for 5 min and proteins were separated on 17.5% low-crosslinking acrylamide gels (acrylamide: bisacrylamide ratio 200 to 1. Gels were run were run at 100mA (in the stacking gel) -150mA (separating gel) in SDS running buffer. Proteins were transferred to PVDF or nitrocellulose membranes by semi-dry blotting for 60-

120 min at 1-2.5 mA/cm^2 gel, depending on the size of the protein of interest. Stacks for blotting were assembled as follows: the nitrocellulose membrane and six pieces of 3mm chromatography 'Whatman paper' (Schleicher& Schuell), all of the same size as the gel, were soaked in transfer buffer. Three pieces of paper were placed on the anode, followed by the membrane, the SDS-gel, another three pieces of paper and the cathode (bottom to top). After transfer, the membrane was rinsed in deionized water (dH_2O), incubated for 90 min with blocking buffer, rinsed with PBST and incubated with the primary antibody. Primary antibodies were diluted in PBS/2% BSA and 0.01% sodium azide or in PBS/5% fat-free milk and sodium azide. Dilutions used for the antibodies are given in appendix II. The membrane was washed three times with PBST and incubated with the appropriate secondary antibody (diluted in blocking buffer) coupled to horseradish peroxidase (HRP) for one hour. After washing the membrane at least three times in PBST, it was developed using enhanced chemoluminescence (ECL) detection system (Amersham Pharmacia) as instructed by the manufacturer. Bands were visualized on Fuji SuperRX films.

2.6 Electron and light microscopy

2.6.1 Preparation of gold particles coupled to BSA (BSA gold)

Preparation of colloidal gold solutions and coupling to BSA was done essentially as described [102]. Homodisperse colloidal gold solutions were prepared by reduction of gold ions in aqueous solutions by using a mixture of tannic acid and citrate as reducing agents.

Reduction of gold chloride leads to condensation of metallic gold particles, with the particle size depending on the amount of reducing agent. Thus, the use of different concentrations of tannic acid influences the size of the gold particles during gold sol formation (Table 2) and allows preparation of gold particles in the size range of 17 to approximately 3 nm [103] with a very narrow variation in particle size.

Gold particle diameter (nm)	1% Tannic acid for 100ml final solution (ml)
3	5
4	2.5
5	1
6	0.5
7.5	0.25
9.5	0.1
10	0.08
11.5	0.05
14	0.025

Table 2. Influence of the amount of tannic acid on gold particle size during preparation of colloidal gold solutions.
When 1 ml or more of tannic acid is used, an equal amount of 25 mM potassium carbonate must be added to neutralize the reducing solution.

Coupling hydrophilic macromolecules such as proteins to gold particles renders colloidal gold solutions both stable and hydrophilic in aqueous solutions. Under pH conditions close to the isoelectric point of a protein, incubation of gold particles with proteins leads to spontaneous and stable coupling at room temperature. After cooling down the gold solution to room temperature, its pH was adjusted with pH paper (colloidal gold may block pH electrodes). The isoelectric point of BSA is around pH 7.0. A final BSA concentration of 0.2% was added and the solution was incubated for several minutes at room temperature. Depending on particle size, the absorption peak of BSA gold solutions is between 480 nm and 550 nm, and optical density (OD) was determined with a spectrophotometer at 520 nm (OD_{520}). BSA-gold solutions were stored at 4ºC.

A detailed protocol of BSA gold preparation is given in appendix III.

2.6.2 Fluid phase uptake of BSA gold

Primary human macrophages were starved over night in DMEM/5%, followed by additional 2 hrs of starvation in serum-free DMEM prior to BSA-gold feeding. To fill endocytic compartments with BSA gold, primary human macrophages were incubated for the indicated times with BSA coupled to 5nm or 10 nm gold (final OD_{520}= 10) in DMEM/10% + 10% HAB at 37°C. Excess BSA was washed away on ice three times with PBS. To fill all endocytic structures including early endocytic

vesicles and EEs with BSA gold, cells were directly fixed for EM (see below). To chase the internalized gold to late endocytic structures, cells were incubated for additional 30 min or 2 hrs at 37ºC. When indicated, macrophages were fed with BSA coupled to 16nm gold for 90 min, followed by an overnight chase to label LEs/lysosomes. In the latter case cells were incubated for 10 min with BSA coupled to 5nm gold to fill early endocytic structures before fixation.

MT4 cells or primary T cells were fed for 40 min with BSA coupled to 5nm gold (OD_{520}= 5); The fact that these cells grow in suspension rather than adherent and their low endocytic activity precluded detailed BSA-gold pulse-chase experiments. The efficiency of BSA gold was generally lower than in endocytically active macrophages. Under the given conditions early endosomes and MVBs were labeled with BSA gold. LEs were generally poorly filled and lysosomes did not contain BSA gold.

2.6.3 Sample processing for immunoelectron microscopy

Adherent cells were fixed by adding an equal volume of a 2x fixative I (8%PFA, 0.2%GA in 0.2M PHEM, pH 6.9) to the cell culture medium. After 5-10 min this mixture was removed and replaced with 1x fixative (4% PFA, 0.1% GA in 0.1M PHEM, pH 6.9) for 90-120 min at room temperature. Cells were scraped, pelleted by centrifugation and either immediately processed (see below) or stored at 4ºC in fixative II containing 4% PFA in 0.1M PHEM, pH 6.9. Suspension cells were carefully collected by low-speed centrifugation for 10 min, the supernatant was removed and cells were directly fixed as a pellet with 4% PFA, 0.1% GA in 0.1M PHEM, pH 6.9 for 90-120 min. If cells were not processed immediately they were stored as described above.

Fixed cells were processed as detailed in [104]. Cell pellets were washed by resuspending 4-5 times in PBS-glycine and incubated for 10 min in PBS-glycine at 37ºC to quench aldehyde groups. Cells were then resuspended carefully in 10% gelatin/PBS, incubated for 5-10 min at 37ºC, pelleted by centrifugation and immediately placed on ice until the gelatin was hardened. Gelatin-embedded samples were infiltrated with 2.3M sucrose (as a cryoprotectant) either for 2 hrs at room temperature or at 4ºC over night on a rotating wheel, mounted onto sample pins and frozen in liquid nitrogen. 50-70 nm cryosections were obtained with Diatome (DiS-

Galetzka, Weinheim, Germany) or Drukker (Element Six, Hanau, Germany) diamond knives in a Leica EM FCS or EM UC6 ultramicrotome (Leica Microsystems, Wetzlar) at –120ºC. Copper grids were coated with Formvar and a thin carbon layer for stabilization. Sections were thawed in a drop of pickup solution (2% methylcellulose: 2.3M sucrose, mixed 1+1) and transferred to coated copper grids. For immunolabeling, 50-70 nm cryosections were thawed and incubated with primary antibodies and 5 nm, 10 nm or 15 nm protein A gold (PAG) as described (Griffiths 1993) and contrasted with uranyl acetate, which forms electron dense precipitates by reacting with phosphate groups of membrane lipids and nucleic acids. Double labeling was essentially as described by [102]. A detailed immunolabeling protocol is given in appendix IV.

2.6.4 Sample processing for plastic embedded electron microscopy

Cells were fed with BSA gold as described above. Cell culture dishes were placed on ice, washed three times with ice-cold 20mM EDTA/PBS to wash off excess BSA gold and to partially detach cells from the culture dish. After washing, cells were fixed with 2.5% GA in 0.1M ice-cold Na-Cacodylate buffer, pH 7.2 for 1 hour, during which cells were allowed to warm up to room temperature. When indicated, the fixative contained 0.5 mg/ml Ruthenium Red (RR), which was added to stain the cell surface. RR is a small membrane-impermeable compound that binds to carbohydrate moieties of the cell surface and can penetrate into very slender invaginations of the plasma membrane [105]. Cells were washed with 0.1M sodium cacodylate buffer, and post-fixed for 30-60 min with 2% osmium tetroxide (OsO_4) in 0.1M sodium cacodylate buffer at room temperature. OsO_4 is a powerful oxidizing agent and an outstanding electron dense stain for electron microscopy. Again, the fixative contained 0.5 mg/ml RR when indicated. Upon post-fixation in the presence of OsO_4, RR forms an electron dense precipitate which stains the cell surface but not intracellular membranes [106-109]. Cells were washed with 0.1M cacodylate buffer to remove excess Ruthenium Red, and dehydrated in a graded series of 50, 70, 90 and 100% ethanol at room temperature. During the dehydration step in 70% ethanol, cells were contrasted with a saturated solution of uranyl acetate in 70% ethanol, either for 2 hours at room temperature or over night at 4ºC. As uranyl acetate is an electron dense

compound, this step was used for 'en bloc' staining of the whole sample. Cells were then embedded in EPON as described [94].

60-80 nm plastic sections were obtained in a Leica Ultracut UCT microtome with a diamond knife, washed with dH_2O and contrasted for about 2 min with lead citrate according to [110]. Lead citrate is a widely used stain for cellular components such as lipids and nucleic acids and presumably reacts with phosphate groups that have a greater affinity to the lead ion compared to citrate. To avoid reaction of lead citrate with CO_2, which would yield a precipitate of lead carbonate, contrasting was always done in the presence of potassium hydroxide pellets. All plastic and cryo-sections were examined with a Zeiss EM10 or a Philips/FEI Morgagni TEM.

2.6.5 EM quantification techniques

Quantification of protein distribution was done essentially as described by [111, 112]. For quantification of the distribution of ESCRT proteins, samples were chosen randomly for sectioning and sections were labeled with primary antibodies and 10 nm PAG. Grids with labeled sections were first examined at low magnification (100x) in order to find a grid square containing sections, sections were then scanned systematically in an unbiased fashion at higher magnification (12.500x) and every gold particle was counted and classified [111, 112]. Per grid a total of 200 gold particles were counted. Values represent counts from at least two different grids and three independent labelings. Quantification in primary T cells and macrophages was done in cells obtained from at least two different donors.

For estimation of labeling densities or reduction of overall labeling upon siRNA treatment, samples and grids with labeled sections were chosen randomly, and grid squares containing sections were chosen at low magnification. Pictures were then taken randomly at 31.500x magnification on at least two different squares per grid using a Gatan MultiScan™ camera and Digital Micrograph™ software. Labeling densities were calculated applying standard stereology methods [94]: each picture was overlaid with a 1cm grid lattice using the open source ImageJ software (available at http://rsb.info.nih.gov/ij/download.html) with a 'stereology' plugin (available at ftp://rsbweb.nih.gov/pub/nih-image/plug-ins/Ster_DropIns.hqx). Membrane intersections of each organelle of interest with the grid were counted and the total membrane length of each organelle was estimated, taking into account the

magnification. For calculation of the labeling density per unit of membrane length (generally 1μm) was calculated by counting gold particles (representing the antigen) on the same pictures.

2.6.4 Immunofluorescence

Cells were grown on glass cover slips and transfected with Fugene6 transfection reagent as described below. At 36 hrs after transfection, they were washed with PBS, fixed for 30 min with 4% PFA/PBS at room temperature and washed three times with 50mM glycine/PBS (PBS-glycine). Cells were permeabilized for 5 min with 0.5% Triton-X100/PBS, washed 5 times with PBS-glycine, blocked for 10 min with IF blocking solution (5% FCS, 50mM glycine in PBS) and incubated with the primary antibody (diluted in blocking solution, dilutions are given in appendix II) for about 30 min at room temperature in a wet chamber. After washing the cells 5 times with PBS-glycine, they were incubated with the appropriate secondary antibody coupled to Cy3 (diluted in IF blocking solution) for 30 min as above. Cells were washed three times with PBS-glycine, three times with dH_2O and mounted onto glass slides with fluorescent embedding medium (Dako Cytomation). Light microscopy images were taken with a 100x lens on a Zeiss Axiovert 200 light microscope, using AxioVision program.

Chapter 3

3. Results

3.1 Localization of ESCRT in T cells and macrophages

In the first part of this study, four selected subunits of the human ESCRT complex were localized in great detail by immuno-electron microcopy (EM) in both HIV-1 infected and uninfected T cells and macrophages. The aims of this ultra-structural localization study were twofold: first, to gain insight into possible unknown functions of ESCRT, besides protein sorting into and formation of MVBs, in uninfected mammalian cells. Second, to examine if in HIV-1 infected cells, the ESCRT protein complex, which was previously shown to be required for HIV-1 release, was actively re-localized to the site of HIV-1 budding and release.

3.1.1 Characterization of antibodies against selected subunits of the ESCRT machinery

At the onset of this study a panel of previously described antibodies [50, 113] were tested for immuno-EM. Affinity-purified antibodies against the ESCRT-I subunit tumor susceptibility gene 101 protein (Tsg101), the ESCRT-associated Vps factor apoptosis-linked gene 2 (ALG-2)-interacting protein 1/ ALG-2-interacting protein X (Aip1/Alix) and against the AAA-type ATPase Vps4B, which was previously shown to be required for ESCRT function, appeared to display specific labeling on cryo-sections. The antiserum against hepatocyte growth factor-regulated tyrosine kinase substrate (Hrs) has been described previously [113], and therefore these four antibodies were used for further study. Since only Tsg101 is currently classified as a *bona fide* ESCRT component, the term ESCRT refers to ESCRT- and ESCRT-associated proteins throughout the remainder of this study.

The specificity of the four antibodies was first tested by western blot analysis of infected and uninfected MT4 cell lysates. The T cell line MT4 was chosen because it can be readily infected with HIV-1 and expresses high amounts of viral proteins [95]. Western blots showed bands of the expected molecular weight for all four antibodies with no obvious difference in expression levels between infected and uninfected cells (Figure 7 A).

The specificity of two of the antibodies was furthermore demonstrated by RNA interference (RNAi) experiments in 293T cells. Cells were transfected with siRNAs specifically interfering with expression of either Tsg101 or Aip1/Alix, lysed and subjected to SDS-PAGE and western blotting. Western blot analysis showed that RNAi with Tsg101 or Aip1/Alix expression led to almost undetectable levels of the respective protein 48 hours after transfection, whereas the expression level of the other ESCRT protein was not affected. An antibody against the abundant cytoskeletal protein actin was used to compare the protein amounts loaded onto the gel (Figure 7 B). To confirm the specificity of the antibodies for immuno-EM, cryosections of 293T cells were labeled with anti-Tsg101 or anti-Aip1/Alix after RNAi-mediated knockdown of either of the two proteins. The labeling density with anti-Tsg101 or anti-Aip1/Alix antibodies was significantly decreased on labeled cryosections (Figure 7 C), confirming the specificity of the antibodies by EM.

Upon detailed inspection of cryosections, the labeling for both Aip1/Alix and Tsg101 was found uniformly decreased over all intracellular structures, with the exception of mitochondria that displayed the same level of (non-specific) labeling after siRNA treatment. The specificity of the Hrs and Vps4B antibodies was not further investigated; the antibody to Hrs was previously used for EM [113]. Furthermore, as shown below, all four antibodies displayed a similar labeling pattern, indirectly confirming their specificity by EM.

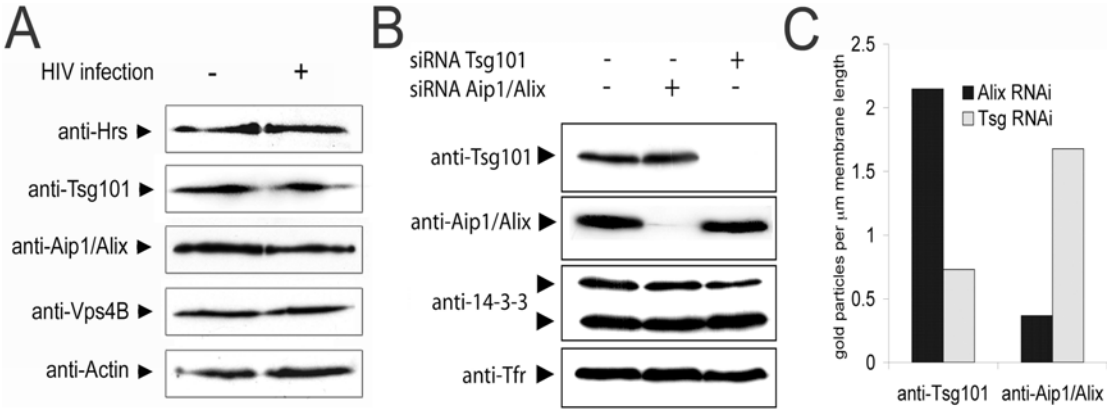

Figure 7: Western blot analysis of Hrs, Tsg101, Aip1/Alix and Vps4B in infected and uninfected MT4 cells; RNA interference with Tsg101 and Aip1/Alix in 293T cells.
(A) Lysates of HIV-1-infected (+) or uninfected (-) MT4 cells (about $7.5x10^4$ cells per lane) were analyzed by SDS-PAGE and western blotting with anti-Hrs, anti-Tsg101, anti-Aip1/Alix, anti-Vps4B and anti-actin antibodies. (B) Lysates of 293T cells, either untransfected or transfected for 48 h with Tsg101- or Aip1/Alix-siRNA, were analyzed by SDS-PAGE and Western blotting. Eighty µg of protein were loaded per lane. Controls are antibodies to the cytosolic 14-3-3θ protein, that appears as two bands on SDS-gels (indicated with arrows), and the membrane-associated transferrin receptor (Tfr). (C) Reduction of the overall Tsg101- and Aip1/Alix- labeling by EM on cryo-sections of 293T cells transfected with either Tsg101- or Aip1/Alix-siRNA. Fifty random photographs of labeled cryo-sections were taken and the average amount of gold particles per µm of membrane length calculated using standard stereology methods.

3.1.2 Defining endocytic compartments in macrophages and T cells

We next set out to determine the localization of components of the ESCRT machinery in target cells for HIV-1 infection. Consequently, we focused on primary human CD4+ T cells, primary human macrophages and the above-mentioned T cell line MT4. From the proposed role of ESCRT in mammalian cells, protein sorting into and formation of MVBs, we expected its subunits to localize throughout the endocytic pathway, perhaps concentrated on MVBs. In contrast to T cells, macrophages have strong endocytic activity. It seemed thus likely that the endocytic pathways of these two cell types show some morphologic differences. Therefore, it was necessary to characterize endocytic organelles in T cells and macrophages prior to localization of ESCRT components immuno-EM.

To define endocytic compartments, primary macrophages are particularly well suited since these cells readily take up fluid phase markers such as bovine serum albumin (BSA) coupled to gold. To identify early and late endocytic compartments,

BSA coupled to 5nm gold was fed to macrophages for 10 or 30 min, fixed directly, or after chasing the internalized gold for 30 min or two hours. These gold-feeding experiments revealed four morphologically distinct endocytic compartments that were filled with gold sequentially, in a time-dependent manner (Figure 8 A-C and E).

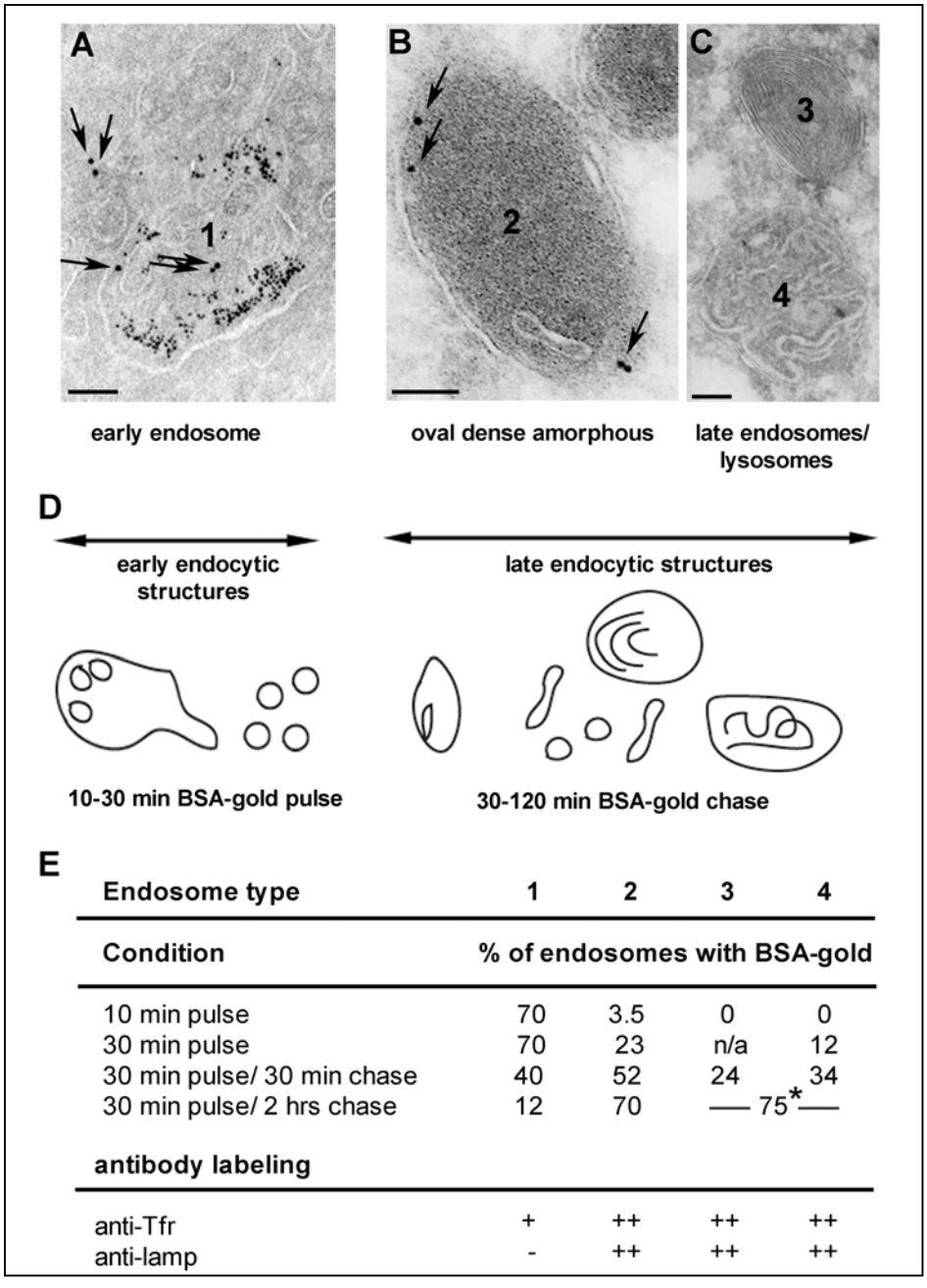

E

Endosome type	1	2	3	4
Condition	**% of endosomes with BSA-gold**			
10 min pulse	70	3.5	0	0
30 min pulse	70	23	n/a	12
30 min pulse/ 30 min chase	40	52	24	34
30 min pulse/ 2 hrs chase	12	70	— 75* —	
antibody labeling				
anti-Tfr	+	++	++	++
anti-lamp	-	++	++	++

Figure 8. Defining the endocytic compartments in primary human macrophages.
In primary macrophages four different endocytic structures (marked 1 to 4) can readily be discriminated. In (A) and (B), cryo-sections of macrophages, fed for 10 min with 5 nm

BSA-gold before fixing, were labeled with anti-Tfr (10nm gold, arrows; arrowheads 5nm internalized BSA gold). (A) A typical early endosome in a macrophage abundantly filled with 5nm BSA-gold. (B) Characteristic oval-shaped dense amorphous structure, abundantly seen in macrophages. (C) Two types of late endosomes/lysosomes in macrophages; these typically accumulated BSA-gold after an overnight chase period. Bars-100nm. (D) Schematic summary of the gold uptake experiments and the definition of early and late endocytic compartments in primary macrophages. For details see text. (E) Primary macrophages were fed with BSA coupled to 5 nm gold for 10 or 30 min. as indicated (pulse) and either fixed directly or after the indicated chase times (30 min or 2 hrs). For each gold feeding condition, the four endocytic structures shown in (A) to (C) were considered and scored as positive if they contained one or more 5nm gold particles. The numbers represent the percentage of each of the endocytic structures labeled with 5 nm gold. N/a: in the sample generated after a 30 min BSA-gold pulse, no endosomes of category '3' were found. -75*-: In the sample obtained after 30 min pulse/ 2 hrs chase the late endocytic structures '3' and '4' were densely packed with gold particles, precluding visualization of the internal membranes. In this particular sample the type '3' and '4' endosomes were therefore counted as one category. Antibody labeling: macrophages were fed for 90 min with BSA coupled to 16 nm gold and the internalized gold chased overnight. Before fixing, the cells were fed for 10 min with BSA coupled to 5 nm gold. Under these conditions, early endosomes (A) accumulate 5nm BSA-gold and the structures shown in (C) accumulate 16nm BSA-gold, whereas the oval dense structures (B) are mostly devoid of internalized gold. Cryo-sections of fixed and BSA gold-fed cells were labeled with anti-lamp-1 or anti-Tfr followed by rabbit anti-mouse and protein A coupled to 10nm gold. The relative distribution of antibody labeling was then quantified. The quantification is displayed qualitatively, + representing low labeling, ++ being abundant labeling while – displays no to very low labeling.

After 10 min of BSA gold internalization, typical early endosomes were abundantly labeled with 5 nm gold particles (Figure 8 A and E, marked as '1'). Upon increasing chase periods, BSA gold was gradually shifted into endocytic structures that were defined as late endosomes/lysosomes (Figure 8 C and E, marked '3' and '4'). The BSA gold pulse-chase experiments also revealed oval-shaped electron dense structures that were generally smaller than late endosomes and that appeared to be an abundant compartment in macrophages (Figure 8 B and E, marked '2'). Since these were filled with gold before late endosomes/lysosomes, they apparently represented intermediates between early and late endosomes/lysosomes. Finally, MVBs, typical round membrane structures containing many internal vesicles, were not prominently seen in macrophages.

We also performed antibody labeling in macrophages using antibodies directed against transferrin receptor (Tfr) and lysosome-associated membrane glycoprotein-1 (lamp-1), generally considered to be markers of early/recycling

endosomes and late endosomes/lysosomes, respectively. For this, we prepared macrophages in which BSA coupled to 16nm gold was chased overnight followed by 10 min incubation with 5nm BSA gold, to more clearly discriminate between early and late endosomes. Under these conditions we found that 16nm BSA gold accumulated in late endosomes/lysosomes (see, for instance, figure 13 F), 5nm gold was found in early endosomes (Figure 8 A) whereas the oval dense structures (Figure 8 B) were mostly devoid of internalized BSA gold (not shown). The cells with two sizes of internalized BSA gold were then used to quantify anti-lamp and anti-Tfr labeling over different endocytic structures (Figure 8 E). Anti-lamp-1 decorated both the oval dense and the late endocytic structures, whereas early endosomes were mostly devoid of this marker (Figure 8 E). We unexpectedly found that anti-Tfr also decorated mainly late endosomal structures (including the oval dense compartments; Figure 8 E) and only about 30% of this marker was found on typical early endosomes.

The BSA-gold feeding and antibody labeling experiments also revealed two types of tubular-vesicular membranes that were part of the endocytic pathway. First, tubular-vesicular membranes that were apparently part of the early endocytic pathway since they readily filled with BSA-gold during a 10 to 30 min pulse and were found close or connected to early endosomes (for an example see figure 13 A). Second, tubular-vesicular membranes that were, albeit inefficiently, filled with BSA-gold after a 30 min chase period. This second type of tubular-vesicular membranes was furthermore found close to late endosomes and often located between late endosomes and the Golgi complex. Since these membranes (for examples see figures 13 F, 14 A and B, 15 A and B) labeled significantly with anti-Tfr, they might be (part of) recycling endosomes.

Throughout this study we defined early endocytic compartments as structures that were readily filled after 10 min BSA gold uptake and that were anti-Tfr positive, but mostly devoid of anti-lamp-1 labeling. Late compartments were those gradually filled with BSA gold after a chase period and that were lamp-1 positive, thus including the oval dense structures, prominently seen in macrophages (see figure 8 D for a model).

Compared to macrophages, fluid phase uptake was poor in primary T cells and MT4, precluding detailed BSA gold pulse-chase experiments. In MT4 cells we nevertheless found that after a 40 min pulse, early endosomes were readily filled with

BSA gold, whereas late endocytic compartments were mostly devoid of BSA gold. In contrast to macrophages, MVBs were readily seen in MT4 cells and could be discriminated from late endosomes because they were significantly filled with BSA gold after a 40 min pulse (see figure 14 D and E). Finally, similar to macrophages, anti-lamp-1 and anti-Tfr labeled mostly late endocytic structures in both MT4 and primary CD4+ T cells. Having operationally defined the different endocytic structures, we next quantified the distribution of ESCRT proteins in uninfected cells.

3.1.3 ESCRT- and ESCRT-associated proteins are differentially distributed in different cell types

Cryosections of MT4 cells, primary human T cells and macrophages were labeled with antibodies directed against ESCRT proteins Hrs, Tsg101, Aip1/Alix and Vps4B and the labeling was quantified as described [111, 112]. Endocytic compartments were defined as described above for macrophages and MT4 cells (using internalized BSA gold as marker) or based on morphological similarity for CD4+ T cells. We found that the relative intracellular distribution of the labeling was similar for each of the four antibodies (Figure 9 A-C), indicating that ESCRT proteins largely co-localize. Unexpectedly, 80% of the signal was associated with membrane structures in each cell type, with only around 10-15% in the cytoplasm (Figure 9 A-C). In T cells (both MT4 and CD4+ T cells) about 15% of the labeling was detected at the plasma membrane with less than 8% on endosomes (Figure 9 A and B), whereas this distribution pattern was essentially reversed in primary macrophages (Figure 9 C). Importantly, in all three cell types the majority of labeling (around 45%) was found associated with a specific set of endosomal membranes (Figure 9 A-C). More specifically, we found that ESCRT was predominantly located on the two types of tubular-vesicular membranes described above that were in close proximity or connected to either early or late endosomes and thus these membranes were denominated ‘endosome-associated’.

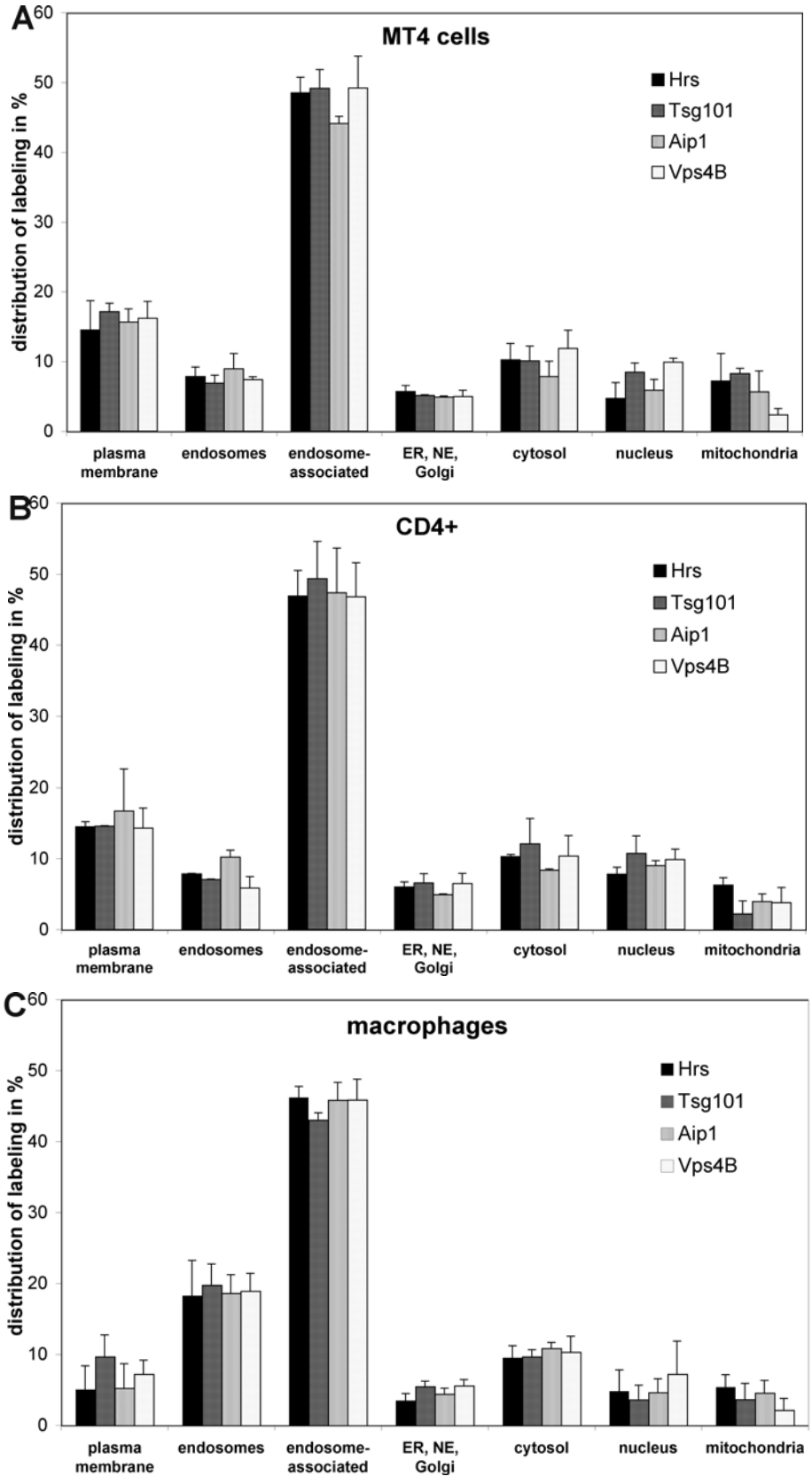
A
MT4 cells
distribution of labeling in %
Hrs
Tsg101
Aip1
Vps4B
plasma membrane
endosomes
endosome-associated
ER, NE, Golgi
cytosol
nucleus
mitochondria
B
CD4+
C
macrophages

Figure 9: Quantification of the localization of ESCRT subunits in uninfected cells by EM.
Thawed cryosections of (A) MT4 cells (B) Primary human CD4+ lymphocytes and (C) Primary human macrophages were labeled with anti-Hrs, anti-Tsg101, anti-Aip1/Alix or anti-Vps4B followed by protein A gold. Quantification was done on MT4 cells with 5nm BSA-gold internalized for 40 min prior to fixing. In the case of macrophages quantification was on cells prepared with two size of internalized BSA-gold as described for figure 8 E. ER endoplasmic reticulum, NE nuclear envelope. A total of 200 gold particles were counted per grid in random sections and attributed to the different categories indicated. Each experiment was repeated at least twice and two grids were counted per experiment. The data represent the relative distribution of gold labeling over different cellular structures, calculated as an average of all experiments and grids. For primary T cells and macrophages the gold counting was performed on sections of cells obtained from at least three different donors. Error bars denote standard deviation.

This quantitative method attributed percentages of labeling to specific organelles irrespective of the size of these membrane structures, which may differ considerably between cell types. To address this, we quantified the relative membrane length of plasma membrane and endosomes (excluding the tubular vesicular membranes) in T cells and macrophages (Figure 10 A). Random pictures of primary T cells and macrophages were overlaid with a grid lattice and intersections of the plasma membrane and of endosomes with the grid were counted on each frame to determine the total membrane length of these two compartments. This quantification revealed a ratio of total plasma membrane- to endosomal membrane length of 2.2 to 1 in T cells and of 1.7 to 1 in macrophages (Figure 10 A). Next, the anti-Hrs and anti-Aip1/Alix labeling densities per unit length of membrane were determined on these two compartments for both cell types (Figure 10 B). For this, gold particles per μm membrane length on the plasma membrane and on endosomes were counted on the same randomly taken frames.

A

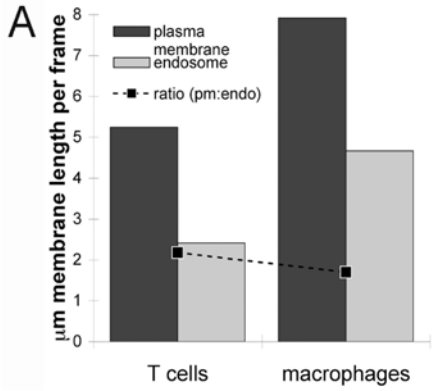

B

	labeling density	T cells	macrophages
Hrs [1]	plasma membrane	0.24 ± 0.04 [2]	0.17 ± 0.03
	endosomes	0.25 ± 0.05	0.57 ± 0.06
Aip1/ Alix [1]	plasma membrane	0.27 ± 0.05	0.12 ± 0.04
	endosomes	0.24 ± 0.06	0.55 ± 0.19

Figure 10: Plasma membrane to endosomal membrane length ratio and labeling densities of Hrs and Aip1/Alix in T cells and macrophages.
(A) 50 random pictures per cell type were taken at 31.500x magnification, overlaid with a 1 cm grid lattice and intersections of the respective membrane type, plasma membrane and endosomal membrane, with the grid were counted. Average membrane length of plasma membrane and endosomal membranes per picture (frame) was calculated from total numbers of intersections with each membrane and ratio of plasma membrane to endosomal membrane length was calculated for both cell types. pm plasma membrane; endo endosomal membrane.
(B) Quantification of Hrs- and Aip1/Alix labeling densities on the same random pictures as in (A). [1] Random pictures were taken from two different labeling experiments for each antibody. Labeling density was determined on the plasma membrane and on endosomes, taking only clearly identifiable endosomes into account and not the tubular-vesicular endosomal membranes. Numbers were determined by applying standard stereology methods. [2] Errors denote standard error of the mean.

In primary CD4+ T cells, the labeling densities of Hrs and Aip1/Alix were approximately the same on the plasma membrane and on endosomes (Figure 10 B). Given a ratio of plasma membrane to endosomal membrane of 2.2 to 1 in these cells (see figure 10 A), 2.1- and 2.5-fold more labeling for Hrs and Aip1/Alix, respectively, was therefore found at the cell surface compared to endosomes. This number corresponds well to the two-fold (Hrs and Aip1/Alix) higher labeling at the cell surface measured by quantifying their relative intracellular distribution (Figure 9 B) and confirms that in T cells ESCRT was more abundant at the plasma membrane than on endosomes. Similar quantification in macrophages, with a plasma membrane to endosome ratio of 1.7 to 1, showed that the labeling density for both antigens was about two-fold higher on endosomes compared to the plasma membrane (Hrs: 2.0-fold, Aip1/Alix: 2.7-fold; figure 10 B), confirming the data shown in figure 9 C. This quantification also confirmed that the labeling density for both Aip1/Alix and Hrs on endosomes was more than twice as high in macrophages compared to T cells.

Thus, the relative ESCRT distribution may vary between cell types. The quantitative EM data furthermore unexpectedly revealed that most of the labeling was associated with membranes, with the majority being associated with tubular-vesicular membranes in the vicinity of, or continuous with, endosomes.

3.1.4 ESCRT antibodies detect both cytosolic and membrane-bound antigen

Our EM observations clearly showed that 80 to 90% of each of the four ESCRT subunits tested were associated with membranes (Figure 9). This finding was unexpected since sequence analysis of the four proteins showed that none of them had a membrane-spanning domain and, with the exception of Hrs, which has a FYVE domain that targets Hrs to membrane lipids, none of the proteins tested had a membrane-targeting domain. Furthermore, it was previously shown that that the bulk of ESCRT proteins comprised a cytosolic pool that was 'recruited' to membranes upon overexpression of a ATPase deficient variant of Vps4 that functions as a dominant negative (dn) protein [63, 114]. These data were largely based on immunofluorescence studies and suggested that overexpression of dnVps4 tagged with green fluorescent protein (dnVps4$_{E228Q}$-EGFP) leads to the formation of aberrant enlarged endosomal structures onto which ESCRT complexes are recruited and trapped [63, 114]. Consistent with the latter studies, the four antibodies displayed a diffuse pattern by fluorescence microscopy in HeLa cells (Figure 11 A, E), interpreted previously as 'cytoplasmic' labeling [62, 114-116]. Furthermore, over-expression of Vps4$_{E228Q}$-EGFP led to the formation of large GFP-positive structures (Figure 11 C, G) that were labeled with antibodies to Hrs (Figure 11 B, D), Aip1/Alix (Figure 11 F, H), Tsg101 and Vps4B (not shown), confirming the above mentioned light microscopy studies. By EM, the Vps4 $_{E228Q}$-induced structures appeared as enlarged, GFP-positive, multi-vesicular membrane structures (Figure 11 I, J). The latter were also decorated with antibodies to Hrs (Figure 11 I), Tsg101 (Figure 11 J) as well as Aip1/Alix and Vps4B (not shown).

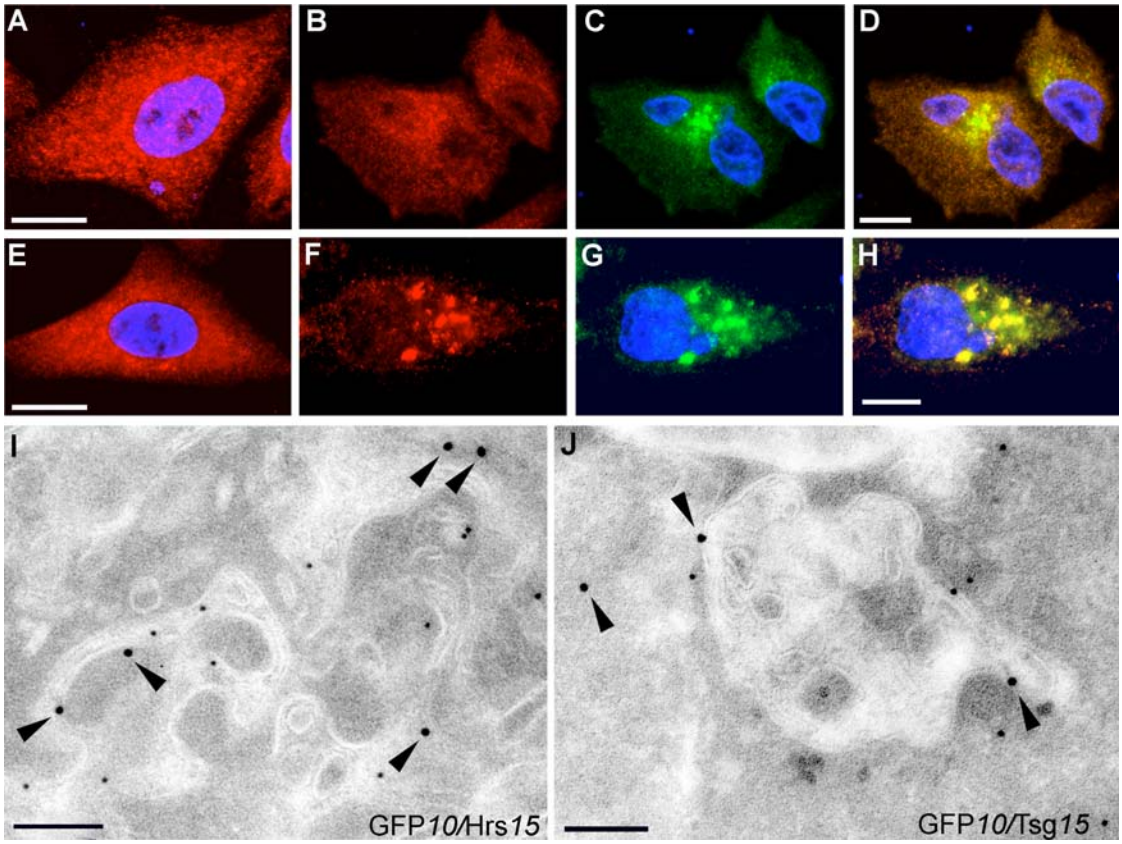

Figure 11: ESCRT-proteins localize to aberrant, dnVps4$_{E228Q}$-induced membrane structures.
HeLaP4 cells were either mock-transfected (A, E) or transfected with dnVps4-EGFP (Vps4$_{E228Q}$-EGFP; B-D, F-H) for 36 hours. (A) to (H) Cells were fixed with PFA, permeabilized and labeled with anti-Hrs (A, B) or anti-Aip1/Alix (E, F). GFP fluorescence is depicted in (C) and (G) with panels (D) and (H) showing the merge of the two signals. In untransfected cells (A) and (E), the proteins display a diffuse localization by light microscopy. Partial redistribution of Hrs and Aip1/Alix to the GFP-positive class E compartment (C and G) is observed upon Vps4$_{E228Q}$-EGFP expression. Bars-10μm. (I, J) Cryosections of Vps4$_{E228Q}$-EGFP-transfected HeLa cells were double-labeled with anti-GFP (10nm) and anti Hrs (15nm) (I, arrowheads) or anti-Tsg101 (15nm, J, arrowheads). Enlarged, GFP-positive aberrant endosomal structures display anti-Hrs- or Tsg101 labeling. Bars-500nm.

To test if the antibodies used detected their antigen preferably in the soluble state or in fully assembled ESCRT complexes, we next quantified the overall labeling density of ESCRT antibodies in HeLa cells overexpressing dnVps4$_{E228Q}$-EGFP compared to untransfected cells. It was shown previously, that in dnVps4$_{E228Q}$-EGFP expressing cells the bulk of ESCRT proteins is present in fully assembled ESCRT complexes, whereas in untreated cells the majority of ESCRT is believed to be disassembled [62, 114-116]. Thus, thawed cryosections of HeLa cells, either

untransfected or dnVps4$_{E228Q}$-EGFP transfected, were double labeled with antibodies directed against GFP and against ESCRT proteins. dnVps4-EGFP expressing cells were identified by anti-GFP labeling and the average amount of gold particles per cell profile was estimated in untransfected and transfected cells. This quantification revealed that the labeling density for Tsg101 and Hrs was similar in both transfected and untransfected cells (Figure 12 A), indirectly showing that disassembled and assembled forms of ESCRT complexes are detected equally well by the antibodies. This excluded the possibility that the unexpected high degree of membrane association of ESCRT proteins seen by EM was due to the inability of antibodies to detect the cytosolic pool of antigen.

The same labeled cryosections were then used to determine if ESCRT proteins were quantitatively recruited to Vps4$_{E228Q}$EGFP-expressing endosomal structures. To this end, we quantified the distributions of Hrs and Tsg101 over the plasma membrane, endosomes and tubular-vesicular membranes by EM (Figure 12 B). Anti-Hrs and anti-Tsg101 labeling on endosomes, including anti-GFP-positive endosomal structures in transfected cells, was increased about 2-fold compared to untransfected control cells (25% versus 12% of total labeling), while the plasma membrane labeling for both antigens was decreased by a factor of 3 (15 versus 5%, figure 12 B). In contrast, the amount of labeling on the tubular-vesicular endosomal membranes or in the cytoplasm was mostly unaffected (approximately 25% and 10%, respectively, see figure 12 B and not shown). This quantitative relocation of ESCRT to enlarged endosomal structures confirmed our light microscopy data and previously published observations, showing a clear re-localization of ESCRT to distinct (membrane) structures upon over-expression of dnVps4-EGFP. Furthermore, this demonstrated that the antibodies used were able to detect the complete pool of antigen, including fully assembled ESCRT complexes and soluble proteins. However, whereas in untransfected cells ESCRT proteins displayed a diffuse pattern by light microscopy, quantitative EM showed that the majority of these proteins were associated with membranes.

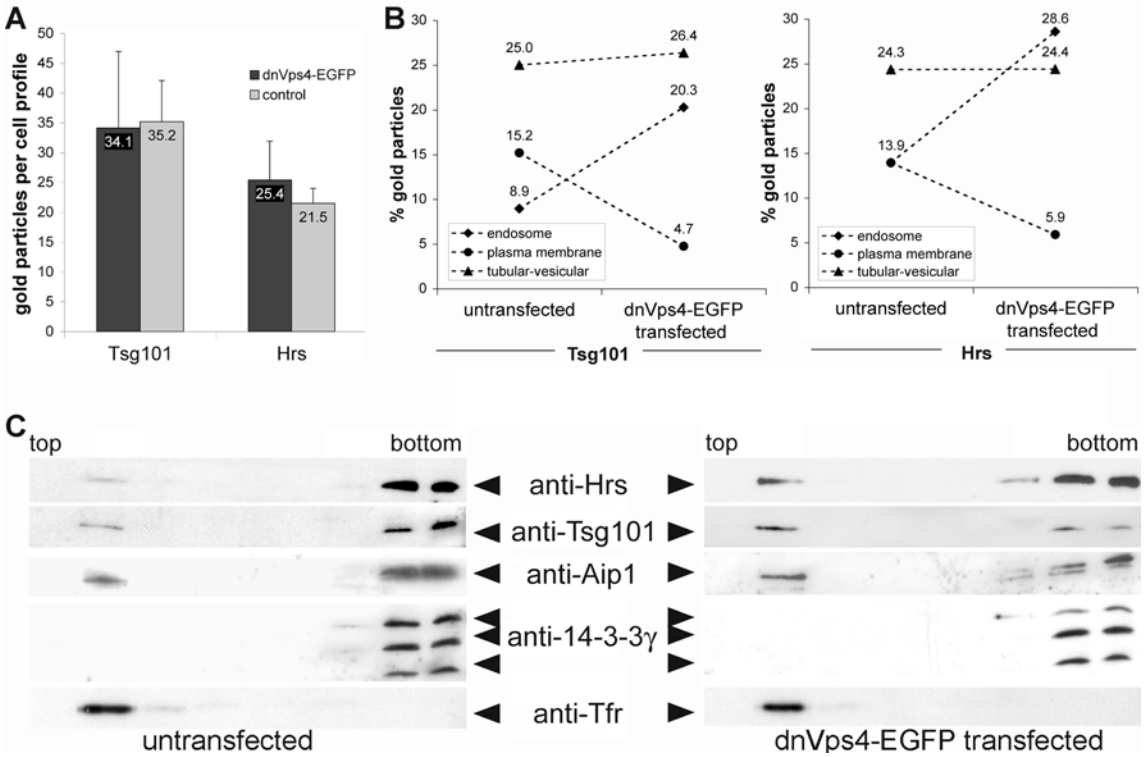

Figure 12: Overexpression of $Vps4_{E228Q}$–EGFP leads to a redistribution of ESCRT but does not change overall labeling density or membrane association of ESCRT proteins.
HeLa cells were either transfected with a dominant-negative Vps4-EGFP construct (dnVps4–EGFP) or left untransfected (control). (A) Quantification of the absolute numbers of gold particles (representing anti-Hrs or anti-Tsg101 labeling) on thawed cryosections of HeLa cells. Values represent counts on at least 10 transfected and 10 control profiles per antibody. Error bars denote standard deviation. (B) Quantification of ESCRT redistribution upon $Vps4_{E228Q}$–EGFP overexpression. Cells were treated as in (A) and gold particles were counted on the plasma membrane, endosomes and tubular-vesicular membranes of transfected and control cells. At least 200 gold particles were counted per antibody. Values were collected in two different labeling experiments and two different grids per experiment. (C) Western blot analysis of gradient fractions from membrane flotation experiments. HeLa cell lysates, either $Vps4_{E228Q}$–EGFP transfected or untransfected, were separated on Optiprep gradients, eight fractions were taken from top to bottom of the gradient and analyzed by western blotting, using antibodies directed against Hrs, Tsg101, Aip1/Alix, the cytosolic protein 14-3-3γ that appears as three bands on SDS gels (arrows) and the membrane protein transferrin receptor (Tfr).

3.1.5 ESCRT proteins are loosely associated with membranes

We next sought to study the membrane association of ESCRT proteins biochemically. As the four ESCRT subunits tested were found mostly on membranes by EM but had no membrane-spanning domains, we expected them to be only loosely associated with membranes. The extent of membrane binding was therefore tested using membrane flotation of non-detergent HeLa lysates. HeLa cells were mechanically homogenized, nuclei were gently spun down and post-nuclear supernatants were subjected to membrane flotation. Gradient fractions were then collected from top to bottom and analyzed by western blotting using three of the four selected antibodies (Figure 12 C). As expected, the majority of ESCRT proteins was detected in the bottom (cytosolic) fractions of the gradient, together with the cytosolic 14-3-3 protein, (Figure 12 C, left panel). Only a minor fraction was found in the top (membrane) fraction, together with the transmembrane protein transferrin receptor (Tfr). Importantly, transfection of HeLa cells with $Vps4_{E228Q}$-EGFP, which is believed to lock ESCRT complexes onto membranes, did not significantly increase the membrane-bound fraction of ESCRT proteins, although transfection efficiency was above 50%, as determined by direct fluorescence microscopy (data not shown). We concluded that ESCRT proteins were lost from membranes during mechanical lysis, indicating that they were only loosely associated with membranes.

3.1.6 Proteins of the ESCRT machinery localize predominantly to tubular-vesicular endosomal membranes

The four ESCRT proteins were next localized in detail by immuno-EM. Primary macrophages were used predominantly, because the endosomal compartment of these cells could readily be filled with BSA gold. However, since typical MVBs were sparse in macrophages, we also localized ESCRT in MT4 cells, in which this endosomal structure is more prominently seen.

Consistent with the observations by Sachse et al. [113], anti-Hrs readily labeled early endocytic structures that were filled with 5nm BSA gold fed to cells 10 min before fixing (Figure 13 A-D). Furthermore, in agreement with their observations, we also found Hrs associated with a conspicuous membrane coat, which has previously been implicated in the recruitment of ubiquitinylated proteins (Figure 13 A, B). Hrs was, however, predominantly found on membranes continuous, or close

to early endosomes (Figure 13 C, D). Although mostly associated with early endosomal membranes, significant labeling for Hrs was also found on late endosomes (Figure 13 G) in particular on the tubular-vesicular membranes continuous with or closely apposed to late endosomes (Figure 13 E-G).

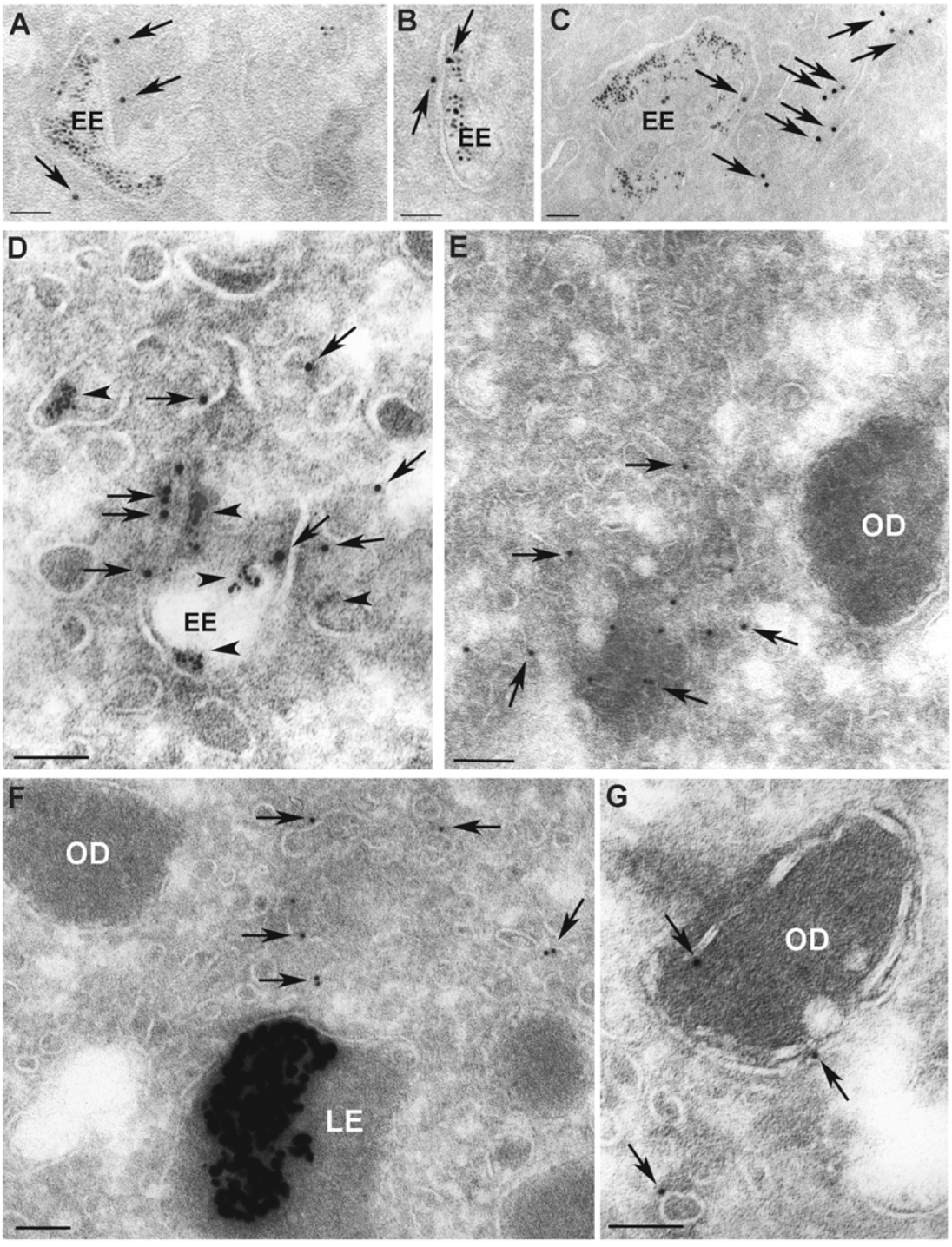

Figure 13. Ultra-structural localization of Hrs in primary human macrophages.
Primary macrophages were fed for 90 min with BSA coupled to 16nm gold particles followed by a chase overnight. Before fixing, macrophages were fed for 10 min with 5nm BSA gold to fill early endosomes (EE). As mentioned in figure 8 E, under these conditions 16nm BSA gold accumulates in late endosomes/lysosomes (LE) but not in the oval-shaped dense amorphous structures (OD) of late endocytic origin. (A)-(D): Hrs (arrows) localizes to early endosomes (EE) abundantly filled with 5 nm BSA gold. In (A) and (B), anti-Hrs labeled an electron-dense coat on early endosomes. In (C) and (D), Hrs was found on the gold-filled early endosomes as well as on tubular-vesicular membranes close by (arrows). (E) to (G) show several oval-shaped dense structures (OD) and (F) one late endosome/lysosome (LE) that is filled with 16nm BSA gold. Low labeling for Hrs (arrows) was found on the oval-shaped dense structures as shown in (G), but more abundant labeling was found on tubular vesicular membranes next to these structures and next to late endosomes. Bars-100nm.

We next performed double-labeling experiments to confirm that the tubular vesicular membranes were of endocytic origin. Both on the 'early' (not shown) and 'late' tubular-vesicular membranes Hrs was found to co-localize with Tfr (Figure 14 A and B), indicating that these membranes might be part of recycling endosomes. Because the 'late' tubular-vesicular membranes were generally inefficiently filled with BSA gold and often closely apposed to the Golgi complex, we suspected that some of these membranes belonged to the trans-Golgi network (TGN) rather than late endosomes. By EM, TGN markers (TGN46, GRP94) invariably labeled the TGN as well as endocytic organelles and were therefore not suitable to unequivocally solve this question (data not shown). We therefore chose to use SA48 HeLa cells, which stably express sialyl-transferase (ST) tagged with a vesicular stomatitis virus G protein epitope that can readily be detected with the monoclonal antibody 'P5D4'. The tagged ST has previously been shown by EM to localize predominantly to the TGN [98]. In SA48 cells, Hrs showed only limited co-localization with the TGN marker, and the majority of Hrs was on tubular-vesicular membranes located some distance away from the labeled TGN (Figure 14 C), suggesting that these membranes were not part of the TGN.

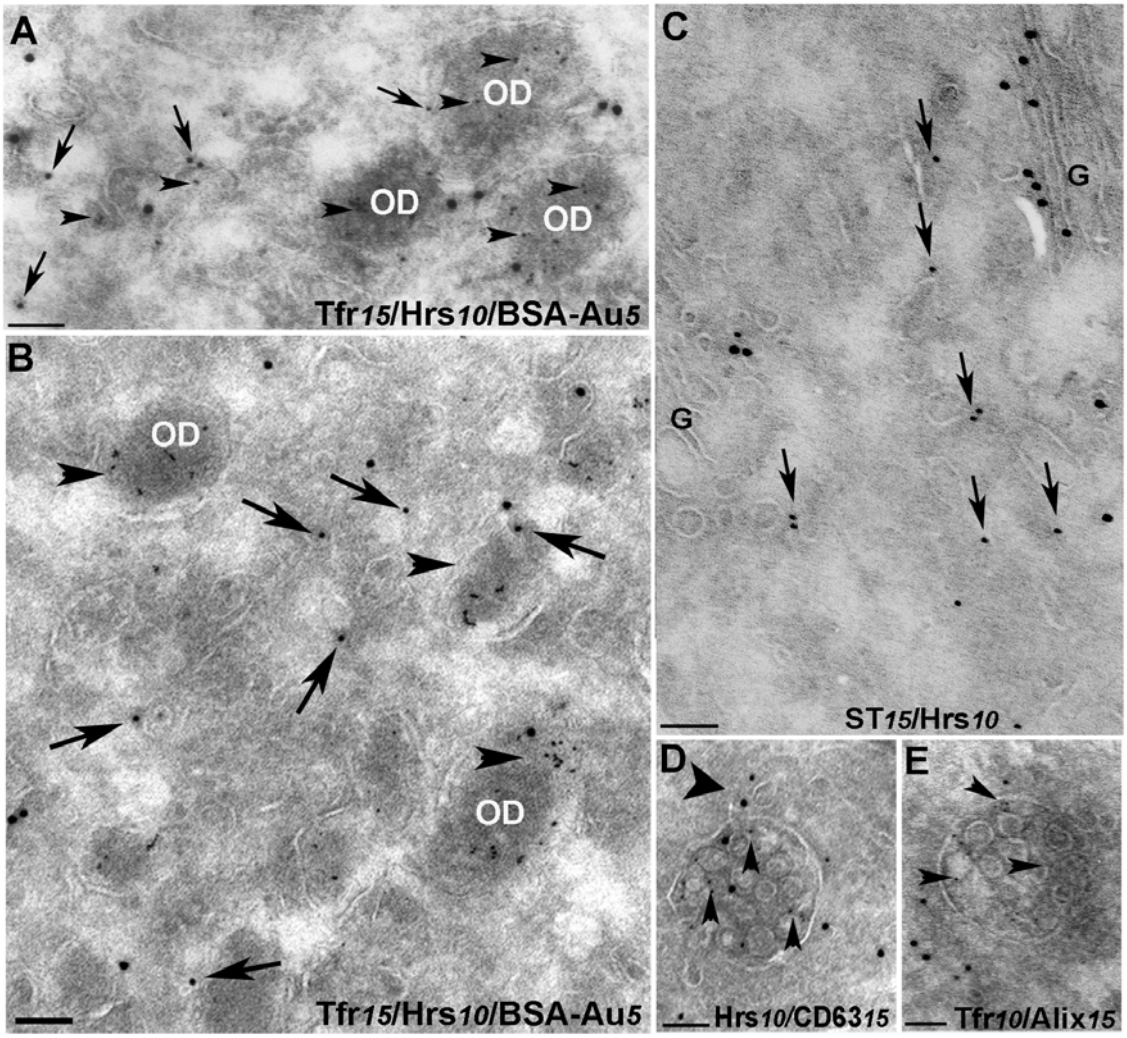

Figure 14. Double labeling experiments with anti-Hrs or anti-Aip1/Alix with anti-Tfr, P5D4-tagged sialyl-transferase (ST) and anti-CD63.
(A) and (B) Primary macrophages were fed with 5nm BSA gold (arrowheads) for 30 min followed by a 30 min chase period. The sections were then double-labeled with anti-Hrs (10nm gold, arrows) and anti-Tfr (15nm gold, not indicated). Both images show several oval-shaped dense structures (OD) filled with internalized BSA gold that are also labeled with both antibodies. Co-localization of Hrs and Tfr is also found on the tubular vesicular membranes next to the late endocytic structures. In (C) SA48 HeLa cells were double-labeled with the P5D4 monoclonal antibody (15nm gold, representing ST tagged with the VSV-G epitope) and anti-Hrs (10nm gold, arrows). Note that Hrs is found apposed to the TGN-region but shows only limited co-localization with ST. (D) and (E) show two typical MVBs in MT4 cells that were fed for 40 min with 5nm BSA gold (arrowheads). (D) Double-labeling for Hrs (10 nm gold) and CD63 (15nm gold). In (E) the section was double-labeled with anti-Tfr (10nm) and anti-Aip1/Alix (15nm) showing that membranes close to the MVB, but not the MVB itself are labeled for both proteins. The large arrowhead in (D) indicates labeled membranes continuous with the MVB. G-Golgi complex. Bars-100nm

We found a very similar labeling pattern for Tsg101, Aip1/Alix (Figure 15 A-D) and Vps4B (not shown) with the exception that these three proteins were more associated with late endocytic structures. Significant labeling for Tsg101 and Aip1/Alix was found on late endosomes (Figure 15 B and D), but the labeling was more frequently detected on the tubular-vesicular membranes located between late endosomes and the Golgi stack (Figure 15 A, B and C). We also used MT4 cells to determine whether ESCRT specifically localized to MVBs. As described above, after 40 min. of incubation with 5nm BSA gold, MVBs but not late endosomes/lysosomes were filled with BSA gold in these cells and this condition was therefore used to localize ESCRT. All four antibodies displayed only low labeling on gold-filled MVBs; instead the labeling for ESCRT was more often associated with membranes close to or in continuity with MVBs rather than MVBs themselves (see figure 14 D and E).

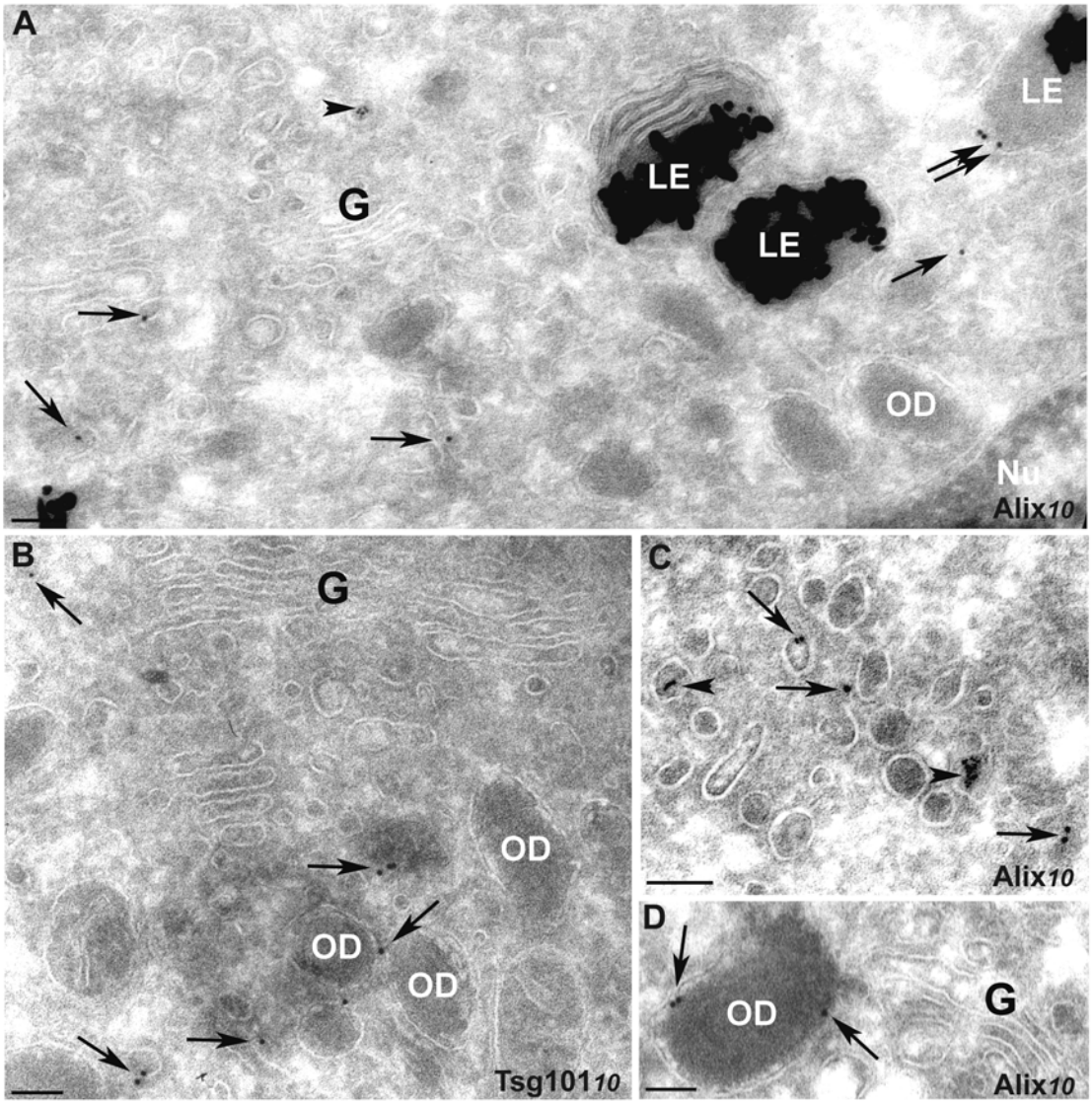

Figure 15: Localization of Aip-1/Alix and Tsg101 in primary macrophages.
In all images primary macrophages were fed with 16 nm and 5 nm BSA-gold (5nm gold is indicated with arrowheads in (A) and (C)) as described in figure 8 E. (A), (C) and (D) Sections labeled with anti-Aip-1/Alix (10nm gold, arrows). (A) shows an extended region with one oval-shaped dense structure (OD) and several late endosomes/lysosomes (LE), closely apposed to a Golgi stack (G). Aip1/Alix was found on the endosomes as well as on tubular-vesicular membranes next to the late endosomes and the Golgi complex. In (B) the section was labeled with anti-Tsg101 (10nm gold arrows) and shows oval-shaped dense structures (OD) close to a Golgi stack (G). Labeling was seen on the dense structures as well as on tubular vesicular membranes closely apposed to these structures. (C) Endosomal vesicles, most likely of early endocytic origin (internalized 5nm gold indicated with arrowheads), labeled with Aip-1/Alix. (D) An oval-shaped dense structure labeled with anti-Aip-1/Alix closely apposed to a Golgi stack (G). Nu-nucleus. Bars-100nm.

Our observations suggested that Hrs localizes predominantly to the early endocytic pathway, while the other three proteins were preferentially associated with domains of late endocytic compartments. To confirm this qualitative impression, we quantified the relative distribution of Hrs and Aip1/Alix over different intracellular membranes in both macrophages and MT4 cells (Table 3). This confirmed that the majority of Hrs was associated with the early endocytic pathway, representing 34-38% of the total labeling. For Aip1/Alix only 10-20% of the label was on early endocytic membranes, whereas 35-40% was associated with late endocytic compartments.

	MT4		**macrophages**	
cellular structure	(%) Hrs[1]	(%) Aip1/Alix	(%) Hrs	(%) Aip1/Alix
plasma membrane	17.2	19.5	7.1	6
early endosome	8.2	1.6	13.5	8.7
early endosome associated	26.2	7.9	24.8	10.5
total early endosome[2]	34.4	9.5	38.3	19.2
late endosome	1.6	8.8	5.4	13.3
late endosome associated	8.8	26.5	13.5	26.2
total late endosome[2]	10.4	35.3	18.9	39.5
MVB	1.8	2.9	n/d[3]	n/d[3]
TGN	3.6	2	4.7	3.9
mitochondria	6.6	6.8	5.3	6
ER/nuclear envelope	5.8	5.9	4.5	2.8
cytosol	12.7	12.8	9.6	9.2
unidentified membranes	7.6	5.4	4	5.9

Table 3. Intra-cellular distribution of Hrs and Aip1/Alix in MT4 cells and human macrophages.

[1] On two different grids from two different labeling experiments, with either anti-Hrs or anti-Aip1/Alix, a total of 200 gold particles per grid were allocated to the cellular structures indicated on the left. In the case of MT4, cells were fed for 40 min with 5nm BSA-gold as described in the text. Quantification in macrophages was done on cells fed with 16nm and 5nm BSA-gold as described in figure 8E. The numbers were obtained by dividing the number of gold particles found on each cellular structure by the total gold particles counted.

[2] Total early/late endosome is the sum of the percentage on early/late endosomes and on membranes associated with early/late endosomes.

[3] n/d: no MVBs were detected in sections of primary human macrophages.

3.1.7 HIV-1 infection does not alter ESCRT localization

Analysis of uninfected T-cells and macrophages revealed that proteins of the ESCRT machinery were enriched at the proposed site of HIV budding, the plasma membrane of T cells and endosomes in macrophages, respectively (see figure 9). This suggested that the endogenous ESCRT pool located at the respective proposed site of budding may suffice for HIV-budding and that this complex might not be recruited to the site of HIV release. All three cell types, MT4 cells, primary human CD4+ T cells and macrophages were therefore infected with HIV-1, and ESCRT proteins were quantified as described above. Infected cells were identified based on their labeling with an antibody against the HIV-1 CA protein and by detection of typical budding profiles and virus particles (for an example, see figure 17 A-F). The MT4 cell line was particularly useful for this quantitative analysis as these cells express high levels of viral antigen and exhibit many budding profiles at the cell surface (Figure 17 B-D). Thus, a redistribution of ESCRT proteins should be easily seen in these cells.

Quantification of antibody labeling to ESCRT proteins showed, however, that HIV-1 infection did not affect the intracellular distribution of ESCRT in any of the three cell-types (Figure 16 A-C, compare to Figure 9 A-C). The percentage of labeling attributed to either the plasma membrane or endosomes (representing the membranes relevant for HIV-1 budding in T cells and macrophages, respectively) was directly compared in uninfected and infected cells (Figure 16D). This comparison revealed that the relative amount of labeling for each of the four antigens increased or decreased by only 1-6%.

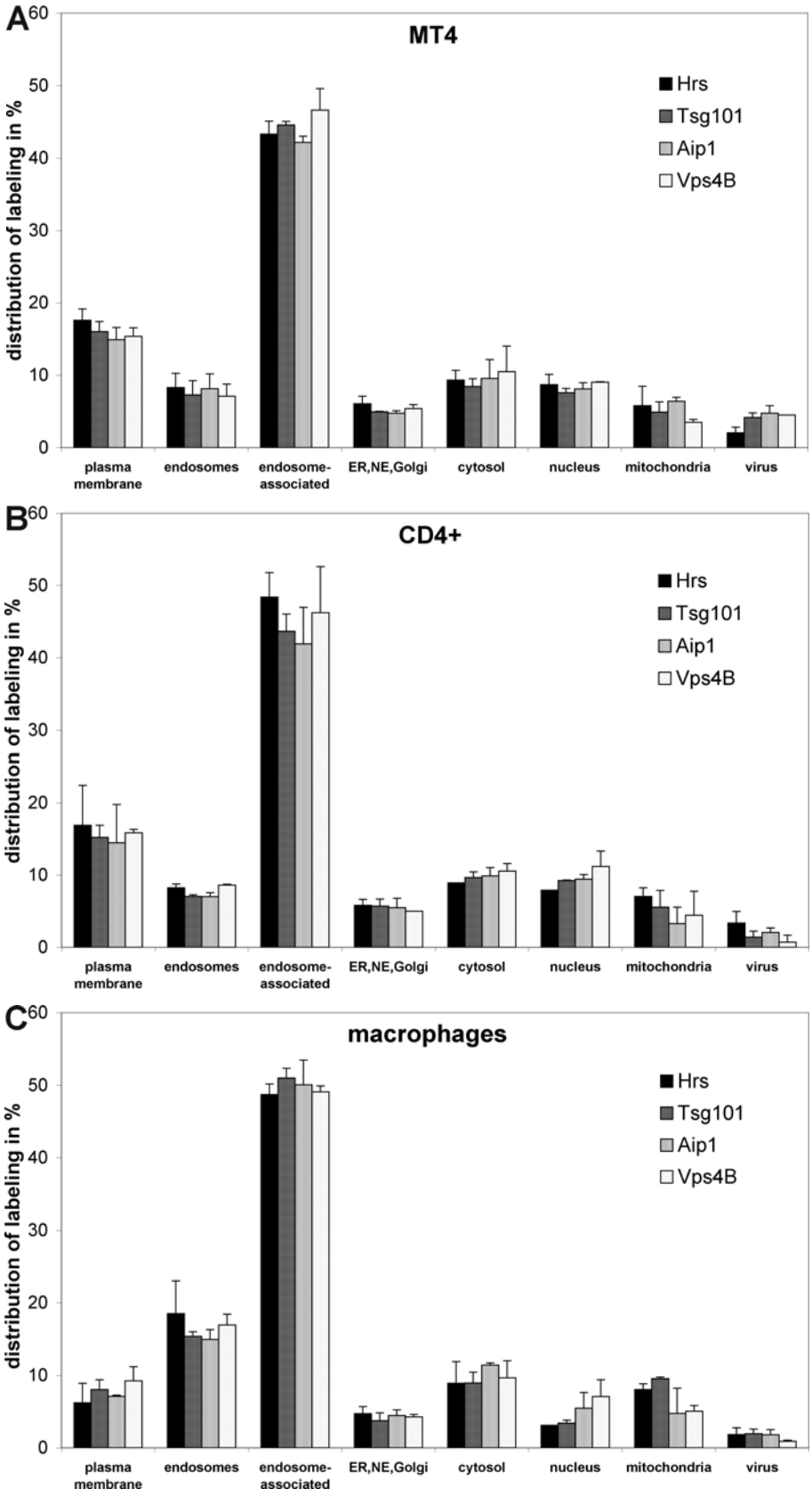
A
MT4
distribution of labeling in %
0
10
20
30
40
50
60
Hrs
Tsg101
Aip1
Vps4B
plasma membrane
endosomes
endosome-associated
ER,NE,Golgi
cytosol
nucleus
mitochondria
virus
B
CD4+
distribution of labeling in %
0
10
20
30
40
50
60
Hrs
Tsg101
Aip1
Vps4B
plasma membrane
endosomes
endosome-associated
ER,NE,Golgi
cytosol
nucleus
mitochondria
virus
C
macrophages
distribution of labeling in %
0
10
20
30
40
50
60
Hrs
Tsg101
Aip1
Vps4B
plasma membrane
endosomes
endosome-associated
ER,NE,Golgi
cytosol
nucleus
mitochondria
virus

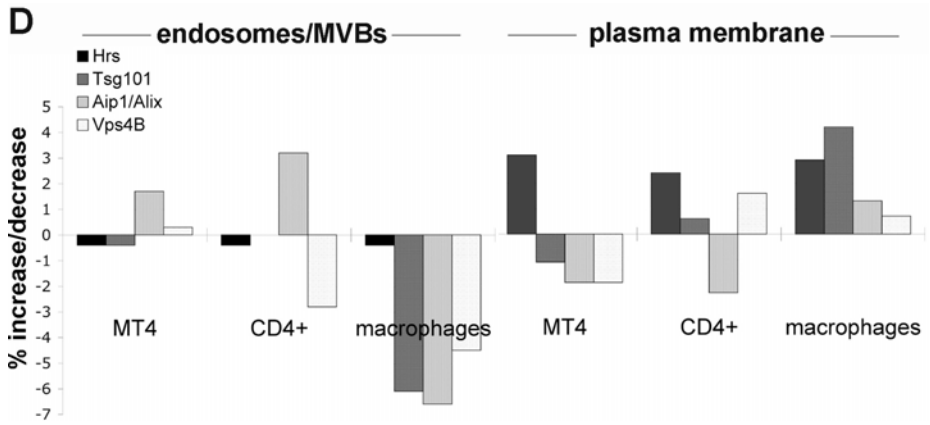

Figure 16: Quantification of the localization of ESCRTsubunits in HIV-1 infected cells by EM.
Thawed cryosections of HIV-1-infected (A) MT4 cells, (B) Primary human CD4+ lymphocytes and (C) Primary human macrophages were labeled with the same antibodies and subjected to the same quantification procedure as described in figure 9. The data in primary T cells and macrophages represent the average of values obtained from two different donors in infected cells. (D) Increase or decrease of ESCRT labeling on the plasma membrane and endosomes of uninfected and infected cells. Values represent relative labeling of the plasma membrane and endosomes in infected cells (figure 16A-C) minus labeling in uninfected cells (figure 9A-C) on the same two compartments.

Importantly, all four antibodies labeled HIV-1 budding profiles (Figure 17 C, D, and data not shown) and extracellular virions (Figure 16 A-C). This confirmed a previous study, biochemically showing incorporation Tsg101, Aip1/Alix and Vps4B into virus particles [50]. Thus, although ESCRT subunits were incorporated into budding virions, we could not provide any evidence that they were specifically enriched at, or relocated to, the site of virus budding. This suggested that on those membranes that are relevant for HIV-1 budding the endogenous pool of ESCRT is sufficient for virus release.

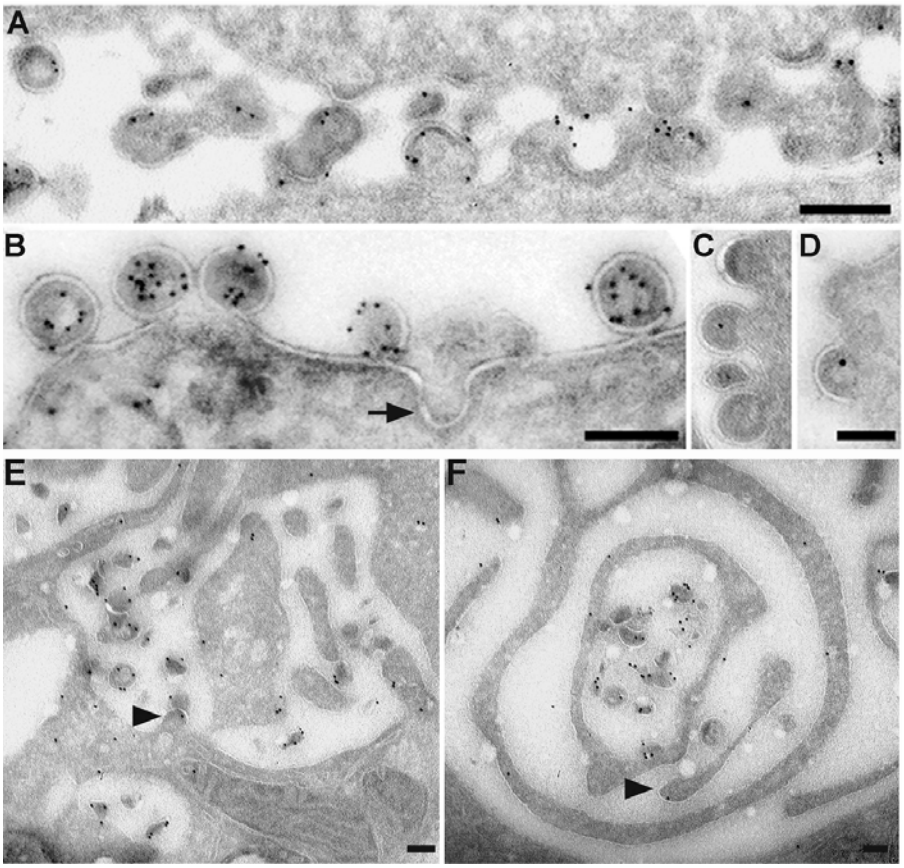

Figure 17: HIV-1 budding in T cells and macrophages.
(A, B) Cryosections of HIV-1-infected primary T cells (A) or MT4 cells (B) showing HIV budding profiles and virus particles at the cell surface labeled with anti-CA and next to a clathrin coated pit (arrow). (C, D) Cryosections of infected MT4 cells labeled with anti-Hrs (C) or anti-Tsg101 (D). (E, F) Cryosections of HIV-1-infected primary macrophages showing virus particles and putative budding profiles (arrowheads) labeled with anti-CA. Bars-200nm (A-D), 100nm (E, F).

HIV-1 was previously proposed to bud primarily on the plasma membrane of T cells and on endosomes in macrophages (see below). Therefore, the differential distribution of ESCRT subunits in T cells and macrophages suggested that ESCRT localization determined the site of HIV-1 budding in these two cell types. In agreement with this, we found that in MT4 cells and in primary T cells budding profiles localized almost exclusively to the cell surface (Figure 17 A-D), frequently next to clathrin-coated pits (Figure 17 B, arrow). In contrast, the site of HIV-1 budding in macrophages was more difficult to determine (figure 17 E, F). Virus particles and viral budding profiles were frequently found on membranes that could not unequivocally be assigned to either the cell surface or endosomes of macrophages

(Figure 16 E, F). Therefore, the site of HIV budding in macrophages was characterized in detail in the second part of this work.

3.2 HIV-1 budding in primary human macrophages

During our above described analysis of HIV-1 infected T lymphocytes and macrophages by immuno EM, we qualitatively observed that in macrophages, virus particles accumulated in the extracellular space (as in T cells) as well as in cytoplasmic vacuolar structures (Figure 17 E, F). Budding also seemed to occur from both the cell surface and vacuolar membranes in these cells. Localization of viral structures to the cell surface of macrophages was unexpected, since earlier studies showed that HIV-1 particles predominantly accumulated in intracellular compartments of monocytes/macrophages [18, 20-27]. Two widely recognized recent studies suggested that this intracellular compartment was of endocytic origin [28, 29]. In the latter studies, it was proposed that in macrophages HIV-1 budded and accumulated in late endosomes from where the virus could be released into the extracellular environment via exocytosis. This obvious discrepancy with our observations prompted us to study the site of HIV budding and accumulation in macrophages in detail.

3.2.1 HIV-1 budding structures and particles are found on the cell surface and in intracellular vacuoles

To characterize budding and release of HIV-1 in detail by electron microscopy (EM), cultures of primary human macrophages were infected with either of the macrophage-tropic HIV-1 strains Ba-L or YU-2 [101]. Virus release into the culture supernatant was monitored by p24 ELISA and cells were fixed when the p24 values in the supernatant had reached a plateau, typically around 12 to 17 days post-infection (data not shown). Cells were then fixed and either processed for immuno-EM or embedded in epoxy resin (Epon). To get an overview of macrophage morphology and localization of virus particles and budding sites, Epon embedded samples were first examined. Epon embedded sections allow morphology-based identification of electron dense virus particles without further treatment such as immunolabeling. Therefore, 60 nm Epon sections were contrasted with lead citrate and examined by EM (Figure 18). In agreement with earlier studies, we found that macrophage profiles had diameters of around 20 to 50µm and a rather complex morphology with many cell surface protrusions, resembling lamellipodia or filopodia, and large cytoplasmic vacuolar structures (Figure 18 D, [24]). Early and late budding

profiles of HIV-1 were identified as typical crescent-shaped or round electron dense structures, respectively (Figure 18 A-C, arrowheads). This electron dense 'shell' most likely represented the main structural HIV-1 Gag protein. HIV-1 buds were seen both intracellularly (Figure 18A, B) and at the cell surface (Figure 18C). Immature and mature HIV-1 particles were also found both at the cell surface (Figure 18F) and in vacuolar structures (Figure 18E) and could be easily identified by their electron dense Gag shell or conical cores, respectively (Figure 18 E, F).

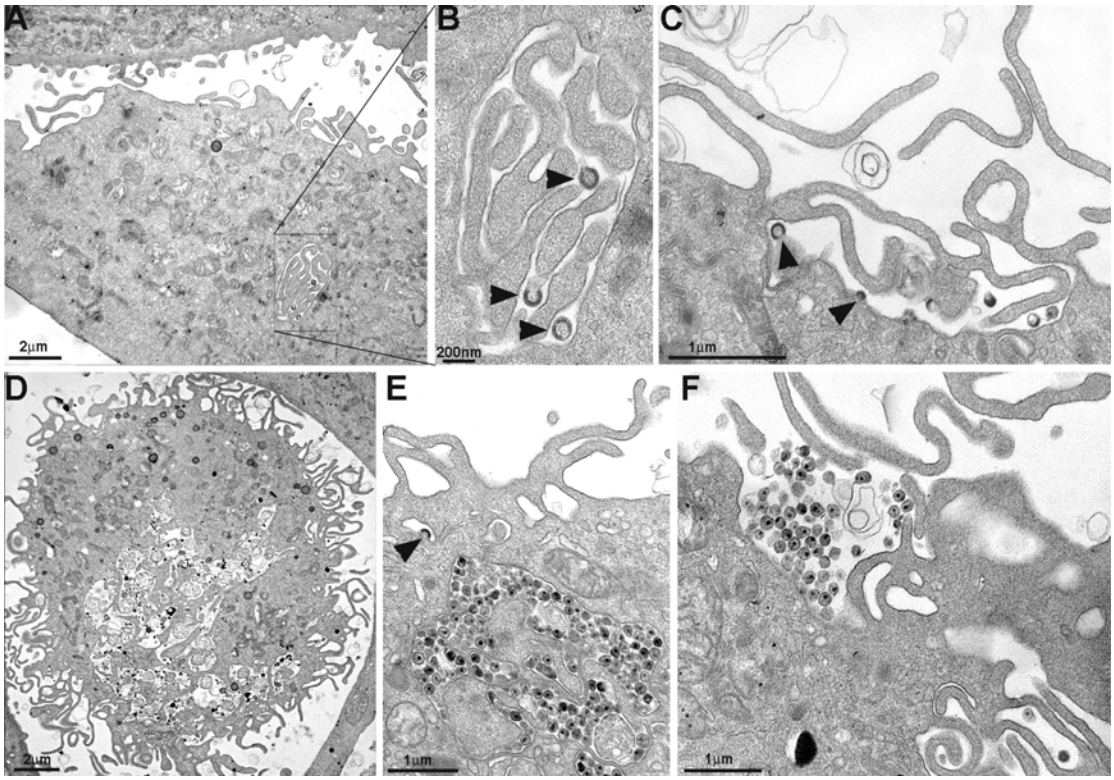

Figure 18: Overview of macrophage morphology and HIV localization in Epon-embedded samples.

Epon sections of primary human macrophages 17 days after infection with the HIV-1 Ba-L strain. (A) Vertical section through an infected macrophage. The flat bottom of the cell is in the left lower corner. (B) Magnification of the boxed area in (A), showing a vacuolar structure containing filopodia-like protrusions and three HIV-1 budding structures (arrowheads). (C) Typical cell surface organization of macrophages, displaying many long filopodia-like protrusions. On the cell surface several HIV-1 budding sites (arrowheads) are found. (D) Horizontal section through an infected macrophage with one or several large virus-filled structures. (E) Section through a large vacuole filled with mature virus particles. The small vacuolar structure contains an early virus bud (arrowhead). (F) Mature virions accumulating on the cell surface. Bars- 2µm (A, D), 1 µm (C, E, F), 200nm (B).

Epon sections are, however, not suitable for immuno labeling with antibodies. Thus, we next used immuno EM to identify viral structures based on their antibody labeling to extend our qualitative observations. Thawed 60 nm cryosections were labeled with an antibody to the viral Capsid (CA) protein to identify infected cells and virus particles. In agreement with the studies of Pelchen-Matthews et al. and Raposo et al. [28, 29], anti-CA labeled HIV particles were readily detected in large vacuoles, seemingly representing an intracellular compartment (Figure 19 A, B). Although the conical cores of mature HIV-1 particles were generally not detected in cryosections, mature virions could easily be identified by the lack of an electron-dense Gag shell. We noted that the limiting membranes of virus-containing vacuoles were often open to the extracellular space and resembled deep plasma membrane invaginations instead (Figure 19 C and F). The virus-filled vacuoles furthermore contained slender membrane protrusions, resembling lamellipodia of the cell surface (Figure 19 D). Finally, on their limiting membrane we frequently observed clathrin-coated pits (Figure 19 E, arrowhead), an endocytic structure that is unique to the plasma membrane. Thus it collectively appeared that at least a subset of the membranes enclosing the budded virions was plasma membrane-derived.

Whereas virus particles were readily seen on cryo-sections, budding profiles were much more rare (see below) and were seen on the vacuolar membranes (Figure 20 A) as well as on the plasma membrane (Figure 20 B-E; [30]. On both sets of membranes budding profiles often occurred next to clathrin-coated pits (Figure 20 A, B, E; arrowheads), again indicating that the limiting vacuolar membrane in such examples was cell surface derived.

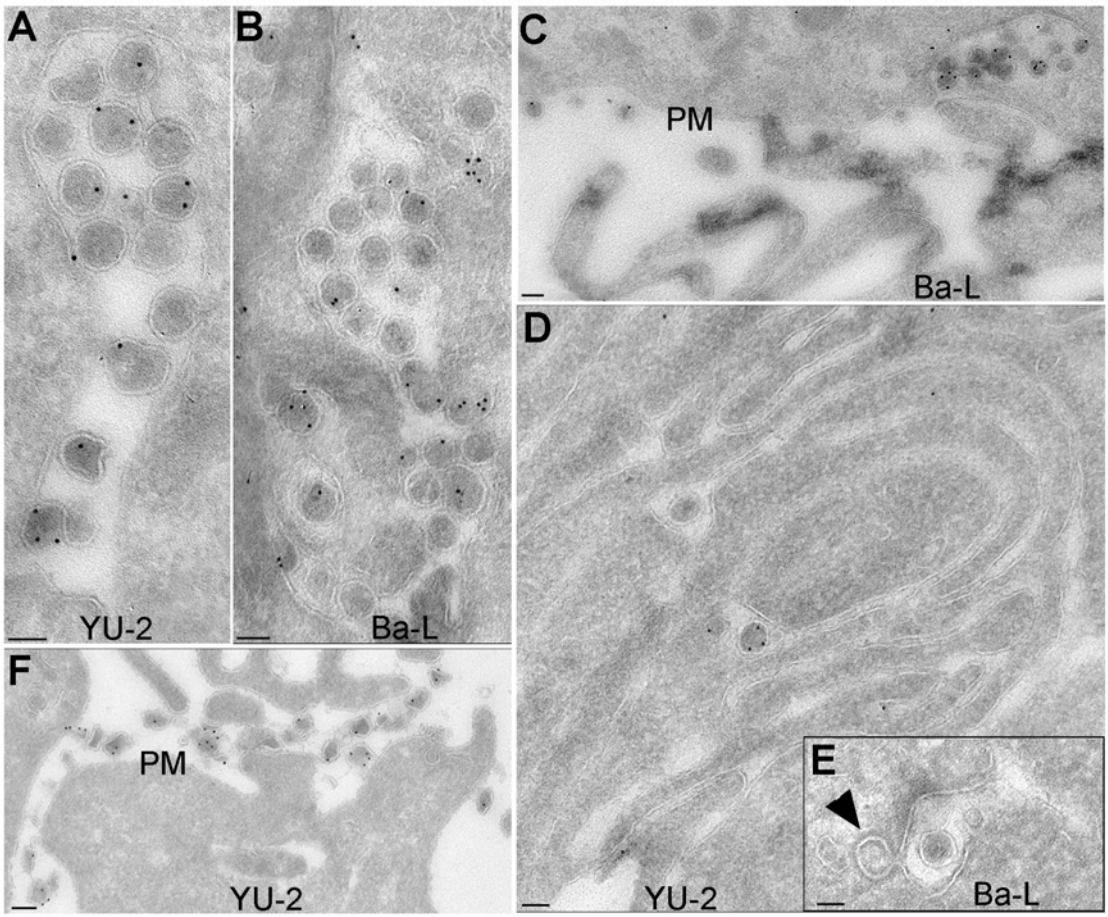

Figure 19. A gallery of primary human macrophages infected with HIV-1 strains YU-2 and Ba-L.
Primary human macrophages were infected with HIV-1 strain YU-2 (A, D, F) or Ba-L (B, C, E). Thawed cryosections were labeled with anti-Capsid antibody followed by 10nm (A-D, F) or 5nm (E) protein A gold. (A) and (B): labeled virions of both HIV-1 strains accumulate in identical looking vacuolar structures. With both strains, labeled virus is also found in plasma membrane invaginations that are directly connected to the extracellular space (C, F) or in vacuolar structures filled with filopodia-like protrusions (D). (E), a virus-containing vacuolar structure with a clathrin coated pit (arrowhead). Bar-100 nm.

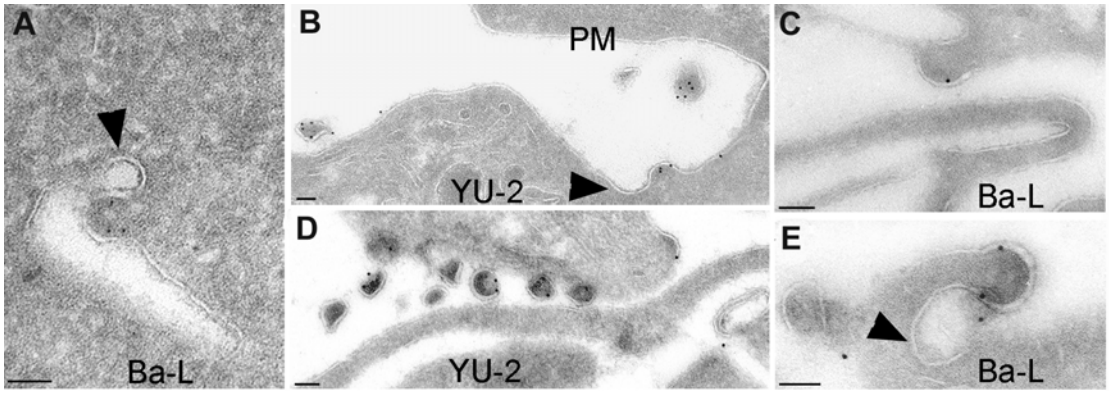

Figure 20. A gallery of budding profiles in primary human macrophages infected with HIV-1 strains YU-2 and Ba-L.
Primary human macrophages were infected with HIV-1 strain YU-2 (A, C, E) or Ba-L (B, D). Thawed cryosections were labeled with anti-Capsid antibody followed by 5nm (A) or 10nm (B-E) protein A gold. Virus budding profiles were found inside vacuolar structures (A) or on the cell surface (B- E). In (A, B, E), budding profiles are next to a clathrin coated pit (arrowheads). Bar-100 nm.

Sections of YU-2 and Ba-L infected macrophages were indistinguishable; with both strains viruses were seen to accumulate in vacuolar structures and budding profiles occurred both at the plasma membrane and at the vacuolar membrane. Replication kinetics for both virus strains were assayed by p24 ELISA and were similar ([100], data not shown). Generally, differences between samples, for instance in the percentage of infected cells, could be attributed to donor variability rather than to difference between the two virus strains (not shown). Throughout the remainder of this study we therefore focused on Ba-L infected macrophages only.

Collectively, we confirmed that in primary human macrophages HIV-1 particles bud into and accumulate in large vacuoles. However, whereas these HIV-1 filled vacuoles were previously proposed to be part of the endocytic pathway [28, 29], we found that at least a subset showed hallmarks of the plasma membrane.

3.2.2 BSA gold-uptake and Ruthenium Red stain to discriminate plasma membrane from endocytic compartments.

We next set out to define the plasma membrane and endosomes in primary macrophages. Our attempts to unequivocally discriminate cell surface and endosomal membranes by using immuno EM and antibodies directed against membrane marker proteins failed. We found that most, if not all, endosomal marker proteins were

distributed over several membranes of the endocytic pathway, including the plasma membrane (see section 3.2.4). Therefore, we decided to make use of a marker independent assay to discriminate endosomal membranes and the plasma membrane of macrophages. This assay is based on sequential marking of endosomes (by endocytic uptake of BSA gold beads) and the plasma membrane (by cell surface staining upon fixation) and was first established in uninfected macrophages.

Macrophages were starved in serum-free medium over night and incubated with BSA coupled to 10nm gold particles (BSA gold). At 37° C, BSA gold is readily taken up by fluid phase endocytosis and therefore marks the endocytic pathway. As shown in chapter 3.1.2, endocytic BSA gold uptake for 2 hrs before fixing leads to filling of at least 75% of all endocytic compartments including late endosomes/lysosomes in primary macrophages. After incubation for 2 hrs, the gold-filled cells were placed on ice to shut down their endocytic activity, washed well to remove excess BSA gold from the cell surface and fixed on ice in the presence of the cell surface stain Ruthenium Red (RR). RR is a membrane-impermeable compound that binds to the cell surface via carbohydrate moieties [108, 109]. Because of its small size, RR can readily penetrate into very small and slender membrane cavities at the cell surface [117], whereas fixation at 4°C prevented its internalization into endosomes. Upon post-fixation with osmium tetroxide (OsO_4), RR and OsO_4 form an electron-dense precipitate that is readily seen on Epon embedded sections [106, 107].

The RR-stain revealed an unexpected complex plasma membrane organization of macrophages (Figure 21); at low magnification the RR stain highlighted many finger-like protrusions at the cell surface (Figure 21 A, B and D). Filopodia from two neighboring cells often formed tight-fitting contact zones (Figure 21 A, arrows) where the RR stain was more electron dense than on single lipid bilayers. The RR-stain also decorated the limiting membrane of large vacuolar structures that were heterogeneous in size and shape (Figure 21 A-F). These contained a complex collection of RR-positive membranes, often resembling plasma membrane filopodia (Figure 21 D, E). Because on sections the RR-stained membranes appeared ‘closed’ and were often found in the peri-nuclear region (Figure 21 C, F), they could readily be mistaken for an intracellular compartment. We noted that a subset of identical looking vacuoles was not stained with RR (Figure 21 E). Since these were never filled with internalized BSA gold, they were obviously not of endocytic origin. Their failure to stain with RR

suggested that they were not directly connected to the cell surface or that they were inaccessible to RR for technical reasons. We noticed, for instance, that the plasma membrane and vacuoles located on the bottom of the cells that was attached to the substrate were not efficiently stained with RR.

BSA gold-filled endosomes (Figure 21 C, E) were always devoid of RR and were typically round or oval-shaped, rather homogenous in size, and significantly smaller than the RR-stained vacuoles. Finally, all other cellular structures such as the Golgi complex or the endoplasmic reticulum were neither labeled with RR nor filled with BSA-gold.

Collectively, the BSA-gold uptake and RR-stain enabled us to discriminate cell surface-derived membranes from endocytic compartments. The RR stain also revealed that human primary macrophages cultured *in vitro* display a complex plasma membrane organization, consisting of many protrusions and invaginations. The latter often resembled profiles of intracellular vacuoles on thin sections.

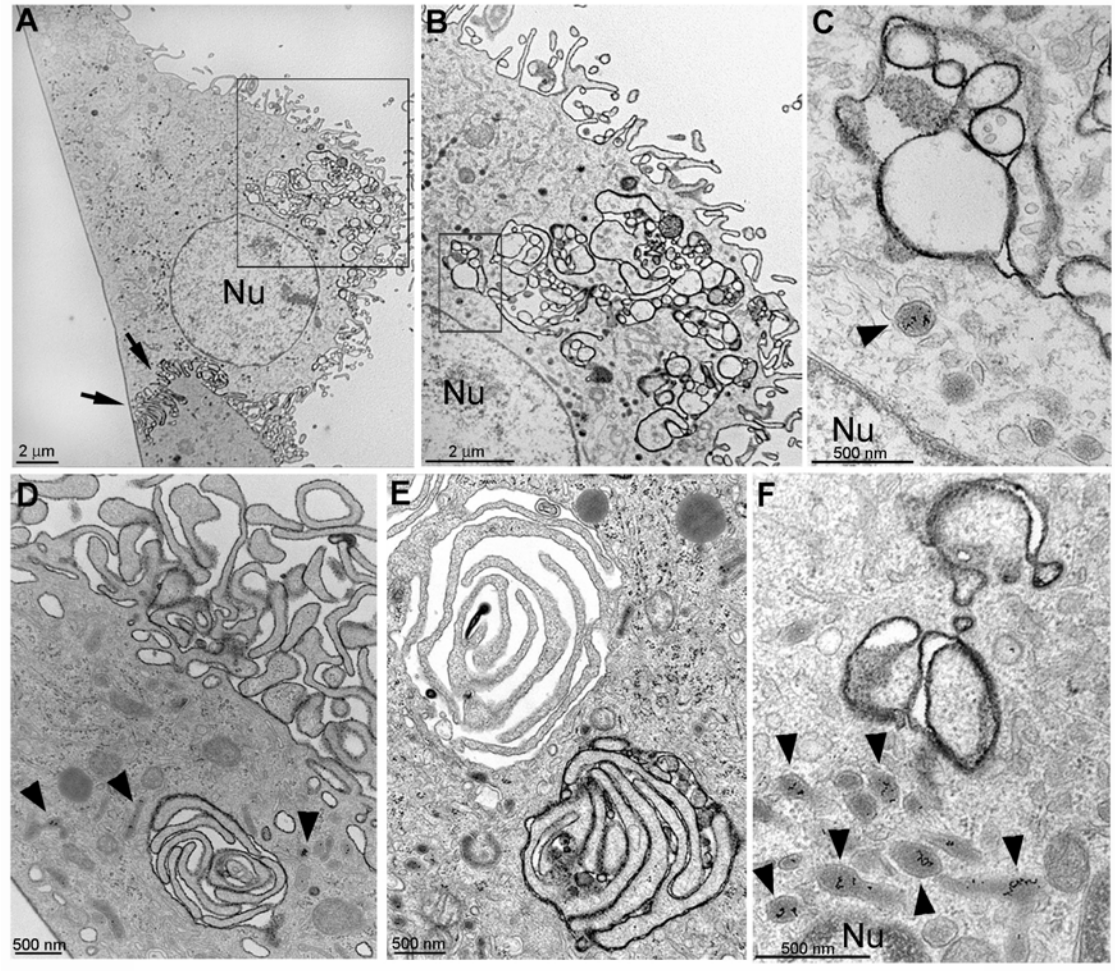

Figure 21. Ruthenium red staining of uninfected macrophages reveals a complex plasma membrane organization.
Primary macrophages were fed for 2 hrs with BSA gold particles, fixed on ice in the presence of Ruthenium Red (RR) and embedded in Epon. (A) Two cell profiles contacting each other, showing the organization of the RR-stained cell surface with many protrusions and RR-positive, seemingly intracellular, vacuolar structures close to the nucleus (Nu). At the tight-fitting contact zones between two cells (arrows) the stain appears more electron-dense than on single lipid bilayers. (B) Higher magnification of the boxed area in (A). It shows the collection of vacuolar structures stained with RR. (C) A higher magnification of the boxed area in (B) showing a RR-positive vacuole next to a BSA-gold filled endosome (arrowhead). (D) Shows a cell profile with many RR-positive filopodia at the cell surface. It also shows an area with RR-positive filopodia that appear intracellular in this section. Note that the BSA gold-filled endosomes (arrowheads) are significantly smaller than the vacuolar structures and that vacuoles have no internalized BSA gold. (E) Two filopodia-containing vacuolar structures. In the upper one the membranes are not RR stained, indicating that not all vacuoles are connected to the cell surface and accessible to the stain. (F) A collection of BSA gold-filled endosomes (arrowheads) next to RR-stained vacuolar structures. Bar-2μm (A, B), 500nm (C-F).

3.2.3 HIV-1 budding occurs on cell surface-derived membranes.

The RR-staining and BSA gold uptake method was next used to identify the origin of the membranes from which HIV-1 budded and that enclosed budded virions in primary human macrophages. Macrophages were differentiated *in vitro* for one week and infected with the macrophage-tropic HIV-1 Ba-L strain. As before, replication kinetics were evaluated by measuring HIV-1 CA amounts in the culture supernatants by ELISA, and cells were fixed and processed for EM at days 12 and 17 post infection (Figure 22A).

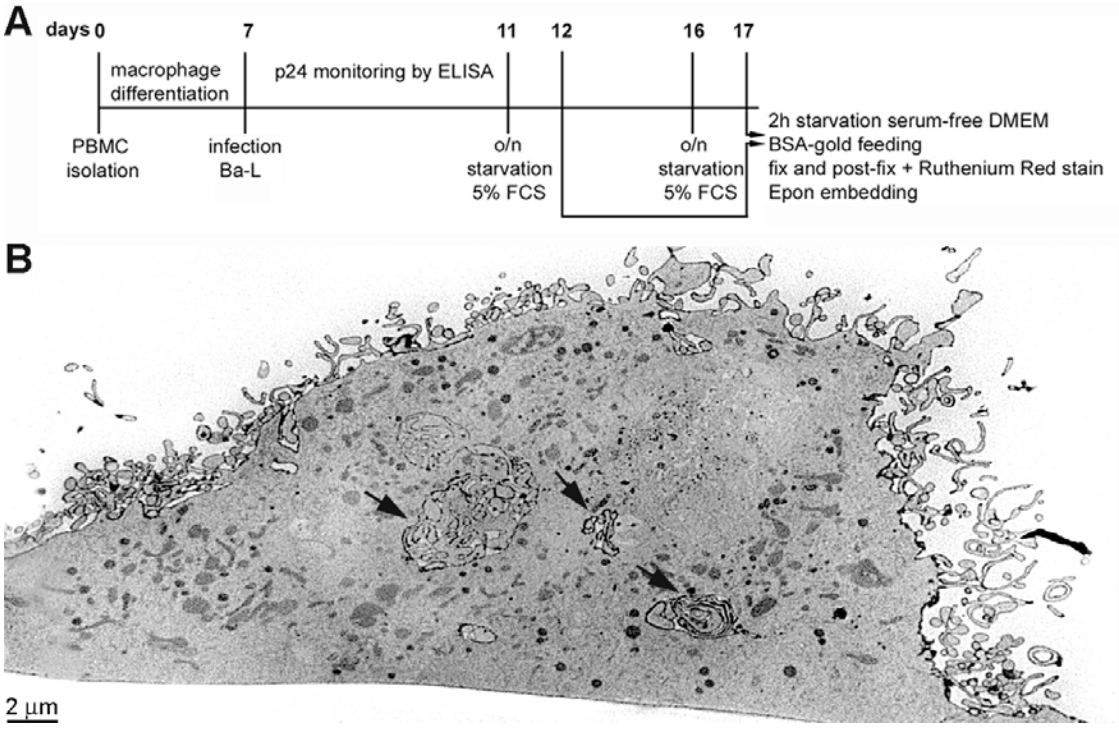

Figure 22: Overview of the experimental setup to discriminate plasma membrane and endosomes in infected macrophages.
Macrophages were infected with HIV-1 Ba-L and treated as described in Materials and Methods. (A) A flow diagram of the time course of macrophage differentiation, infection and processing for EM. (B) A cell profile of an infected macrophage at low magnification displaying a complex RR-stained plasma membrane organization and RR stained vacuolar structures (arrows) that contain virus particles. Bar-2µm.

As seen before in uninfected cells, cell profiles of Epon-embedded infected macrophages displayed complex RR-stained membrane structures, including numerous surface protrusions, invaginations and RR-positive vacuolar structures

(Figure 22 B, arrows), often filled with mature virus particles with a typical conical core, (23 A-C, E, F). These virus-filled vacuoles were devoid of BSA gold whereas their limiting membrane and the surface of the virions they enclosed, were stained with RR (Figure 22 B, C; 23 A-C, E, F), clearly showing that they were directly connected to the cell surface. We also noted that many of the RR-positive virus-containing vacuoles contained plasma membrane-like filopodia (Figure 23 C, J) and that their limiting membrane displayed clathrin-coated pits (Figure 23 E, F, arrows), supporting the fact that they were cell surface-derived.

Consistent with the RR-staining of uninfected macrophages, we found that not all virus-containing vacuoles were stained with RR (see, for instance, Figure 23 J). Such RR-negative vacuoles did not contain BSA-gold excluding the possibility that they were part of the endocytic pathway (Figure 23 J). Instead, gold-filled endosomes appeared significantly smaller, more homogenous in size and never contained virus particles (Figure 23 B, D, E, G, and K, arrowheads).

To substantiate this obvious size difference, we estimated the average profile area of the virus-filled vacuoles and BSA gold-filled endosomes in cells of three individual blood donors (Figure 24 A). The average profile area of gold-filled endosomes was only 0.08μm^2, corresponding to an average diameter of 0.28μm. This value corresponded well to previously published data on the size of the central vesicular elements of endosomes [84]. In contrast, the average profile area of virus-filled vacuoles was 10 to 60 times bigger, between 1 and 3.1μm^2 (Figure 24A). Strikingly, this value corresponded well to the size of HIV-containing vacuoles observed in previous studies (Figure 24A; [28, 29]. Whereas in the latter studies the virus-filled vacuoles were suggested to be of endocytic origin, our data now indicate that they are identical to RR-stained vacuoles representing plasma membrane invaginations.

Budding profiles were either found on the cell surface (Figure 23 H) or on RR-positive (Figure 23 I) and RR-negative vacuolar-like membranes (Figure 23 J, K). They were furthermore found on the tip of filopodia-like protrusions, frequently inside the vacuolar structures (Figure 23 J, arrow).

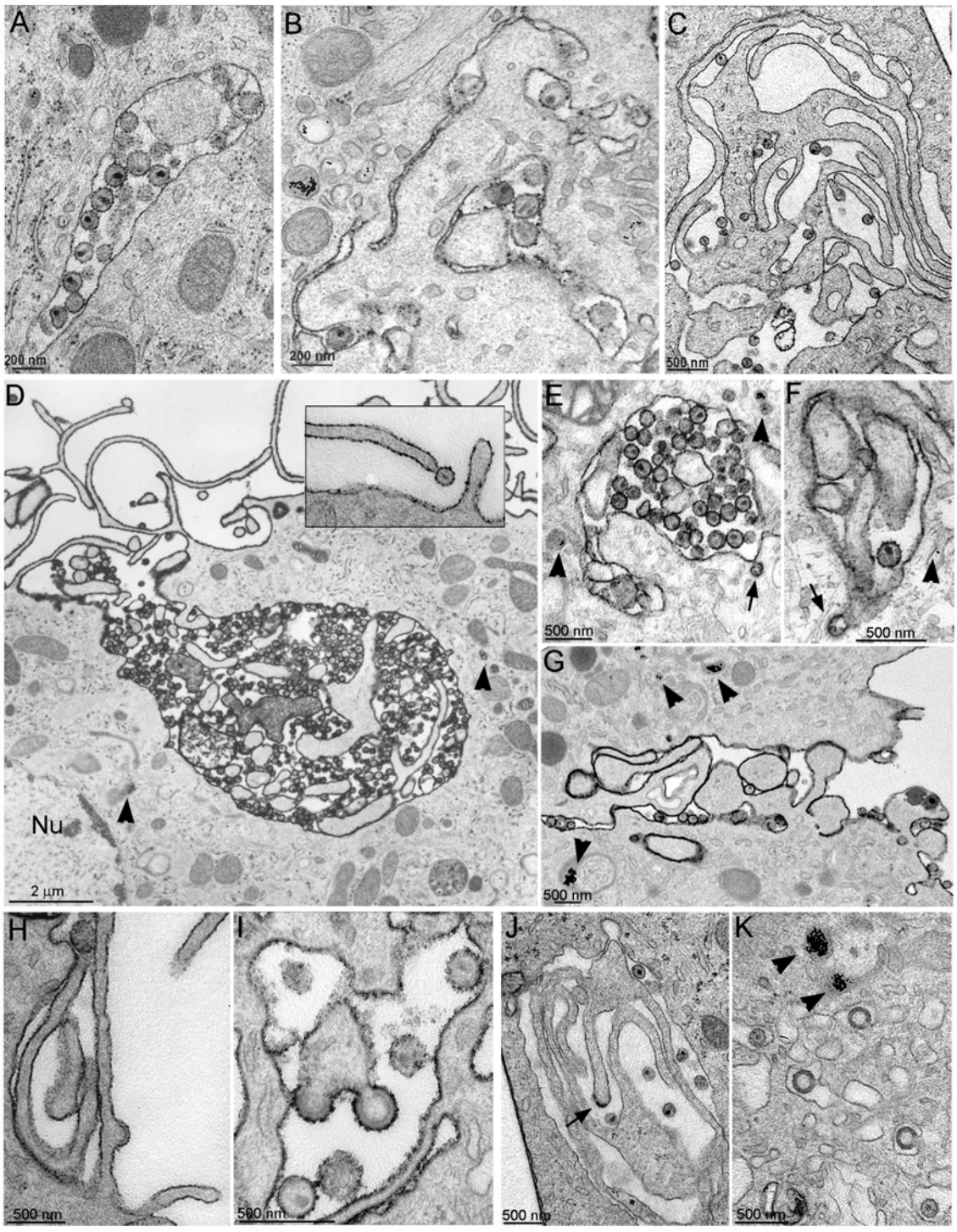

Figure 23. HIV-1 buds into and accumulates in ruthenium red-stained domains.
Macrophages were infected with HIV-1 Ba-L and treated as described in figure 22 and in Materials and Methods. (A) and (B) show virus-containing structures that are apparently intra-cytoplasmic but are stained with RR. (C) Shows a collection of RR-stained filopodia interspaced by RR- stained mature virus particles. In (D) a large vacuolar structure that is directly connected to the RR-stained cell surface and contains numerous RR-stained virions.

The inset shows a mature virus particle on the tip of a finger-like plasma membrane protrusion. (E) and (F) are two RR-stained vacuolar structures that contain virus particles and that display clathrin-coated pits (arrows). The arrowheads indicate gold-filled endosomes that are not RR-stained. (G) RR-stained virus particles that accumulate between the plasma membranes of two neighboring cells. Arrowheads indicate BSA gold-filled endosomes without RR stain. (H) to (K) Budding profiles are found on the RR-stained cell surface (H), on RR-stained vacuolar structures (I) or on vacuolar structures that are devoid of RR and BSA gold (J, K). The arrow in (J) indicates an early viral bud on the tip of a finger-like protrusion. Arrowheads in (K) mark BSA gold-filled endosomes. Nu- nucleus. Bar-200nm (A, B), 2μm (D), 500nm (C, E-K).

Our qualitative observations of the localization of viral structures (as depicted in figure 23) were next analyzed in a quantitative manner (Figure 24 B). To this end, cells from three different donors were analyzed. Free virus particles and budding sites were assigned to either of three categories, i) on RR positive, BSA gold negative membranes (RR+ BSA gold-), ii) on membranes without both markers (RR- BSA gold-) and iii) on membranes lacking RR but with the endocytic marker (RR- BSA gold+). This quantification revealed that over 94% of all viral structures were found on RR stained membranes or in vacuolar structures that were devoid of internalized gold and that were in the majority of the cases stained with RR (Figure 24 B). Only few viral structures were seen in vacuoles containing BSA gold. As mentioned above, the number of free virus particles largely exceeded the number of budding profiles and 91 to 97% of the viral structures was immature or mature virus (Figure 24 B). We nevertheless quantified budding profiles seen over the above-mentioned membrane types in macrophages derived from the same three donors (Figure 24 C). Virtually all of the budding profiles (98-100%) were counted on the RR stained cell surface or on vacuolar membranes that were either RR-positive or RR-negative (but were morphologically indistinguishable) and were devoid of internalized gold (Figure 24 C). We also found two budding profiles on structures that contained BSA-gold (one event each for donor 1 and 3). However, in these two examples the gold-containing structures did not look like typical endosomes and their gold-content likely resulted from an incomplete wash-off of the fluid phase marker from the cell surface.

These data strikingly show that in primary human macrophages, HIV-1 budding occurs predominantly on cell surface derived membranes rather than on endosomal membranes.

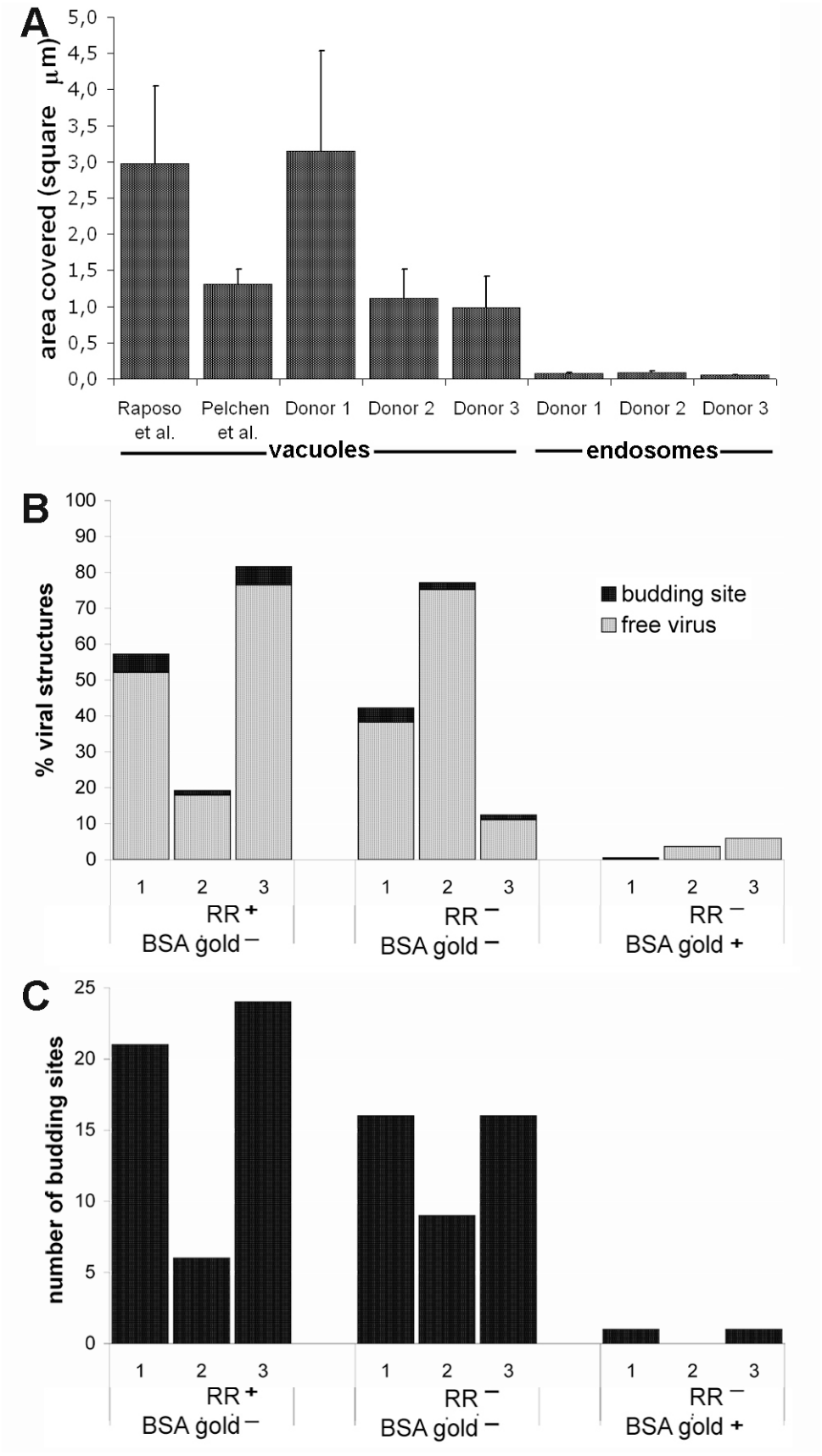
A
area covered (square µm)
5,0
4,5
4,0
3,5
3,0
2,5
2,0
1,5
1,0
0,5
0,0
Raposo et al.
Pelchen et al.
Donor 1
Donor 2
Donor 3
Donor 1
Donor 2
Donor 3
vacuoles
endosomes
B
% viral structures
budding site
free virus
RR +
BSA gold –
RR –
BSA gold –
RR –
BSA gold +
C
number of budding sites
RR +
BSA gold –
RR –
BSA gold –
RR –
BSA gold +

Figure 24: Quantification of the membrane compartments where HIV-1 accumulates and buds.
Infected macrophages were infected and processed as described in figure 22. (A) Quantification of the average profile area of virus containing vacuoles and BSA gold-filled endosomes. The average profile area of virus-filled vacuoles in the left panel is based on the images of figure 1A,B; 2A; 3A-C in the publication by Raposo et al., the figure 3A-D; 4A,B; 5A; 6A-C; 7A in Pelchen-Matthews et al. These two studies used cryo-sections of infected macrophages only. The values Donor 1 to Donor 3 therefore represent the average area covered by virus-filled vacuoles or gold-filled endosomes estimated on cryo-sections of infected macrophages from three donors. The size was estimated in at least 10 electron micrographs per donor using standard stereological methods. For estimation of endosome size, clearly identifiable endosomal profiles, abundantly filled with BSA-gold were considered. Error bars denote standard error of the mean. (B) Quantification of the percentage of free virus particles and budding profiles in infected macrophages prepared from the same three blood donors as in (A), but embedded in Epon. Three types of cellular membranes that either surrounded free virus or that displayed budding sites were considered: 1. RR-positive without internalized BSA gold (RR^+, BSA $gold^-$), 2. RR-negative without BSA gold (RR^-, BSA $gold^-$) and 3. RR-negative with BSA gold (RR^-, BSA $gold^+$). 'Free virus' included mature virions with a typical conical core and immature particles displaying an electron dense Gag shell. 'Budding sites' included 'late buds' consisting of spherical profiles that are connected to a membrane via a stalk (see, for instance figure (23 K)) and 'early buds', half-moon-shaped membrane profiles with an electron-dense (Gag) shell on their concave side (see, for instance, figure 23 H). In (C) the distribution of budding profiles was quantified in the same three donors as in (B).

3.2.4 HIV-1 particles acquire the late endosomal membrane proteins CD63 and lamp-1 and the cell surface protein CD44.

Pelchen-Matthews et al. have previously demonstrated the incorporation of the late endosomal marker proteins CD63 and lamp-1 into the HIV-1 envelope. This incorporation was taken as important evidence that HIV-1 buds into endosomes in primary human macrophages and was based on the assumption that CD63 and lamp-1 localized to late endosomes/lysosomes preferentially. Our data implied, however, that HIV-1 buds predominantly at cell surface-derived membranes in these cells, consistent with results showing that HIV-1 also acquires the cell surface protein CD44 [118]. We therefore localized the late endosomal marker proteins CD63 and lamp-1 as well as the cell surface protein CD44 in infected macrophages by EM.

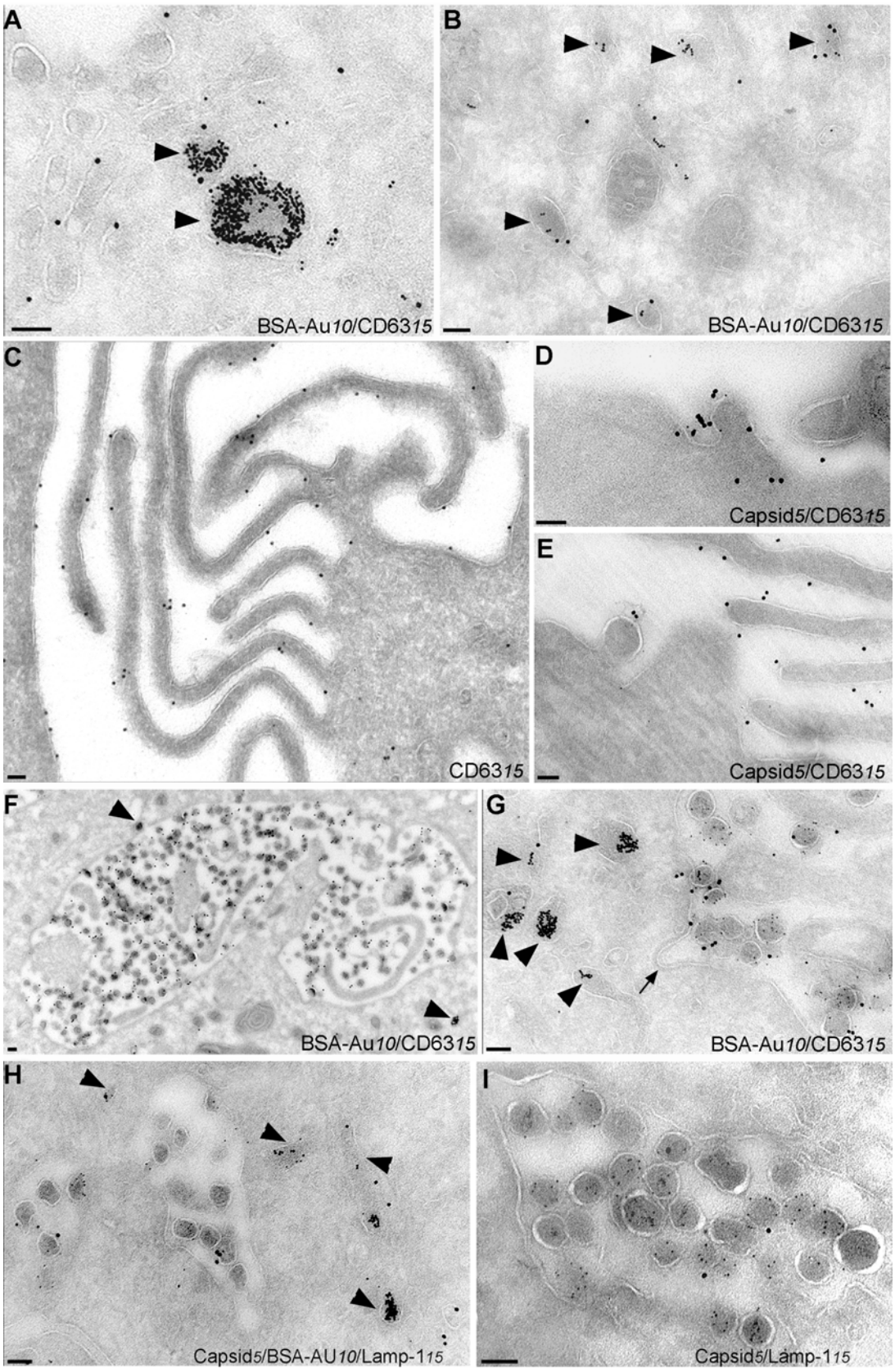
A
BSA-Au10/CD6315
B
BSA-Au10/CD6315
C
CD6315
D
Capsid5/CD6315
E
Capsid5/CD6315
F
BSA-Au10/CD6315
G
BSA-Au10/CD6315
H
Capsid5/BSA-AU10/Lamp-115
I
Capsid5/Lamp-115

Figure 25: Localization of the late endosomal/ lysosomal markers CD63 and lamp-1.
Primary human macrophages were infected with HIV-1 strain Ba-L and fed with BSA coupled to 10 nm gold. Thawed cryosections were labeled with mouse monoclonal antibodies to endosomal/lysosomal membrane markers followed by rabbit anti-mouse IgG and 15nm protein A gold (A-C) or double-labeled with the same membrane markers and rabbit anti-Capsid antibody followed by 5nm protein A gold. (D-I). (A) to (C) Thawed cryosections were labeled with anti-CD63, followed by rabbit anti-mouse IgG and 15nm protein A gold. In (A) and (B), anti-CD63 localizes to BSA-gold-filled endosomes (arrowheads) and the tubular vesicular membranes nearby. In (C) CD63 localizes to extended regions of the plasma membranes of two adjacent macrophages. (D) and (E) show anti-CD63 positive budding profiles at the cell surface that are also labeled with anti-Capsid (5nm). (F, G) CD63 is efficiently incorporated into the envelope of virus particles that accumulate in vacuolar structures and also localizes to BSA gold-filled endosomes (arrowheads in (F)). Note that the limiting vacuolar membrane in (G) is decorated with a clathrin-coated pit (arrow). (H, I) Thawed cryosections were double-labeled with anti-lamp-1 followed by 15nm protein A gold and anti-CA followed by 5nm protein A gold. Lamp-1 localizes to BSA gold-filled endosomes (arrows in H) and the tubular-vesicular membranes nearby and is incorporated at low levels into viral particles (H, I). Bar-100nm

First, cryosections of infected macrophages were labeled with antibodies to CD63 or lamp-1. Examination of these cryosections revealed that both proteins did not only localize to BSA gold-filled endosomes and the tubular-vesicular membranes nearby (Figure 25 A, B and H), but also to the plasma membrane (Figure 25 C and E and not shown). Typically, cells contained large plasma membrane patches where CD63 seemed highly concentrated as well as regions that had less CD63 labeling (not shown). We also found that the virus incorporated CD63 during budding at the plasma membrane (Figure 25 D, E). Extracellular viruses (not shown) as well as virions inside vacuolar structures were significantly labeled with anti-CD63 (Figure 25 F, G) and to a lesser extent with lamp-1 (Figure 25 H, I). Thus, under our infection conditions these late endosomal/lysosomal proteins were also incorporated into virions.

Immunolabeling of thawed cryosections with anti-CD44 revealed that this protein localized almost exclusively to the cell surface (Figure 26 A) and was not present at all on BSA gold-filled endosomes (Figure 26 A, C; arrowheads). Budding profiles on vacuolar structures (Figure 26 B) as well as virus particles (Figure 26 C) were decorated with the cell surface protein CD44, further evidencing that HIV-1 budding occurred on the cell surface.

Thus, although HIV-1 buds predominantly at cell surface derived membranes, the virus not only incorporates plasma membrane proteins such as CD44 but also readily incorporates endosomal/lysosomal proteins such as CD63 and lamp-1.

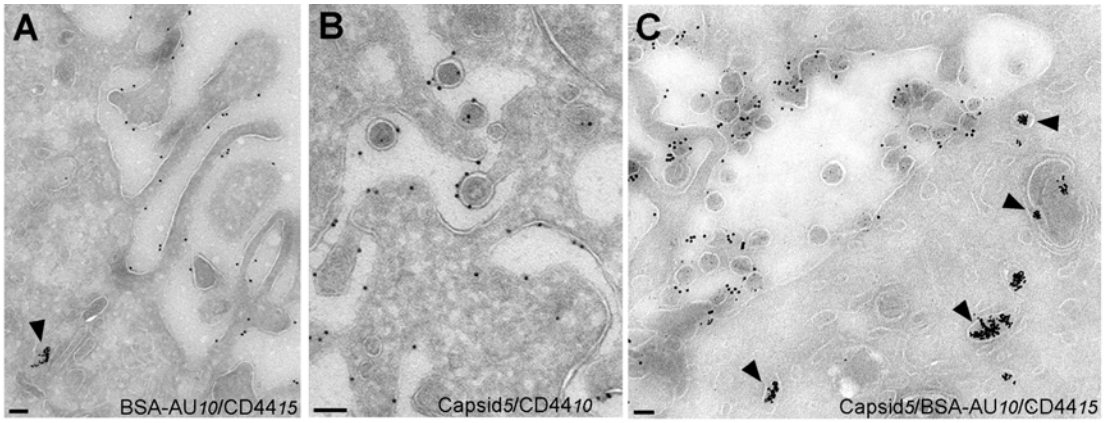

Figure 26: Localization of the cell surface protein CD44.
Primary human macrophages were infected with HIV-1 strain Ba-L and fed with BSA coupled to 10 nm gold (except in (B)). Thawed cryosections were labeled with a mouse monoclonal antibody to CD44 followed by rabbit anti-mouse IgG and 15nm (A, C) or 10nm protein A gold (B). In (B) and (C), sections were double-labeled with anti-CD44 and rabbit anti-Capsid antibody followed by 5nm protein A gold. In (A), CD44 localizes to the cell surface, especially to filopodia-like membrane protrusions, but is absent from BSA gold-filled endosomes (arrowhead). (B) Shows a set of membranes displaying a late budding profile and virus particles decorated with anti-CD44 and anti-CA. (C) Shows a large intracellular vacuole containing numerous virus particles which are labeled with anti-CD44. Note that the BSA gold-filled endosomes (arrowheads) are devoid of anti-CD44 labeling. Bars- 100 nm

The distribution of CD63 and CD44 over different membranes was next analyzed in a quantitative manner by estimating the labeling density of these markers on late endosomes, on the cell surface and on the limiting membrane of the virus-filled vacuolar structures in cells from three different donors (Figure 27). We also included virions in this quantification since we expected the labeling density on virus particles to resemble the one of the plasma membrane. Quantification showed that both in uninfected and infected macrophages, significant amounts of CD63 localized to the cell surface (Figure 27), confirming our qualitative observations. Depending on the donor, the labeling density on BSA gold-filled late endosomes was around three times higher compared to the cell surface (Figure 27). On the vacuolar membranes surrounding the viruses the density was similar to the plasma membrane, providing

additional evidence for its plasma membrane-, rather than endocytic, origin. We unexpectedly found that the labeling density on the viral envelope was intermediate between the plasma membrane and endosomes (Figure 27). This suggested that HIV budded preferentially from plasma membrane regions that concentrated CD63. However, although we readily found budding profiles at the cell surface that were labeled with CD63 (Figure 25 D, E) and lamp-1 (not shown), we did not find any evidence that budding occurred from those regions that were significantly enriched in CD63 (see Discussion).

When CD44 was quantified in a similar way, we found that this protein localized predominantly to the cell surface, with very low labeling on endosomes (Figure 27, right panel). Importantly, the labeling density of this protein on the viral envelope and on the virus-filled vacuolar membrane was identical to the one of the plasma membrane (Figure 27, right panel). These results additionally confirm that HIV-1 buds from the cell surface and that the limiting membrane of the vacuolar structures is plasma membrane-derived.

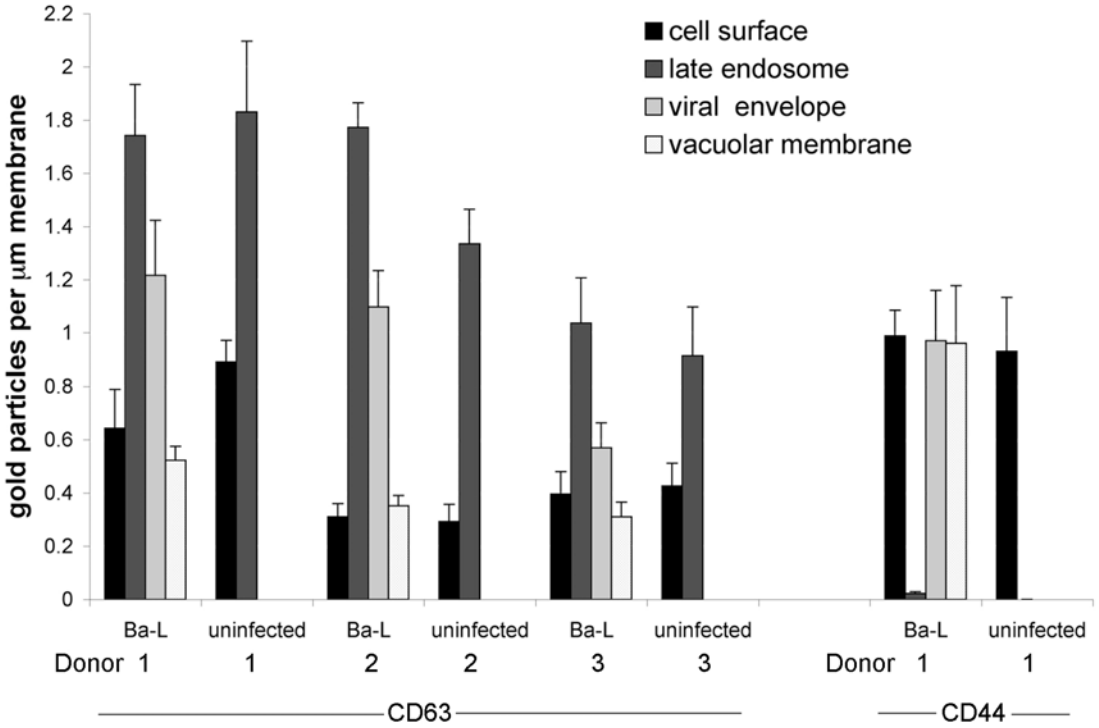

Figure 27: Quantification of CD63 and CD44 on different cellular membranes and on virus particles.
The labeling densities for CD63 and CD44 were quantified on late endosomes and the cell surface of uninfected and infected macrophages and additionally on virions and the limiting membrane of virus-containing vacuolar structures in infected macrophages. The donors 1 to 3 are the same as those used in figure 24 to quantify the distribution of budded virions and budding profiles. CD44 labeling density was determined in donor 1 only. The values represent the average from two independent labeling experiments and two different grids per experiment. At least 200 gold particles were counted per labeling experiment and donor. Error bars denote standard error. The cell surface was defined as plasma membrane profiles that were clearly external and ignoring intracellular membranes with plasma membrane-like morphology. Late endosomes were identified by the presence of internalized BSA gold and their typical morphology.

Our data thus confirm previous studies showing that HIV-1 incorporates both endosomal and cell surface proteins into its envelope [118]. However, whereas it was previously proposed that endosomal as well as cell surface proteins were incorporated into the viral envelope during the budding process on endosomes, our collective data show that HIV-1 budding occurs on the cell surface, where both types of proteins are incorporated into virus particles. Collectively, our EM data provided strong evidence

that HIV-1 buds on cell surface-derived membranes of primary human macrophages. This is in contrast to previous studies [28, 29] and will be discussed below.

Chapter 4

4. Discussion

4.1 Localization of ESCRT in T cells and macrophages

At the onset of this study T cells and macrophages, the two major target cell types for HIV-1 infection, were believed to promote HIV-1 budding and release from different membranes, the plasma membrane and endosomal membranes, respectively. The cellular ESCRT complex was shown to be required for HIV-1 budding and release in both cell types and it was therefore proposed that ESCRT was actively recruited to the plasma membrane of T cells upon HIV-1 infection. However, a detailed localization study of endogenous ESCRT proteins in HIV-1 susceptible cells was not available before the onset of this study. We therefore localized four subunits of the ESCRT machinery in detail by quantitative EM in uninfected and HIV-1 infected human T cells and macrophages. Our data contribute to the understanding of ESCRT localization and function in these cells.

4.1.1 Membrane association of ESCRT proteins

Our analysis of ESCRT localization by quantitative EM showed that more than 80% of ESCRT is associated with membrane structures. Previous studies addressing the role of ESCRT in mammalian cells showed that the cellular ESCRT machinery has several functional roles that involve interaction with membranes of the endocytic pathway: First, targeting of ubiquitinated receptors to the intralumenal vesicles of MVBs for subsequent degradation was shown to depend on ESCRT function (reviewed in [51, 57]). Second, formation of the intralumenal MVB vesicles, which is intimately linked to protein sorting to these vesicles, is believed to depend on ESCRT function as well, although the mechanism of ESCRT action during this process is not entirely clear. It was, however, shown that ATPase activity of the ESCRT-associated protein Vps4 is required for MVB formation. In particular, overexpression of the inactive form of Vps4 (dnVps4) led to formation of an aberrant endosomal compartment (the mammalian class E compartment), believed to represent

enlarged MVBs lacking internal vesicles [60]. Furthermore, knock-down of the ESCRT-associated protein Aip1/Alix by RNA interference indicated that this protein also plays a role in the formation of the internal endosomal membranes [119], as originally proposed in yeast. Recent results suggested, however, that Aip1/Alix may have additional functions such as endosome positioning and the organization of the actin network [120].

Although these established functions for ESCRT involve interaction with endosomal membranes, previous studies suggested that ESCRT proteins are mainly found in the cytoplasm [69, 114, 116, 121]. In contrast to previous reports, this study showed by electron microscopy that ESCRT proteins localize predominantly on membrane structures with only a minor fraction in the cytoplasm. Previous studies were predominantly based on the localization of overexpressed and tagged proteins by light microscopy [63, 69, 122, 123], whereas we localized and quantified endogenous protein in T cells and macrophages by EM. Importantly, we were able to reproduce the reported diffuse localization pattern of ESCRT proteins by immunofluorescence microscopy and suggest that the tubular-vesicular membranes, to which the majority of ESCRT localized by EM, could be mis-interpreted as 'cytoplasmic' localization in light microscopy analyses.

Since we could formally exclude the possibility that cytosolic ESCRT proteins were only poorly detected by EM compared to their membrane associated forms, the fact that ESCRT was predominantly cytosolic by membrane flotation indicated that ESCRT proteins are peripherally attached to membranes and that this membrane association was lost upon mechanical cell lysis [114, 116, 121, 124]. This idea was supported by the fact that overexpression of Vps4^{E228Q}, reported in several independent studies to recruit and lock ESCRT to membranes [60, 63, 114, 125], did not affect the amount of ESCRT in the membrane fractions.

4.1.2 ESCRT localization throughout the endocytic pathway

Our detailed EM localization study of Hrs, Tsg101, Aip1/Alix and Vps4B showed that ESCRT localizes throughout the endocytic pathway, including the plasma membrane. Comparison of the distributions of the four proteins suggested, however, that the relative subcellular distribution of ESCRT varied depending on the cell type. Whereas in both T cells and macrophages the majority of ESCRT proteins

was found on tubular-vesicular membranes associated with endosomes, the amounts of ESCRT on the plasma membrane and on endosomes differed between the two cell types. The relatively high amounts of ESCRT on endosomes of macrophages may simply reflect their function as professional antigen-presenting cells. As such they may need a more elaborate endosomal system, particularly equipped to carry out processes such as antigen processing and subsequent presentation of processed antigen at the cell surface, processes which involve endosomal protein sorting and recycling.

Our results confirm a previous light microscopy study showing that the localization of Hrs and Tsg101 only partially overlaps [124]. Whereas Aip1/Alix, Tsg101 and Vps4B were preferentially associated with late endocytic structures, Hrs localized mostly to early endosomes, confirming previous data [126]. We propose that this difference reflects different functions of subunits of the ESCRT machinery. Hrs has been predicted to bind to at least six different factors, most of which are preferentially associated with the early endocytic pathway, suggesting that this protein may have more than one function [127]. A significant, but lower amount of Hrs was found on late endosomes, in particular on tubular-vesicular membranes associated with late endosomes. This fraction of Hrs co-localized with Aip-1/Alix, Tsg101 and Vps4B and it appears likely that this colocalization reflects a function of Hrs that overlaps with the other ESCRT subunits.

4.1.3 ESCRT localization to tubular-vesicular endocytic membranes

Surprisingly, the amount of ESCRT on tubular-vesicular endosomal membranes was significantly higher than on MVBs. Since ESCRT has been linked to the formation of the intra-lumenal endosomal vesicles of MVBs, the predominant localization to tubular-vesicular membranes was unexpected, raising the question about the function of this pool of ESCRT. Based on morphological similarity [92, 128, 129] and labeling for Tfr it seems likely that these tubular-vesicular endocytic membranes are involved in endosomal recycling and/or sorting. Similar membrane appendages of endosomes have been suggested to be the site of receptor/ligand uncoupling [128] and to be involved in endosomal sorting [129]. Our data thus suggest that ESCRT may play a role in protein sorting and recycling in addition to its known function in MVB formation. An alternative possibility is that the pool of ESCRT on tubular-vesicular

endosomal membranes represents unassembled ESCRT components that are rapidly recruited into functional complexes to support MVB formation. In this scenario, functional complexes may be present only transiently on MVBs and, accordingly, ESCRT proteins do not significantly accumulate on MVBs themselves. Instead, inactive (unassembled) ESCRT proteins may preferentially localize to tubular-vesicular membranes, rather than being cytoplasmic. However, the expression of ATPase-deficient Vps4, which is believed to trap assembled ESCRT complexes, did not result in depletion and relocation of this ESCRT pool to enlarged endosomal structures. The latter result suggested that ESCRT proteins found on tubular-vesicular membranes associated with endosomes also represented (functional) ESCRT complexes and that ESCRT-dependent sorting steps may occur on tubular-vesicular membranes rather than MVBs. In this scenario, MVBs would play a minor role during endosomal protein sorting. The latter would be in agreement with our observation that, even upon close inspection of endosomes in BSA-gold pulse-chase experiments, the endocytic pathway of primary human macrophages appeared to be almost devoid of MVBs.

In conclusion, our collective data suggested an unexpected role for endosome-associated tubular vesicular membranes in the function of ESCRT, most likely in protein sorting and recycling in the endocytic pathway.

4.1.4 ESCRT proteins are not recruited to HIV-1 budding sites

HIV-1 infection of T cells or macrophages did not lead to a detectable re-localization of ESCRT. This was in contrast to previous studies concluding that ESCRT was recruited to the site of HIV budding. However, these studies were based on Gag over-expression analyses [69]. It is likely that in this Gag over-expression context, ESCRT does not suffice to support virus-like particle formation, leading to the observed redistribution. Since infection did not result in a redistribution of ESCRT to the site of budding, our data would argue that on those membranes that are relevant for HIV-1 budding, the endogenous pool of ESCRT is sufficient for virus release. Our data showed furthermore that ESCRT was enriched at those membranes presumed to be the site of HIV budding in T cells and macrophages, the plasma membrane and endosomes, respectively, suggesting that ESCRT plays a role in determining the site of budding. However, recent studies make a direct role for ESCRT in HIV-Gag

targeting to certain membranes unlikely, as Gag was shown to accumulate on endosomes independently of the interaction of the p6 subunit of Gag with Tsg101 [130]. The collective evidence furthermore suggested that Gag may traffic through endocytic compartments, even in cells where budding occurs at the cell surface [50, 131-133]. Although ESCRT is clearly required for the process of HIV-1 budding, the collective data were more consistent with an indirect role for ESCRT in determining the site of HIV budding in different cell types.

Our qualitative observations in infected T cells confirmed the plasma membrane as predominant site of HIV budding. The complex morphology of macrophages, however, made it difficult to identify the predominant site of virus budding in these cells. Interestingly, almost no MVBs were found in macrophages, arguing against a pivotal role of MVBs in both protein sorting and HIV-1 budding in these cells.

4.2 HIV-1 budding in macrophages

HIV-1 budding and release from human macrophages has gained much interest in recent years for several reasons. Whereas it was previously believed that HIV-1 buds from the plasma membrane of most cell types including monocytes and macrophages [18, 30], several independent studies suggested that HIV-1 buds on intracellular membranes and accumulates in an intracellular compartment of human macrophages [20, 24, 26, 28, 29]. It was therefore proposed that this compartment of HIV-1 infected macrophages comprised a reservoir of infectious virions that could be disseminated to T cells upon contact [38]. Whereas earlier EM studies suggested that this intracellular virus-filled compartment belonged to the Golgi network [20, 24], it was recently proposed to be of late endocytic origin. This was mainly based on the observation that HIV-1 particles acquired late endosomal proteins such as CD63, lamp-1 [28] and major histocompatibility complex type II (MHC II) molecules [29]. Here, the morphology of primary human macrophages and the site of HIV-1 budding and release was analyzed in detail, and our data have strong implications for our view on budding, release and storage of HIV-1 in these cells.

4.2.1 Analysis of macrophage morphology

In this study, we analyzed primary human macrophages, derived by *in vitro* differentiation from peripheral blood monocytes. Our EM analysis revealed that macrophages cultured *in vitro* exhibit an unexpectedly complex plasma membrane organization with many long protrusions and deep invaginations. Unexpectedly, a variety of apparently intracellular large vacuolar structures were also found to be delineated by the plasma membrane, since the cell surface stain Ruthenium red (RR) highlighted many of these apparently intracellular vacuolar structures, besides the 'obvious' plasma membrane regions (regions delineating the cell borders). The fact that the limiting membrane of these vacuolar structures often showed hallmarks of the plasma membrane (filopodia-like protrusions and clathrin coated pits) provided additional evidence for its cell surface origin. Importantly, we found that this complex system of vacuolar structures was morphologically distinct and spatially separated from the intracellular endosomal system of macrophages. The two sets of structures could furthermore be distinguished by their disability or ability of endocytic BSA gold uptake, respectively. Collectively, our data argued that the vacuolar structures

were limited by a cell surface-derived membrane and were not of endocytic origin. The combined use of BSA gold as an endocytic tracer molecule and RR as a cell surface stain was especially useful for the analysis of macrophage morphology and was more unambiguous compared to immuno EM using antibodies (see below).

4.2.2 HIV-1 particles bud and accumulate on cell-surface-derived membranes of macrophages

Analysis of HIV-1 infected macrophages confirmed previously published data, showing that most virus particles accumulated in large cytoplasmic vacuoles and that the virus budded from the limiting membranes of these vacuolar structures [28, 29]. However, our collective data demonstrated that the virus-containing vacuoles and the cell surface-derived vacuolar structures were identical. The vacuolar membrane (as well as the envelopes of virus particles inside vacuoles) was accessible to RR, indicating that it was derived from the plasma membrane. Furthermore, virus-filled vacuolar structures failed to internalize BSA gold and showed the same hallmarks of plasma membrane as the above mentioned vacuolar structures, long filopodia and clathrin coated pits. Strikingly, the latter two features can also be seen in previous studies (Figures 2 A and 3 B from [29]; Figures 5 B, C; 6 A, C; 7 A, B from [28]), but were not discussed in these studies. Thus, together with the fact that the size of the vacuoles corresponded well to previous studies, it must be clear that the virus-filled compartment observed in the present study is identical to the one previously described.

HIV-1 budding sites were found to localize to the same vacuolar compartment as virions. However, they were also frequently seen on the plasma membrane, together with single or few virus particles. Whereas free virus particles in the extracellular space are easily lost during sample preparation, the distribution of budding profiles in EM sections should quantitatively reflect their distribution in intact cells. Strikingly, EM quantification of budding profiles demonstrated that in primary human macrophages HIV-1 buds at the cell surface and on plasma membrane derived vacuolar membranes but never at BSA gold-filled endosomes.

Therefore, our ultra-structural analyses of both infected and uninfected macrophages cultured *in vitro* contributed in an unexpected way to the proposed role of these cells in HIV-1 persistence. The finding that HIV-1 budding occurs on the cell

surface of macrophages raises the question whether the deep invaginations of the plasma membrane may provide domains for HIV-1 to be stored and hidden. It was previously shown that cultured human macrophages store infectious virus for weeks or months [38]. Although this study proposed a model in which virus was stored in a late endosomal compartment/ in MVBs, it did not exclude the possibility that this storage compartment consisted of deep plasma membrane invaginations, e.g. on the bottom of the cells. In fact, we frequently observed virus particles trapped in the space between cells and the underlying substrate by EM, and this viral 'reservoir' could not be removed by washing the cell monolayer [38]. Our data thus aids at explaining how these cells could create pockets where the virus is stored and can be released occasionally in small amounts. Although this scenario is not much different from the exosome-release hypothesis, it is likely that the regulation of virus storage and release may underlie an entirely different mechanism.

4.2.3 HIV-1 envelopes incorporate endosomal and cell surface proteins

Previous studies, which proposed that the vacuolar virus-containing compartment of macrophages was of endocytic origin, were mostly based on the finding that endosomal membrane markers were present on the surface of virus particles [28, 29, 118]. Our study confirmed these data showing that HIV-1 particles acquired cellular proteins that are used as markers for endosomal membranes and plasma membrane [28, 29, 118, 132, 134-137]. However, in contrast to previous studies, we provide evidence that these proteins, including the endosomal marker proteins, are acquired at the cell surface.

Although demonstrated in several independent studies [28, 118, 138, 139], it is unclear why the HIV-1 envelope incorporates a subset of cellular proteins. One proposal is that HIV-1 buds at specialized membrane domains such as 'lipid raft' membrane microdomains [139-142]. In fact, is has been shown that the membrane composition of HIV-1 envelopes resembles that of such microdomains and differs from the overall composition of host cell membranes [143]. Whether this composition reflects that of pre-existing microdomains in intact cellular membranes is, however, unclear.

The fact that the labeling density of CD63 was higher in virions compared to the plasma membrane, suggests that certain proteins are specifically enriched during

the budding process. Such enrichment could be achieved by budding at specific plasma membrane domains that concentrate or exclude cellular proteins, as recently suggested [134]. However, although CD63 appeared highly concentrated in some parts of the cell surface of macrophages, we could not find any evidence that the virus preferentially budded from such domains. Whereas the significance of these CD63 cell surface patches for HIV-budding remains to be investigated, they may have important implications for the use of anti-CD63 as a putative MVB-marker (see below).

Collective evidence showed that the ESCRT machinery, proposed to be required for the biogenesis of MVBs, is also needed for HIV-1 release (reviewed in [51, 65]. This led to the idea that HIV-1 budding, and consequently Gag-targeting, are linked to late endosomes/MVBs. Data supporting the role for the endocytic pathway in HIV-1 budding and/or Gag targeting using various cell types mostly relied on light microscopy, often using CD63 as a presumed MVB marker [130-132, 144, 145]. By EM, however, CD63 was found throughout the endocytic pathway including the cell surface [91] and is not particularly enriched on MVBs, as was shown in the first part of this study. It is questionable whether double-labeling experiments at the light microscopy level can discriminate between CD63-positive plasma membrane domains, MVBs and late endosomes (for a review see [146]) and such data should thus be interpreted with caution. The fact that the late endosome/lysosome marker lamp-1 also localized partially to the cell surface of macrophages together with the finding that Tfr, often used as a marker for early/recycling endosomes, localized predominantly to late endocytic membranes of these cells, indicated that the use of marker proteins may not be sufficient for most quantitative microscopic analyses.

Given our unequivocal results in primary macrophages and T cells, we propose that plasma membrane budding of HIV-1 predominates in most cells. EM images obtained in HeLa and 293T cell lines apparently showing budding of retroviruses into endosomes [131, 132], require a re-evaluation using the two markers (RR-stain and internalized gold) used in the present study. Thus, our present data, together with the EM localization of ESCRT in primary T cells and macrophages, question the proposed pivotal role of MVBs in the HIV-1 life cycle.

4.3 Future directions

For further study of HIV-1 infection in macrophages it will be important to analyze *in vivo* differentiated macrophages by EM. Whether their morphology is comparable to that of cells cultured *in vitro* and whether the sites of HIV-1 budding and release are identical is unknown, since no ultrastructural HIV infection study has been done yet with *ex vivo* macrophages. Culture and HIV-1 infection of explanted human tonsils has been recently established in the lab of Oliver T. Keppler ([147] and unpublished results), and EM analysis of HIV-1 infected tonsil histoculture can easily be done in the near future. First experiments indicated that tonsils contain macrophages that look very similar to the *in vitro* cultured cells. However, identification of macrophages was based on morphological similarity, and macrophage-specific surface markers will be needed to identify these cells in the tissue. Furthermore, the accessibility of the tissue for the cell surface stain RR is inefficient, most likely due to tight cell-cell contacts, and it will therefore be challenging to analyze the organization of cell surfaces inside tissues. Since macrophages were previously proposed to store infectious HIV-1 in endosomal compartments for long periods [38] it will be important to formally demonstrate if infectious virus can be stored in plasma membrane invaginations of macrophages or other cell types.

The concentration of CD63 on virus particles suggested that HIV-1 budding occurred from plasma membrane regions where CD63 was enriched. Although we could show that CD63 accumulated in extended regions of the plasma membrane, it was not possible to determine if HIV-1 budding predominated in these regions. Statistic analysis was mainly hampered by the low numbers of budding structures observed, and therefore a testable system, yielding higher numbers of budding sites, could result from using HIV-1 L-domain mutants displaying a late budding defect.

From our finding that several vacuolar structures of macrophages were not stained with RR (although the presence of filopodia and clathrin coated pits clearly showed that they were limited by the plasma membrane) we concluded that this RR-inaccessibility was due to technical reasons. Another possibility for formation of such RR-inaccessible vacuoles would be membrane fusion of adjacent cells. Such cell-cell fusion events, induced by HIV-1 Env expression on the cell surface, were shown to occur frequently in HIV-1 infected macrophages and are known to lead to syncytia

formation. Whether RR negative vacuolar structures of macrophages (or other cell types) are a result of cell-cell fusion could be tested using viral constructs encoding fusion-deficient Env glycoprotein.

Since our EM data suggest a role for ESCRT in protein sorting and recycling, further experiments will be required to determine whether sorting of ubiquitinated proteins into the lysosomal degradation pathway is the predominant function of ESCRT in the endocytic pathway. Furthermore, for future studies of ESCRT in HIV-1 infected cells it will be important to address the functional roles of different ESCRT subunits in HIV-1 budding and release. Whereas abrogation of ESCRT binding to Gag (by mutation of L domains in Gag, or Tsg101 depletion) was proposed to lead to induce an 'early' HIV-1 budding arrest (represented by crescent-shaped budding sites), overexpression of dnVps4 is thought to lead to a late HIV-1 budding arrest (represented by 'lollipop' shaped budding sites) due to a block in membrane fission. However, this model has not been proven yet. This could be addressed by interfering with ESCRT-Gag interactions and ESCRT function by different means, e.g. by making use of truncated or mutated Gag constructs lacking the p6 domain or L domain motifs, respectively, by RNA interference with expression of Tsg101 and Aip1/Alix or by overexpression of dnVps proteins. Whether this correlates with distinct HIV-1 budding phenotypes can be addressed by quantitative EM and will now be studied by Stefanie Jaeger, a PhD student in our lab.

Finally, one could address the question whether ESCRT association with membranes is mediated solely by Hrs or if ESCRT proteins can participate in other, yet unknown, interactions with membrane- or membrane-associated proteins. Such proteins, e.g. bearing PT/SAP motifs, could serve as alternative binding partners for Tsg101. Another possibility would be that ESCRT subunits, similar to what was proposed for Aip1/Alix [119], directly interact with membrane lipids.

Appendix I List of abbreviations

µl	microliter
µm	micrometer
aa	amino acid
Aip1/Alix	Apoptosis-linked gene 2 (ALG-2)-interacting protein 1/ ALG-2-interacting protein X
APS	Ammonium persulfate
BIS	N,N'-methylene bisacrylamide
bp	Base pair
BSA	bovine serum albumine
BSA gold	collidal gold particles coupled to BSA
CA	Capsid protein
cm	centimeter
DDSA	2-Dodecenylsuccinic acid anhydride
dH_2O	deionized water
DMP-30	2,4,6 Tris(dimethylaminomethyl)phenol
dn	dominant negative
DNA	deoxyribonucleic acid
EGTA	ethylene glycol-bis(β-aminomethylether)-N,N,N',N'-tetraacetic acid)
ELISA	enzyme-linked immunosorbent assay
EM	electron microscopy
ESCRT	endosomal sorting complex required for transport
EtOH	ethanol
GA	glutaraldehyde
Gag	Group specific antigen
gp	glycoprotein
HAB	human AB serum
HEPES	N-2-hydroxyethylpiperazine-N'-2-ethane sulfonic acid

HIV	human immuno deficiency virus
hrs	hours
Hrs	hepatocyte growth factor kinase substrate
IF	immunofluorescence
kb	kilobase
kDa	kilodalton
KOH	potassium hydroxide
M	molar; mol/liter
MA	Matrix protein
MC	methyl cellulose
min	minute(s)
ml	milliliter
mm	millimeter
MNA	methylnadic anhydride
NaCl	sodium chloride
NC	nucleocapsid protein
nm	nanometer
ºC	degrees centigrade
p	pico
p.i.	post infection
PAG	protein A gold
PBG	immuno-EM blocking solution (PBS/BSA/gelatin)
PBS	phosphate buffered saline
PBST	PBS with 0.1% Tween-20
PFA	paraformaldehyde
PIPES	piperazine-N,N'-bis(2-ethane sulfonic acid)
PR	Protease enzyme
PVDF	polyvinylidene fluoride
RNA	ribonucleic acid

RR	Ruthenium Red
RT	reverse transcriptase enzyme
SDS	sodium dodecyl sulfate
SDS-PAGE	SDS-polyacrylamide gel electrophoresis
TEM	transmission electron microscope
TEMED	N,N,N’N’-tetramethylenediamine
Tsg101	Tumor susceptibility gene 101 protein
U	unit
UA	uranyl acetate
Vps	vacuolar protein sorting
wt	wild type

Appendix II List of antibodies

antibody	reactivity	remarks	provided by/ purchased from	dilution
rabbit **Anti-Hrs**	human	polyclonal antiserum	Sylvie Urbe	EM, IF 1:200 WB 1:1000
mouse **Anti-Tsg101**	human, mouse	monoclonal, clone 4A10	Genetex MS-TSG10-PX1/ abcam ab83	EM, IF 1:100 WB 1:500
rabbit **anti-Alix**	human	polyclonal, affinity purified	Wesley Sundquist	EM 1:5, IF 1:100 WB 1:1000
rabbit **anti-Vps4B**	human	polyclonal, affinity purified	Wesley Sundquist	EM 1:5 WB 1:3000
mouse **anti-CD63**	human	mouse IgG1, affinity purified CLB-gran/12, 435	Sanquin PeliCluster M1544	EM 1:80
mouse **anti-CD63**	human	monoclonal, clone 1B5	Mark Marsh	EM 1:100
mouse **anti-TfR**	human	monoclonal mouse IgG1, clone H68.4	Zymed Cat.-No 13-6800	EM 1: 100 WB 1:1000
mouse **anti-CD44**	human	affinity purified, Clone F10-44-2	Chemicon CBL154	EM 1:60
mouse **anti-lamp1**	human	mouse IgG1, clone H4A3	DSHB	EM 1: 80
goat anti-**actin**	mouse, rat, human, zebrafish, C. elegans, S. cerevisiae, X. laevis	goat polyclonal IgG, C-11	Santa Cruz Cat.No. sc-1615	WB 1:1000
rabbit **anti-14-3-3 γ** rabbit **anti-14-3-3 θ**	mouse, rat, human	C-17 C-16	Santa Cruz Cat.No. sc-732	WB 1: 500
rabbit **Anti-capsid**	HIV-1 NL-4.3 Capsid (preparations CA1, CA3)	polyclonal antiserum	Hans-Georg Kraeusslich	EM, IF 1:50 WB 1:1000
mouse **anti- SialylT**	VSV-G tagged sialyl transferase	monoclonal, P5D4 culture supernatant	Thomas Kreis	EM 1:100
rabbit anti-**mouse**	mouse IgG whole molecule	polyclonal, IgG	ICN Cappel Cat. #55436	EM 1:75
donkey **anti-rabbit IgG**	rabbit IgG (H+L)	coupled to Cy3	Jackson, Dianova 711-165-152	IF 1:700
goat **anti-mouse IgG**	mouse IgG whole molecule	coupled to Cy3	Jackson, Dianova 115-165-003	IF 1:400
goat **anti-mouse IgG**	mouse IgG	coupled to HRP	Dianova	WB 1:2000
goat **anti-rabbit IgG**	rabbit IgG	coupled to HRP	Dianova	WB 1:3000

Appendix III Preparation of BSA gold

stock solutions required:

- 1% (w/v) gold chloride in dH_2O (Sigma #G-4022). Can be stored for several weeks at 4ºC, protect from light.
- 1% (w/v) tri-sodium citrate· $2H_2O$ in dH_2O
- 1% (w/v) tannic acid in dH_2O (Serva #35753), prepare freshly
- 25mM potassium carbonate in dH_2O
- 20% (w/v) BSA in dH_2O (Biomol #01400, BSA Fraction V)

gold conden-sation	**5nm gold**	**10nm gold**	**16nm gold**
gold solution A	790ml dH_2O 10ml 1% $AuCl_2$	790ml dH_2O 10ml 1% $AuCl_2$	960ml dH_2O 10ml 1% $AuCl_2$
reducing solution B	40ml 1% tri-Na citrate 10ml 1% tannic acid 10ml 25mM K_2CO_3 140ml dH_2O	20ml 1% tri-Na citrate	40ml 1% tri-Na citrate 0.5ml 1% tannic acid 159.5ml dH_2O
	Heat each solution to 60ºC Quickly pour B into A while rapidly stirring, color of solution changes to red immediately, heat up to 95ºC for 5 min		Heat solution A to 100ºC while stirring quickly add 20 ml 1% tri-Na citrate re-heat to 100ºC until color changes to red
BSA coupling			
	let cool down to room temperature adjust pH using pH paper to the isoelectric point of BSA (~pH 7.0). Colloidal gold blocks pH electrode! Add 10ml 20% BSA (final BSA concentration 0.2%), stir slowly for 10 min		
Centrifugation (all steps at 4ºC)			
Beckman 45 Ti	45.000 rpm, 90 min remove supernatant, resuspend pellet carefully in 0.2%BSA/PBS		8.000 rpm, 45 min, remove supernatant, resuspend pellet carefully in 0.2%BSA/PBS
Beckman 70 Ti	38.000 rpm, 30 min collect supernatant	18.000 rpm 30 min collect supernatant	
Beckman 70 Ti	spin supernatant at 45.000 rpm, 30 min	spin supernatant at 27.000 rpm, 30 min	
	remove supernatant resuspend pellet carefully in 0.2%BSA/PBS		

Appendix IV Immunolabeling

- place grids section-side-down on 2 % gelatin plate, incubate to melt away gelatin	> 20 min at 37°C
at room temperature, grids section-side-down on a drop of solution	
- wash	4x 2 min, PBS
- block	10 min, PBG
- primary antibody	30 min, diluted in PBG
- wash	5x 2 min, PBS
if required:	
- rabbit-anti-mouse bridging antibody	30 min, diluted in PBG
- wash	5x 2 min, PBS
- protein A gold (PAG)	20 min, diluted in PBG
- wash	5x 2 min, PBS
- wash	5x 2 min, ddH_2O
for double labeling experiments:	
- fix	5min, 2% GA in ddH_2O
- wash	5x 2 min, PBS-glycine
- wash	3x 2 min PBS
- block	10 min, PBG
- antibody-, PAG-incubation and wash steps as above	
on ice:	
- contrast	3-10 min, 2%MC /3%UA (mixed 0.85+ 0.15)
- loop out grids from MC/UA solution	
at room temperature:	
- dry on Whatman #1 filter paper	
- air-dry	~10 min
- store in grid box at room temperature	forever

References

1. UNAIDS/WHO, *UNAIDS/WHO report on the global AIDS epidemic*. 2006, UNAIDS. p. Chapter 2 Overview of the global AIDS epidemic.
2. Vogt, V.M., *Retroviral virions and genomes*, in *Retroviruses*, J.M. Coffin, S.H. Hughes, and H.E. Varmus, Editors. 1997, Cold Spring Harbor Laboratory Press: New York, USA.
3. Telesnitsky, A. and S. Goff, *Reverse transcription and the generation of retroviral DNA*, in *Retroviruses*, J.M. Coffin, S.H. Hughes, and H.E. Varmus, Editors. 1997, Cold Spring Harbor Laboratory Press: New York, USA.
4. Gao, F., et al., *Origin of HIV-1 in the chimpanzee Pan troglodytes troglodytes*. Nature, 1999. **397**(6718): p. 436-41.
5. Briggs, J.A., et al., *The mechanism of HIV-1 core assembly: insights from three-dimensional reconstructions of authentic virions*. Structure, 2006. **14**(1): p. 15-20.
6. Wiegers, K., et al., *Sequential steps in human immunodeficiency virus particle maturation revealed by alterations of individual Gag polyprotein cleavage sites*. J Virol, 1998. **72**(4): p. 2846-54.
7. Borsetti, A., A. Ohagen, and H.G. Gottlinger, *The C-terminal half of the human immunodeficiency virus type 1 Gag precursor is sufficient for efficient particle assembly*. J Virol, 1998. **72**(11): p. 9313-7.
8. Bryant, M. and L. Ratner, *Myristoylation-dependent replication and assembly of human immunodeficiency virus 1*. Proc Natl Acad Sci U S A, 1990. **87**(2): p. 523-7.
9. Wilk, T., et al., *Organization of immature human immunodeficiency virus type 1*. J Virol, 2001. **75**(2): p. 759-71.
10. Cimarelli, A., et al., *Basic residues in human immunodeficiency virus type 1 nucleocapsid promote virion assembly via interaction with RNA*. J Virol, 2000. **74**(7): p. 3046-57.
11. Demirov, D.G. and E.O. Freed, *Retrovirus budding*. Virus Res, 2004. **106**(2): p. 87-102.
12. Clapham, P.R. and A. McKnight, *HIV-1 receptors and cell tropism*. Br Med Bull, 2001. **58**: p. 43-59.
13. Daecke, J., et al., *Involvement of clathrin-mediated endocytosis in human immunodeficiency virus type 1 entry*. J Virol, 2005. **79**(3): p. 1581-94.
14. Jacque, J.M. and M. Stevenson, *The inner-nuclear-envelope protein emerin regulates HIV-1 infectivity*. Nature, 2006. **441**(7093): p. 641-5.
15. Wodrich, H. and H.G. Krausslich, *Nucleocytoplasmic RNA transport in retroviral replication*. Results Probl Cell Differ, 2001. **34**: p. 197-217.
16. Fields, B.E., *Virology*, ed. D.M.K. Bernard N. Fields, Peter M. Howley, Robert M. Chanock, Thomas P. Monath, Joseph L. Melnick, Bernard Roizman, Stephen E. Straus. 3rd Ed. 1995.
17. Resh, M.D., *Intracellular trafficking of HIV-1 Gag: how Gag interacts with cell membranes and makes viral particles*. AIDS Rev, 2005. **7**(2): p. 84-91.

18. Bourinbaiar, A.S. and D.M. Phillips, *Transmission of human immunodeficiency virus from monocytes to epithelia*. J Acquir Immune Defic Syndr, 1991. **4**(1): p. 56-63.
19. Garrus, J.E., et al., *Tsg101 and the vacuolar protein sorting pathway are essential for HIV-1 budding*. Cell, 2001. **107**(1): p. 55-65.
20. Blom, J., C. Nielsen, and J.M. Rhodes, *An ultrastructural study of HIV-infected human dendritic cells and monocytes/macrophages*. Apmis, 1993. **101**(9): p. 672-80.
21. Carr, J.M., et al., *Rapid and efficient cell-to-cell transmission of human immunodeficiency virus infection from monocyte-derived macrophages to peripheral blood lymphocytes*. Virology, 1999. **265**(2): p. 319-29.
22. Gendelman, H.E., et al., *Efficient isolation and propagation of human immunodeficiency virus on recombinant colony-stimulating factor 1-treated monocytes*. J Exp Med, 1988. **167**(4): p. 1428-41.
23. Meltzer, M.S., et al., *Role of mononuclear phagocytes in the pathogenesis of human immunodeficiency virus infection*. Annu Rev Immunol, 1990. **8**: p. 169-94.
24. Meltzer, M.S., et al., *Macrophages and the human immunodeficiency virus*. Immunol Today, 1990. **11**(6): p. 217-23.
25. Munn, R.J., et al., *Ultrastructural comparison of the retroviruses associated with human and simian acquired immunodeficiency syndromes*. Lab Invest, 1985. **53**(2): p. 194-9.
26. Orenstein, J.M., et al., *Cytoplasmic assembly and accumulation of human immunodeficiency virus types 1 and 2 in recombinant human colony-stimulating factor-1-treated human monocytes: an ultrastructural study*. J Virol, 1988. **62**(8): p. 2578-86.
27. Palmer, E., et al., *Morphology and immunoelectron microscopy of AIDS virus*. Arch Virol, 1985. **85**(3-4): p. 189-96.
28. Pelchen-Matthews, A., B. Kramer, and M. Marsh, *Infectious HIV-1 assembles in late endosomes in primary macrophages*. J Cell Biol, 2003. **162**(3): p. 443-55.
29. Raposo, G., et al., *Human macrophages accumulate HIV-1 particles in MHC II compartments*. Traffic, 2002. **3**(10): p. 718-29.
30. Perotti, M.E., X. Tan, and D.M. Phillips, *Directional budding of human immunodeficiency virus from monocytes*. J Virol, 1996. **70**(9): p. 5916-21.
31. Gould, S.J., A.M. Booth, and J.E. Hildreth, *The Trojan exosome hypothesis*. Proc Natl Acad Sci U S A, 2003. **100**(19): p. 10592-7.
32. Janeway, C.A., et al., *Immunobiology*. 2001, New York: Garland Publishing.
33. Coffin, J.M., *HIV population dynamics in vivo: implications for genetic variation, pathogenesis, and therapy*. Science, 1995. **267**(5197): p. 483-9.
34. Piguet, V. and Q. Sattentau, *Dangerous liaisons at the virological synapse*. J Clin Invest, 2004. **114**(5): p. 605-10.
35. McDonald, D., et al., *Recruitment of HIV and its receptors to dendritic cell-T cell junctions*. Science, 2003. **300**(5623): p. 1295-7.
36. Kwon, D.S., et al., *DC-SIGN-mediated internalization of HIV is required for trans-enhancement of T cell infection*. Immunity, 2002. **16**(1): p. 135-44.

37. Venzke, S. and O.T. Keppler, *The role of macrophages in HIV infection and persistence*. Expert Review of Clinical Immunology, 2006. **in press**.
38. Sharova, N., et al., *Macrophages archive HIV-1 virions for dissemination in trans*. Embo J, 2005. **24**(13): p. 2481-9.
39. Herbein, G., et al., *Macrophage activation and HIV infection: can the Trojan horse turn into a fortress?* Curr Mol Med, 2002. **2**(8): p. 723-38.
40. Rothman, J.H., et al., *Protein targeting to the yeast vacuole*. Trends Biochem Sci, 1989. **14**(8): p. 347-50.
41. Rothman, J.H. and T.H. Stevens, *Protein sorting in yeast: mutants defective in vacuole biogenesis mislocalize vacuolar proteins into the late secretory pathway*. Cell, 1986. **47**(6): p. 1041-51.
42. Bankaitis, V.A., L.M. Johnson, and S.D. Emr, *Isolation of yeast mutants defective in protein targeting to the vacuole*. Proc Natl Acad Sci U S A, 1986. **83**(23): p. 9075-9.
43. Horazdovsky, B.F., D.B. DeWald, and S.D. Emr, *Protein transport to the yeast vacuole*. Curr Opin Cell Biol, 1995. **7**(4): p. 544-51.
44. Lemmon, S.K. and L.M. Traub, *Sorting in the endosomal system in yeast and animal cells*. Curr Opin Cell Biol, 2000. **12**(4): p. 457-66.
45. Babst, M., et al., *Endosomal transport function in yeast requires a novel AAA-type ATPase, Vps4p*. Embo J, 1997. **16**(8): p. 1820-31.
46. Hurley, J.H. and S.D. Emr, *The ESCRT Complexes: Structure and Mechanism of a Membrane-Trafficking Network*. Annu Rev Biophys Biomol Struct, 2006.
47. Piper, R.C., et al., *VPS27 controls vacuolar and endocytic traffic through a prevacuolar compartment in Saccharomyces cerevisiae*. J Cell Biol, 1995. **131**(3): p. 603-17.
48. Eastman, S.W., et al., *Identification of human VPS37C, a component of endosomal sorting complex required for transport-I important for viral budding*. J Biol Chem, 2005. **280**(1): p. 628-36.
49. Stuchell, M.D., et al., *The human endosomal sorting complex required for transport (ESCRT-I) and its role in HIV-1 budding*. J Biol Chem, 2004. **279**(34): p. 36059-71.
50. von Schwedler, U.K., et al., *The protein network of HIV budding*. Cell, 2003. **114**(6): p. 701-13.
51. Slagsvold, T., et al., *Endosomal and non-endosomal functions of ESCRT proteins*. Trends Cell Biol, 2006. **16**(6): p. 317-26.
52. Babst, M., et al., *Escrt-III: an endosome-associated heterooligomeric protein complex required for mvb sorting*. Dev Cell, 2002. **3**(2): p. 271-82.
53. Babst, M., et al., *Endosome-associated complex, ESCRT-II, recruits transport machinery for protein sorting at the multivesicular body*. Dev Cell, 2002. **3**(2): p. 283-9.
54. Bowers, K., et al., *Protein-protein interactions of ESCRT complexes in the yeast Saccharomyces cerevisiae*. Traffic, 2004. **5**(3): p. 194-210.
55. Katzmann, D.J., M. Babst, and S.D. Emr, *Ubiquitin-dependent sorting into the multivesicular body pathway requires the function of a conserved endosomal protein sorting complex, ESCRT-I*. Cell, 2001. **106**(2): p. 145-55.

56. Gruenberg, J. and H. Stenmark, *The biogenesis of multivesicular endosomes*. Nat Rev Mol Cell Biol, 2004. **5**(4): p. 317-23.
57. Raiborg, C., T.E. Rusten, and H. Stenmark, *Protein sorting into multivesicular endosomes*. Curr Opin Cell Biol, 2003. **15**(4): p. 446-55.
58. Bache, K.G., et al., *The ESCRT-III subunit hVps24 is required for degradation but not silencing of the epidermal growth factor receptor*. Mol Biol Cell, 2006. **17**(6): p. 2513-23.
59. Babst, M., *A protein's final ESCRT*. Traffic, 2005. **6**(1): p. 2-9.
60. Fujita, H., et al., *A dominant negative form of the AAA ATPase SKD1/VPS4 impairs membrane trafficking out of endosomal/lysosomal compartments: class E vps phenotype in mammalian cells*. J Cell Sci, 2003. **116**(Pt 2): p. 401-14.
61. Raiborg, C., et al., *FYVE and coiled-coil domains determine the specific localisation of Hrs to early endosomes*. J Cell Sci, 2001. **114**(Pt 12): p. 2255-63.
62. Bache, K.G., et al., *STAM and Hrs are subunits of a multivalent ubiquitin-binding complex on early endosomes*. J Biol Chem, 2003. **278**(14): p. 12513-21.
63. Bishop, N. and P. Woodman, *ATPase-defective mammalian VPS4 localizes to aberrant endosomes and impairs cholesterol trafficking*. Mol Biol Cell, 2000. **11**(1): p. 227-39.
64. Pornillos, O., J.E. Garrus, and W.I. Sundquist, *Mechanisms of enveloped RNA virus budding*. Trends Cell Biol, 2002. **12**(12): p. 569-79.
65. Morita, E. and W.I. Sundquist, *Retrovirus budding*. Annu Rev Cell Dev Biol, 2004. **20**: p. 395-425.
66. Freed, E.O., *Viral late domains*. J Virol, 2002. **76**(10): p. 4679-87.
67. Pornillos, O., et al., *HIV Gag mimics the Tsg101-recruiting activity of the human Hrs protein*. J Cell Biol, 2003. **162**(3): p. 425-34.
68. Strack, B., et al., *AIP1/ALIX is a binding partner for HIV-1 p6 and EIAV p9 functioning in virus budding*. Cell, 2003. **114**(6): p. 689-99.
69. Martin-Serrano, J., T. Zang, and P.D. Bieniasz, *HIV-1 and Ebola virus encode small peptide motifs that recruit Tsg101 to sites of particle assembly to facilitate egress*. Nat Med, 2001. **7**(12): p. 1313-9.
70. VerPlank, L., et al., *Tsg101, a homologue of ubiquitin-conjugating (E2) enzymes, binds the L domain in HIV type 1 Pr55(Gag)*. Proc Natl Acad Sci U S A, 2001. **98**(14): p. 7724-9.
71. Patnaik, A., V. Chau, and J.W. Wills, *Ubiquitin is part of the retrovirus budding machinery*. Proc Natl Acad Sci U S A, 2000. **97**(24): p. 13069-74.
72. Schubert, U., et al., *Proteasome inhibition interferes with gag polyprotein processing, release, and maturation of HIV-1 and HIV-2*. Proc Natl Acad Sci U S A, 2000. **97**(24): p. 13057-62.
73. Gottwein, E. and H.G. Krausslich, *Analysis of human immunodeficiency virus type 1 Gag ubiquitination*. J Virol, 2005. **79**(14): p. 9134-44.
74. Martin-Serrano, J., T. Zang, and P.D. Bieniasz, *Role of ESCRT-I in retroviral budding*. J Virol, 2003. **77**(8): p. 4794-804.

75. Griffiths, G., *On vesicles and membrane compartments*. Protoplasma, 1996. **195**: p. 37-58.
76. Griffiths, G., et al., *The mannose 6-phosphate receptor and the biogenesis of lysosomes*. Cell, 1988. **52**(3): p. 329-41.
77. McDowall, A., et al., *The structure of organelles of the endocytic pathway in hydrated cryosections of cultured cells*. Eur J Cell Biol, 1989. **49**(2): p. 281-94.
78. Schmid, S.L., *Clathrin-coated vesicle formation and protein sorting: an integrated process*. Annu Rev Biochem, 1997. **66**: p. 511-48.
79. Smith, A.E. and A. Helenius, *How viruses enter animal cells*. Science, 2004. **304**(5668): p. 237-42.
80. Pelkmans, L. and A. Helenius, *Endocytosis via caveolae*. Traffic, 2002. **3**(5): p. 311-20.
81. Damm, E.M., et al., *Clathrin- and caveolin-1-independent endocytosis: entry of simian virus 40 into cells devoid of caveolae*. J Cell Biol, 2005. **168**(3): p. 477-88.
82. Keller, G.A., M.W. Siegel, and I.W. Caras, *Endocytosis of glycophospholipid-anchored and transmembrane forms of CD4 by different endocytic pathways*. Embo J, 1992. **11**(3): p. 863-74.
83. Becich, M.J., S. Mahklouf, and J.U. Baenziger, *Wheat germ agglutinin is selectively transported to multivesicular bodies*. Eur J Cell Biol, 1991. **55**(1): p. 83-93.
84. Marsh, M., et al., *Three-dimensional structure of endosomes in BHK-21 cells*. Proc Natl Acad Sci U S A, 1986. **83**(9): p. 2899-903.
85. Aniento, F., et al., *Cytoplasmic dynein-dependent vesicular transport from early to late endosomes*. J Cell Biol, 1993. **123**(6 Pt 1): p. 1373-87.
86. Gruenberg, J., G. Griffiths, and K.E. Howell, *Characterization of the early endosome and putative endocytic carrier vesicles in vivo and with an assay of vesicle fusion in vitro*. J Cell Biol, 1989. **108**(4): p. 1301-16.
87. Pelchen-Matthews, A., G. Raposo, and M. Marsh, *Endosomes, exosomes and Trojan viruses*. Trends Microbiol, 2004. **12**(7): p. 310-6.
88. Katzmann, D.J., G. Odorizzi, and S.D. Emr, *Receptor downregulation and multivesicular-body sorting*. Nat Rev Mol Cell Biol, 2002. **3**(12): p. 893-905.
89. Sachse, M., G.J. Strous, and J. Klumperman, *ATPase-deficient hVPS4 impairs formation of internal endosomal vesicles and stabilizes bilayered clathrin coats on endosomal vacuoles*. J Cell Sci, 2004. **117**(Pt 9): p. 1699-708.
90. Stoorvogel, W., et al., *The biogenesis and functions of exosomes*. Traffic, 2002. **3**(5): p. 321-30.
91. Mobius, W., et al., *Recycling compartments and the internal vesicles of multivesicular bodies harbor most of the cholesterol found in the endocytic pathway*. Traffic, 2003. **4**(4): p. 222-31.
92. Griffiths, G., R. Back, and M. Marsh, *A quantitative analysis of the endocytic pathway in baby hamster kidney cells*. J Cell Biol, 1989. **109**(6 Pt 1): p. 2703-20.

93. Kleijmeer, M.J., G. Raposo, and H.J. Geuze, *Characterization of MHC Class II Compartments by Immunoelectron Microscopy*. Methods, 1996. **10**(2): p. 191-207.
94. Griffiths, G., *Fine Structure Immunocytochemistry*. 1993, Berlin: Springer Verlag.
95. Harada, S., Y. Koyanagi, and N. Yamamoto, *Infection of HTLV-III/LAV in HTLV-I-carrying cells MT-2 and MT-4 and application in a plaque assay*. Science, 1985. **229**(4713): p. 563-6.
96. Pear, W.S., et al., *Production of high-titer helper-free retroviruses by transient transfection*. Proc Natl Acad Sci U S A, 1993. **90**(18): p. 8392-6.
97. Charneau, P., M. Alizon, and F. Clavel, *A second origin of DNA plus-strand synthesis is required for optimal human immunodeficiency virus replication*. J Virol, 1992. **66**(5): p. 2814-20.
98. Rabouille, C., et al., *Mapping the distribution of Golgi enzymes involved in the construction of complex oligosaccharides*. J Cell Sci, 1995. **108 (Pt 4)**: p. 1617-27.
99. Adachi, A., et al., *Production of acquired immunodeficiency syndrome-associated retrovirus in human and nonhuman cells transfected with an infectious molecular clone*. J Virol, 1986. **59**(2): p. 284-91.
100. Konvalinka, J., et al., *An active-site mutation in the human immunodeficiency virus type 1 proteinase (PR) causes reduced PR activity and loss of PR-mediated cytotoxicity without apparent effect on virus maturation and infectivity*. J Virol, 1995. **69**(11): p. 7180-6.
101. Westervelt, P., et al., *Macrophage tropism determinants of human immunodeficiency virus type 1 in vivo*. J Virol, 1992. **66**(4): p. 2577-82.
102. Slot, J.W., et al., *Translocation of the glucose transporter GLUT4 in cardiac myocytes of the rat*. Proc Natl Acad Sci U S A, 1991. **88**(17): p. 7815-9.
103. Slot, J.W. and H.J. Geuze, *A new method of preparing gold probes for multiple-labeling cytochemistry*. Eur J Cell Biol, 1985. **38**(1): p. 87-93.
104. Ghosh, P., et al., *Mammalian GGAs act together to sort mannose 6-phosphate receptors*. J Cell Biol, 2003. **163**(4): p. 755-66.
105. Damke, H., et al., *Dynamin GTPase domain mutants block endocytic vesicle formation at morphologically distinct stages*. Mol Biol Cell, 2001. **12**(9): p. 2578-89.
106. Blanquet, P.R., *Ultrahistochemical study on the ruthenium red surface staining. I. Processes which give rise to electron-dense marker*. Histochemistry, 1976. **47**(2): p. 63-78.
107. Blanquet, P.R., *Ultrahistochemical study on the ruthenium red surface staining. II. Nature and affinity of the electron dense marker*. Histochemistry, 1976. **47**(3): p. 175-89.
108. Luft, J.H., *Ruthenium red and violet. II. Fine structural localization in animal tissues*. Anat Rec, 1971. **171**(3): p. 369-415.
109. Luft, J.H., *Ruthenium red and violet. I. Chemistry, purification, methods of use for electron microscopy and mechanism of action*. Anat Rec, 1971. **171**(3): p. 347-68.

110. Reynolds, E.S., *The use of lead citrate at high pH as an electron-opaque stain in electron microscopy*. J Cell Biol, 1963. **17**: p. 208-12.
111. Mayhew, T.M., J.M. Lucocq, and G. Griffiths, *Relative labelling index: a novel stereological approach to test for non-random immunogold labelling of organelles and membranes on transmission electron microscopy thin sections*. J Microsc, 2002. **205**(Pt 2): p. 153-64.
112. Lucocq, J.M., et al., *A rapid method for assessing the distribution of gold labeling on thin sections*. J Histochem Cytochem, 2004. **52**(8): p. 991-1000.
113. Sachse, M., et al., *Bilayered clathrin coats on endosomal vacuoles are involved in protein sorting toward lysosomes*. Mol Biol Cell, 2002. **13**(4): p. 1313-28.
114. Yoshimori, T., et al., *The mouse SKD1, a homologue of yeast Vps4p, is required for normal endosomal trafficking and morphology in mammalian cells*. Mol Biol Cell, 2000. **11**(2): p. 747-63.
115. Zhong, Q., et al., *Perturbation of TSG101 protein affects cell cycle progression*. Cancer Res, 1998. **58**(13): p. 2699-702.
116. Vito, P., et al., *Cloning of AIP1, a novel protein that associates with the apoptosis-linked gene ALG-2 in a Ca2+-dependent reaction*. J Biol Chem, 1999. **274**(3): p. 1533-40.
117. Damke, H., et al., *Induction of mutant dynamin specifically blocks endocytic coated vesicle formation*. J Cell Biol, 1994. **127**(4): p. 915-34.
118. Kramer, B., et al., *HIV interaction with endosomes in macrophages and dendritic cells*. Blood Cells Mol Dis, 2005. **35**(2): p. 136-42.
119. Matsuo, H., et al., *Role of LBPA and Alix in multivesicular liposome formation and endosome organization*. Science, 2004. **303**(5657): p. 531-4.
120. Cabezas, A., et al., *Alix regulates cortical actin and the spatial distribution of endosomes*. J Cell Sci, 2005. **118**(Pt 12): p. 2625-35.
121. Komada, M., et al., *Hrs, a tyrosine kinase substrate with a conserved double zinc finger domain, is localized to the cytoplasmic surface of early endosomes*. J Biol Chem, 1997. **272**(33): p. 20538-44.
122. Morino, C., et al., *A role for Hrs in endosomal sorting of ligand-stimulated and unstimulated epidermal growth factor receptor*. Exp Cell Res, 2004. **297**(2): p. 380-91.
123. Katoh, K., et al., *The ALG-2-interacting protein Alix associates with CHMP4b, a human homologue of yeast Snf7 that is involved in multivesicular body sorting*. J Biol Chem, 2003. **278**(40): p. 39104-13.
124. Bache, K.G., et al., *Hrs regulates multivesicular body formation via ESCRT recruitment to endosomes*. J Cell Biol, 2003. **162**(3): p. 435-42.
125. Babst, M., et al., *The Vps4p AAA ATPase regulates membrane association of a Vps protein complex required for normal endosome function*. Embo J, 1998. **17**(11): p. 2982-93.
126. Urbe, S., et al., *The UIM domain of Hrs couples receptor sorting to vesicle formation*. J Cell Sci, 2003. **116**(Pt 20): p. 4169-79.
127. Clague, M.J. and S. Urbe, *Hrs function: viruses provide the clue*. Trends Cell Biol, 2003. **13**(12): p. 603-6.

128. Geuze, H.J., et al., *Intracellular site of asialoglycoprotein receptor-ligand uncoupling: double-label immunoelectron microscopy during receptor-mediated endocytosis*. Cell, 1983. **32**(1): p. 277-87.
129. Peden, A.A., et al., *Localization of the AP-3 adaptor complex defines a novel endosomal exit site for lysosomal membrane proteins*. J Cell Biol, 2004. **164**(7): p. 1065-76.
130. Ono, A., et al., *Phosphatidylinositol (4,5) bisphosphate regulates HIV-1 Gag targeting to the plasma membrane*. Proc Natl Acad Sci U S A, 2004. **101**(41): p. 14889-94.
131. Sherer, N.M., et al., *Visualization of retroviral replication in living cells reveals budding into multivesicular bodies*. Traffic, 2003. **4**(11): p. 785-801.
132. Nydegger, S., et al., *HIV-1 egress is gated through late endosomal membranes*. Traffic, 2003. **4**(12): p. 902-10.
133. Perlman, M. and M.D. Resh, *Identification of an intracellular trafficking and assembly pathway for HIV-1 gag*. Traffic, 2006. **7**(6): p. 731-45.
134. Booth, A.M., et al., *Exosomes and HIV Gag bud from endosome-like domains of the T cell plasma membrane*. J Cell Biol, 2006. **172**(6): p. 923-35.
135. Ott, D.E., *Potential roles of cellular proteins in HIV-1*. Rev Med Virol, 2002. **12**(6): p. 359-74.
136. Arthur, L.O., et al., *Cellular proteins bound to immunodeficiency viruses: implications for pathogenesis and vaccines*. Science, 1992. **258**(5090): p. 1935-8.
137. Orentas, R.J. and J.E. Hildreth, *Association of host cell surface adhesion receptors and other membrane proteins with HIV and SIV*. AIDS Res Hum Retroviruses, 1993. **9**(11): p. 1157-65.
138. Esser, M.T., et al., *Differential incorporation of CD45, CD80 (B7-1), CD86 (B7-2), and major histocompatibility complex class I and II molecules into human immunodeficiency virus type 1 virions and microvesicles: implications for viral pathogenesis and immune regulation*. J Virol, 2001. **75**(13): p. 6173-82.
139. Nguyen, D.G., et al., *Evidence that HIV budding in primary macrophages occurs through the exosome release pathway*. J Biol Chem, 2003. **278**(52): p. 52347-54.
140. Liao, Z., et al., *Lipid rafts and HIV pathogenesis: host membrane cholesterol is required for infection by HIV type 1*. AIDS Res Hum Retroviruses, 2001. **17**(11): p. 1009-19.
141. Nguyen, D.H. and J.E. Hildreth, *Evidence for budding of human immunodeficiency virus type 1 selectively from glycolipid-enriched membrane lipid rafts*. J Virol, 2000. **74**(7): p. 3264-72.
142. Campbell, S.M., S.M. Crowe, and J. Mak, *Lipid rafts and HIV-1: from viral entry to assembly of progeny virions*. J Clin Virol, 2001. **22**(3): p. 217-27.
143. Brugger, B., et al., *The HIV lipidome: a raft with an unusual composition*. Proc Natl Acad Sci U S A, 2006. **103**(8): p. 2641-6.
144. Grigorov, B., et al., *Assembly of Infectious HIV-1 in Human Epithelial and T-Lymphoblastic Cell Lines*. J Mol Biol, 2006. **359**(4): p. 848-62.

145. Lindwasser, O.W. and M.D. Resh, *Human immunodeficiency virus type 1 Gag contains a dileucine-like motif that regulates association with multivesicular bodies*. J Virol, 2004. **78**(11): p. 6013-23.
146. Griffiths, G., et al., *The immunofluorescent era of membrane traffic*. Trends Cell Biol, 1993. **3**(7): p. 214-9.
147. Jayakumar, P., et al., *Tissue-resident macrophages are productively infected ex vivo by primary X4 isolates of human immunodeficiency virus type 1*. J Virol, 2005. **79**(8): p. 5220-6.

List of publications

Sonja Welsch, Oliver T. Keppler, Anja Haberman, Ina Allespach, Jacomine Krijnse-Locker, Hans-Georg Kräusslich: „The Primary Site of HIV-1 Budding in Infected Macrophages is the Plasma Membrane", in preparation.

Welsch S., Habermann A., Jäger S., Müller B., Krijnse-Locker J., Kräusslich HG: "Ultrastructural analysis of ESCRT proteins suggests a role for endosome-associated tubular-vesicular membranes in ESCRT function". Re-submitted for publication in "Traffic".

Palacios S., Perez L.H., Welsch S., Schleich S., Chmielarska K., Melchior F., Locker JK. "Quantitative SUMO-1 modification of a vaccinia virus protein is required for its specific localization and prevents its self-association." Mol Biol Cell. 2005 Jun; 16(6): 2822-35.

Welsch S, Doglio L, Schleich S, Krijnse Locker J. "The vaccinia virus I3L gene product is localized to a complex endoplasmic reticulum-associated structure that contains the viral parental DNA." J Virol. 2003 May; 77(10): 6014-28.

Melzner I., Sommer A., Schulte M., Roederer S., Welsch S., von Baehr A., Wegmann M. and Moeller P. "Quantification of the Expression of *obese* Messenger Ribonucleic Acid in Human Adipose Tissue by Reverse Transcription Polymerase Chain Reaction: A Methodologic Contribution. In Blum W.F., Kiess W., Rascher W. (Eds.): "Leptin - the voice of adipose tissue": J.A. Barth 1997: 110-114.